MULTIVARIATE ANALYSIS APPLIED TO DISCRETE PART MANUFACTURING

MULTIVARIATE ANALYSIS APPLIED TO DISCRETE PART MANUFACTURING

By

DARRYL WALLACE, B.Eng.

A Thesis

Submitted to the School of Graduate Studies

in Partial Fulfilment of the Requirements

for the Degree

Master of Applied Science

McMaster University

MASTER OF APPLIED SCIENCE (2007)	McMaster University
(Mechanical Engineering)	Hamilton, Ontario

TITLE:	Multivariate Analysis Applied to Discrete Part Manufacturing
AUTHOR:	Darryl Wallace, B.Eng. (McMaster University)
SUPERVISOR:	Professor S.C. Veldhuis
NUMBER OF PAGES:	xii, 139

ABSTRACT

The overall focus of this thesis is the implementation of a process monitoring system in a real manufacturing environment that utilizes multivariate analysis techniques to assess the state of the process. The process in question was the medium-high volume manufacturing of discrete aluminum parts using relatively simple machining processes involving the use of two tools. This work can be broken down into three main sections.

The first section involved the modeling of temperatures and thermal expansion measurements for real-time thermal error compensation. Thermal expansion of the Z-axis was measured indirectly through measurement of the two quality parameters related to this axis with a custom gage that was designed for this part. A compensation strategy is proposed which is able to hold the variation of the parts to ±0.02mm, where the tolerance is ±0.05mm.

The second section involved the modeling of the process data from the parts that included vibration, current, and temperature signals from the machine. The modeling of the process data using Principal Component Analysis (PCA), while unsuccessful in detecting minor simulated process faults, was successful in detecting a miss-loaded part during regular production. Simple control charts using Hotelling's T^2 statistic and Squared Prediction Error are illustrated. The modeling of quality data from the process data of good parts using Projection to Latent Structures by Partial Least Squares (PLS) data did not provide very accurate fits to the data; however, all of the predictions are within the tolerance specifications.

The final section discusses the implementation of a process monitoring system in both manual and automatic production environments. A method for the integration and storage of process data with Mitutoyo software MCOSMOS and MeasurLink® is described. All of the codes to perform multivariate analysis and process monitoring were written using Matlab.

ACKNOWLEDGEMENTS

I would like to thank Dr. Stephen Veldhuis for his continued support and for providing this wonderful opportunity. I would also like to thank Dr. John MacGregor for his assistance with multivariate analysis.

I would like to thank James Nixon and Frank Nixon and the rest of the staff from Nixon Integrated Machining Designs Ltd. for providing me with assistance and allowing me to use their facilities throughout this project.

For their help here at McMaster University, I would like to thank the members of the labs: Warren Reynolds, Jim McLaren, Mark MacKenzie, Joe Verhaeghe, Ron Lodewyks, and Dave Schick. Their assistance and patience in the lab was greatly appreciated.

Finally, I would like to thank my family, friends, and most of all Kristin Davies, for their continued support and encouragement throughout my studies.

TABLE OF CONTENTS

LIST OF FIGURES

LIST OF TABLES

Chapter 1 – Introduction

1.1 Overview

This thesis outlines the investigation of a process monitoring system for machining in a production environment using multivariate modeling techniques. This process monitoring system is to provide a variety of functions from the multitude of process sensor data acquired during the manufacturing of discrete parts. Furthermore, the role of a manufacturing process monitoring system can be outlined by three main criteria as defined by Inasaki and Tönshoff (2001):

- Capable of detecting undesirable process
- Capturing information regarding the process and using this information to optimize the process
- Relating the input of the process to the output

The work presented in this thesis attempts to satisfy these criteria, as well as provide some additional functionality. While capturing the information of the process, it must be able to relay the information regarding the state of the process in a simple yet effective way to operators and employees. Through the use of principal component analysis (PCA) and projection to latent structures or partial least squares (PLS) multivariable modeling techniques, it is possible to create simple control charts using parameters such as Hotelling's T^2 statistic. Furthermore, these modeling techniques provide easy to understand diagnostic tools, such as contribution plots, which can be used to determine the cause of problematic process conditions by identifying the process variables most responsible for the poor quality.

With much of the research in this field performed in the laboratory, it was necessary to develop a monitoring system which is still capable of satisfying the three main criteria while implementing a solution that can be seamlessly integrated into an existing process in a real production environment. An example of this is the use of table force dynamometers for measurement of cutting forces; a sensor that is frequently used in highly controlled laboratory experiments, but is not generally compatible with the machining process that is investigated throughout this thesis. With this being said, a sensor fusion system is developed, based on the literature review of sensors, which can satisfy the requirements of measuring crucial machining process parameters while providing no interference or alteration to the process. Using the sensor information it is possible to develop process monitoring schemes that are capable of satisfying criteria specified by the customer, such as modeling the quality data with process information and real-time thermal error compensation.

Finally, with all of this process data now becoming available, there are commercially only few options available when it comes to storing the process data, as these process monitoring systems (including laboratory based systems) are often custom designed to suit their respective applications. Inspection information, however, is frequently stored in databases and statistical packages, like Mitutoyo's MCOSMOS CMM inspection software and STATMeasure Plus which links to MCOSMOS through MeasurLink. Using these software packages developed by Mitutoyo, a method of relaying the process information to a database is developed and information is tagged to the parts using a simple part ID tagging convention. Once this data is stored in an easily accessible location, multivariate statistical analysis can easily be performed.

1.2 Thesis Layout

This document follows a standard thesis layout. The main goals here are to effectively outline the experimentation procedures and results while providing justification for the methods used and to conclude on the findings made.

This first chapter provides an overview for the thesis while illustrating the main criteria that a process monitoring system must satisfy. The multivariate tools that are implemented throughout this thesis and the need for a sensor fusion system capable of meeting these criteria are introduced. Finally, the idea that the large amounts of new data coming do not have a place to be stored is addressed.

In the second chapter the literature review is performed where several key topics are investigated. A brief look at errors that are experienced in machining is discussed followed by a look at the sensors used on a machine for various process quantities such as force, vibrations, temperatures, etc. The next section involves a look at existing process monitoring schemes, with emphasis on the measured process quantities and modeling techniques in order to assess pros and cons of these systems. All of the schemes that are discussed here consider the cases where all of the modeling is done on controlled laboratory experiments with little emphasis on monitoring machining in a production environment. Finally, the theory and techniques used for multivariate analysis of the process data is mentioned, along with addressing the control charts that are used to relay process information to the operators.

The third chapter outlines the experimental methods that are performed during this work. The methods described for the design of a real-time thermal error compensation system using temperature measurements from machining conditions during production. The need for the investigation of this compensation is verified by the measurement of the thermal expansion of the Z-axis using proximity sensors and later the indirect measurement of this quantity through the measurement of the height quality parameter on the parts. The sensor fusion system is described for the overall process monitoring of a discrete part manufacturing system. The description of the sensors used to fulfill the requirement that the system must yield seamless integration into the existing manufacturing process is also outlined. The experimental and analysis techniques used in this research are also described.

Chapter four addresses the analysis of this experimental work while providing the results and discussion of these experiments. The analysis of the real-time thermal error compensation involves the use of modeling the expansion of the machine via PLS. Using quality measurements during the production to indirectly measure thermal distortion, a model was created and was found to yield predictions that can hold the quality parameters to within tolerance. The model is applied to new data and a compensation strategy is proposed and investigated. The monitoring of the machining process using a combination of vibration, current, and temperature sensors is investigated. The experimental simulation of the process faults is then investigated and the use of control charts is illustrated. The modeling and application of several quality parameters affected by machining is illustrated here using PLS.

The fifth chapter discusses the implementation of this process monitoring system. The structure of the data collection environment is illustrated here, as well as the integration with the Mitutoyo software. Since codes were developed to perform the PCA and PLS algorithms in Matlab, a comparison is performed with the modeling results generated by commercial software such as SIMCA-P+.

The final chapter concludes on the work presented here and outlines the key results and findings of the various experimental work performed here. Ideas for future work are also presented here.

Chapter 2 – Literature Review

2.1 Errors in machining

Ramesh *et al.* (2000) stated that while accuracies in machine tools have reached the range of 0.005mm which is a result of improved design practices and material selection; it is still difficult, however, to completely remove all forms of error. Furthermore, errors are broadly classified in four categories which include geometric and kinematic; thermal; cutting force induced; and other errors (tool wear and fixturing errors fit in this category). Ramesh *et al.* also go on to distinguish between accuracy and error; with accuracy being how close the final part matches the desired geometry and error being the "deviation from the position of the cutting edge from the theoretically required value" needed to attain a specific accuracy. The goal in much research is simply to compensate for this error through its measurement. The only requirement, however, is that the errors are repeatable in order to track and compensate for these changes. There has also been much research into real-time error compensation where by continuous error tracking is performed and corrections are made frequently to the process while it is running (Ramesh, Mannan, & Poo, 2000).

2.2 Sensors

Within a manufacturing environment, there are a number of aspects related to the process that can be measured. It has become standard practice to use multiple sensors, both multiple locations and types, in a method known as *sensor fusion* (Inasaki & Tönshoff, 2001). The combination of these sensors enables the user to observe or capture effects from a complex process, such as machining, in order to determine if the process is good or give the ability to predict certain quality parameters. Using various sensors, it is important to measure process variables such as forces, acoustic emissions (AE), cutting power (Byrne *et al*, 1995), as well as vibrations and temperatures (Inasaki & Tönshoff, 2001). From this information the user is able to relate process variables to quality parameters via modeling techniques. Another benefit of sensor fusion comes from the ability to "provide data for the decision-making process that has a low uncertainty owing to the inherent randomness or noise in the sensor signals (Inasaki & Tönshoff, 2001)." Furthermore, Figure 2.1 provides an example of process sensor locations on a both milling and turning machines.

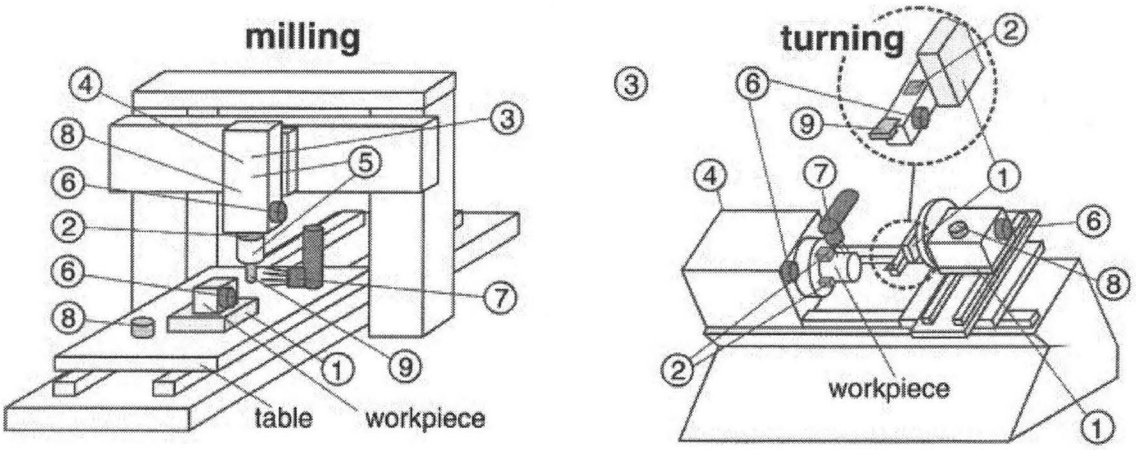

Figure 2.1: Possible sensor locations on machine tools. Sensors: 1 – piezo-electric dynamometer; 2 – strain gauge; 3 - force measuring bearing; 4 – power sensor; 5 – torque sensor; 6 – AE sensor, surface mounted; 7 – AE Sensor, fluid coupled; 8 – acceleration sensor; 9 – tool inbuilt sensor (Inasaki & Tönshoff, 2001).

2.2.1 Force

In any machining process, the interaction of the tool with the work piece generates forces at the interface of the two objects (Tlusty, 2000). This is true for both single-point tool operations like boring or multipoint tool operations like milling; however the nature of the force differs with process. Furthermore, the detection of a change in the force signal from the process could be the result of tool chipping or breakage and is required for assessing the current tool condition (Inasaki & Tönshoff, 2001).

Strain gauges have been used for measuring forces; however, methods using these sensors suffer from the need to place the sensor as close to the element under load as possible (Inasaki & Tönshoff, 2001).

Piezoelectric table dynamometers for use in milling and smaller tool shank mounted dynamometers (as seen in Figure 2.1) have been reported as being the most accurate force measurement devices (Byrne *et al*, 1995; Inasaki & Tönshoff, 2001; and others). The use of these types of sensors, however, have been limited to the laboratory due to their high costs (Byrne *et al*, 1995) and lack of robustness under the harsh machining environment. Furthermore, the charge-based nature of the piezoelectric effect requires the use of charge amplifiers that need to be reset in between tests making it difficult for implementation in a high volume production environment.

While other methods of measuring forces in machine tools have been reported (e.g. Byrne *et al*, 1995), the common factor relating all of these methods of directly measuring forces are not ideal for production environments as they may interfere with processes involving multiple tool changes (e.g. the tool shank placement dynamometer in turning) or production environments with custom fixturing.

2.2.2 Indirect Force Measurement

Due to some of the difficulties mentioned in the previous section with regards to direct measurement of forces, there has been research into methods regarding indirect force sensing. These techniques often involve the measurement and recording of other sensors, process information and parameters within the machine and using these signals to estimate the actual forces.

A method which relies on using capacitance displacement sensors to measure the deflection of spindle was developed by Albrecht *et al.* (2005). Initially, a single displacement sensor is placed next to the spindle in the X-direction and cutting tests were performed in this direction. In addtion, the cutting forces were monitored using a Kistler piezoelectric table dynamometer. In the process of measuring the spindle displacement, the dynamics of the spindle are also observed. Compensation using a Kalman filter was used to remove the structural dynamics of the spindle and remove high frequency noise while maintaining an accurate model of the measured forces. This method was used to increase the bandwidth of the sensor system from approximately 350 Hz to 1,000 Hz. Cutting tests were performed at spindle speeds ranging from 1,000 RPM to 12,000 RPM with a five-fluted endmill (corresponds to 83.3Hz to 1,000Hz tooth passing frequencies). The Kalman filter compensation is able to reduce the error of the displacement sensor model in all cases and is able to replicate the measurements of the dynamometer with good agreement, with exception to the case at 12000 RPM. Here the bandwidth limit of the dynamometer was reached at 1,000 Hz which caused errors in the measurement of the forces and thus difficulties in modeling. In addition, the authors presented methods to compensate for thermal effects, roundness errors and unbalanced spindles by different and mulitple sensor configurations.

Jeong and Cho (2002) presented a method of using feed motor currents on a milling machine for the estimation of cutting forces. Cutting tests were performed in both X and Y directions and forces were measured using a table dynamometer. Current signals from the X and Y axis motors were measured using Hall effect current transducers. One of the interesting things to note was the mention of the measured current of the stationary axis motor. The current of the stationary axis motor flucutated in order keep the axis steady. Relationships between the stationary axis current and forces in that axis were developed. While Figure 2.2 shows good agreement with the estimation of cutting force from the current measurement, the limitation of the method described was the bandwidth of the current sensor at 130 Hz.

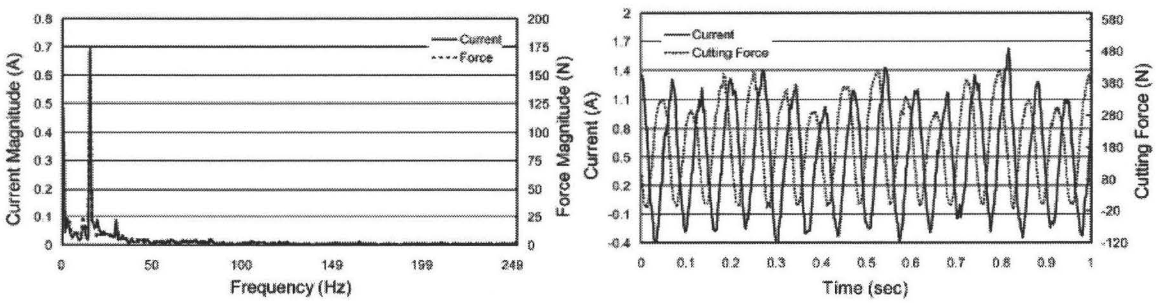

Figure 2.2: Cutting forces vs. current measurement in both time and frequency domain for tooth passing frequency of 15 Hz. Note the phase lag in the current measurements compared to the forces (Jeong & Cho, 2002).

Although the limitations of this work are limited to relatively low tooth passing frequencies, it is still an illustration of how measuring the feed motor currents can be used as a tool to indirectly measure forces.

Spiewak (1995) demonstrated the use of acceleration measurements in the spindle as indirect force measurements. There were two main sources of error in this method of measuring forces which included the flexible mode vibrations and the motions associated with the spindle structure causing inertial and viscous forces. A filtering system was developed using an adaptive filter that was tuned using process information and sensor information in order to attenuate information from the spindle dynamics. External excitation forces were presented to the spindle and, after filtering, the estimated force from the acceleration signal was in good agreement with the measured forces.

2.2.3 Temperature

There has been much research into the measurement of temperatures on machine tools for use in error compensation. Geometric deviations caused by the thermal expansion of the components in a machine during operation lead to errors in the machined parts. Much of this research involves the use of thermocouples (Ramesh, Mannan, & Poo, 2000a). An exaggerated example of how machine tools geometrically deform due to increases in temperatures can be found in Figure 2.3. In general, this heat generation is primarily caused by the operation of actuators within the machine.

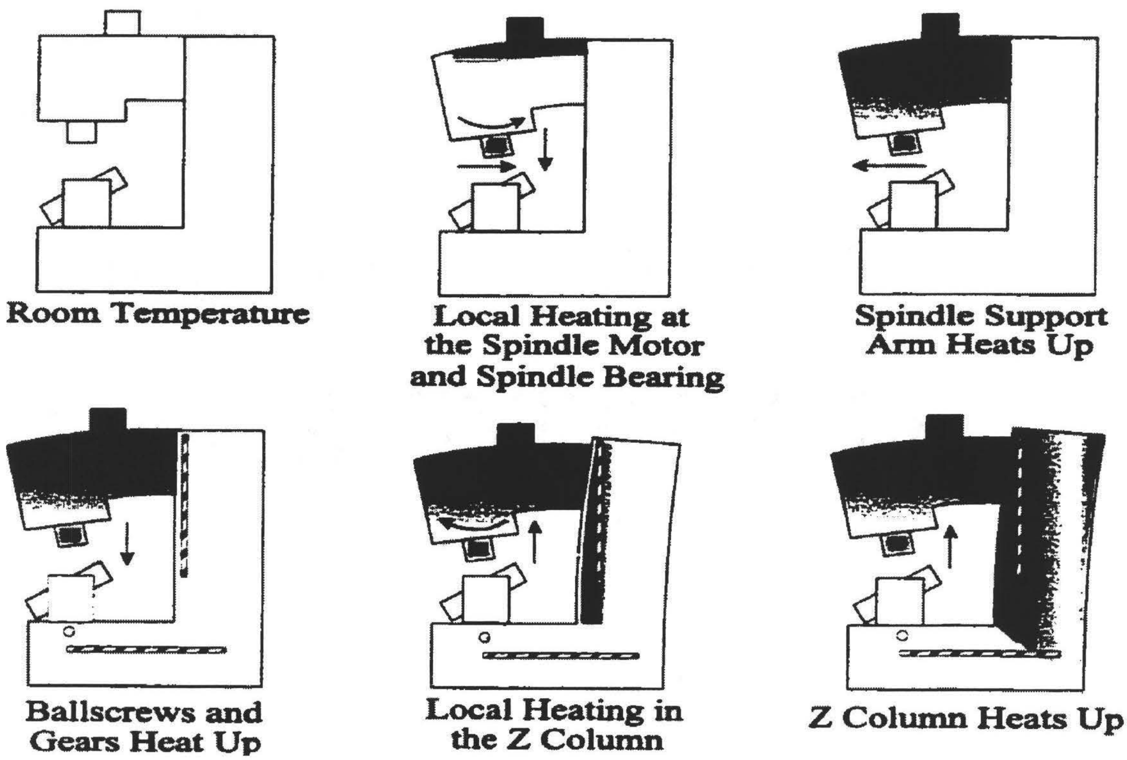

Figure 2.3: Illustration of thermal errors in machine tools (Veldhuis, 1998)

It has been reported by Attia and Kops (1993) that E-type thermocouples provided the best performance when taking surface temperature measurements in machine tools. This type of thermocouple has higher sensitivity when compared to other types of thermocouples such as K-type. Furthermore, this type of thermocouple has been used in practice with success in several studies, including (Chen J. , 1996), (Chen & Ling, 1996) and (Veldhuis, 1998).

2.2.4 Vibration

The measurement of vibrations in a machine tool has been used for various reasons including: tool condition monitoring (Inasaki & Tönshoff, 2001) and surface quality (Azouzi & Guillot, 1996), for example.

Dimla and Lister (2000) showed how the use of piezoelectric based accelerometers (used in conjunction with a tool shank mounted dynamometer) can be used for assessing tool condition monitoring in turning. Vibration signatures in the frequency domain were used to illustrate the effects of increasing tool wear and are shown in Figure 2.4. Note how the vibration signature increases in two locations: slightly at ~2.5 kHz and more so at ~10kHz. It was found that the force and vibration signatures in the Z-direction were most effective at identifying tool wear.

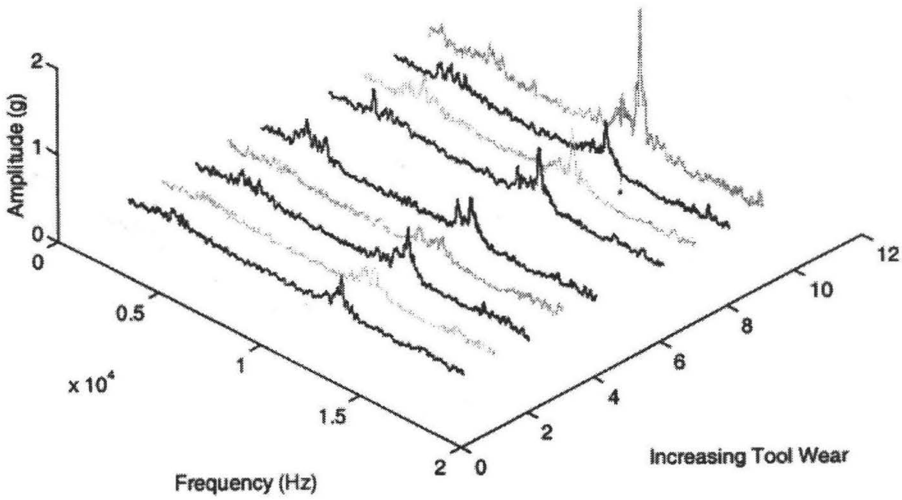

Figure 2.4: Vibration spectra showing an increase in vibrations with tool wear (Dimla & Lister, 2000)

Furthermore, it has also been noted that acceleration based sensors do not need to be mounted close to the tool/workpiece in order to capture important information in the process. Also, they are suitable for use in the rough environments of machining (Inasaki & Tönshoff, 2001).

2.2.5 Acoustic Emissions (AE)

Regarded as one of the most popular methods for monitoring tool wear and breakage, AE sensors suffer from the drawback that they must typically be placed close to the tool/workpiece interface. In an industrial setting with frequent tool changes it is not always practical or possible to use AE signals in assessing tool condition or surface quality (Inasaki & Tönshoff, 2001). Still, many studies have used AE signals for tool condition monitoring (e.g. Byrne *et al*, 1995; Inasaki & Tönshoff, 2001) and surface quality (e.g. Azouzi & Guillot, 1996; Axinte *et al*, 2004; Huessin, 2007).

2.2.6 Current

Another method of assessing the state of the machine tool during cutting is through the measurement of cutting power. With most machine tools using three-phase AC motors for spindle drives, the measurement of the current is a direct measurement of power consumption during cutting. Hall-effect style current transducers are often desirable because of their ease of installation. Either toroidal sensors or split-ring clamp style sensors, where the current-carrying wire passes through the sensor, are commonly used. One of the benefits of this sensor over an inline device is that the original connections to the controller are used. Another benefit of using current sensors is they are often placed in the back of the machine and away from the workspace preventing them from interfering with the process. Li *et al.* (2003) reported using Hall-effect sensors to monitor spindle current for the diagnosis of a tapping process while monitoring spindle with a 93% success rate in differentiating between five different process conditions. While, used for a tapping process it was suggested that the presented approach is generic and can be used for any process that can be "characterized using motor current signals." Hussein (2007) used spindle current signals from Hall-effect sensors in the multivariate sensor fusion for the prediction of surface quality in milling.

Previously mentioned in section 2.2.2, the use of Hall-effect sensors for current signal measurements from feed motors was performed by Jeong & Cho (2002) for the indirect measurement of forces in milling.

2.3 Machine Process Monitoring

There has been much research conducted on the monitoring and control of various machining processes. The motivation behind this research is explained by Liang *et al.* when they describe the main idea being to improve product quality and reduce manufacturing costs, and go on to define process monitoring as "the measurement and estimation of process variables" (Liang, Hecker, & Landers, 2004). The process monitoring of machining, however, can be very complex; often requiring the use of intensive data preprocessing to extract the important information contained within the signals. Monitoring a machining process includes the measurement of various process variables including forces, vibrations, acoustics and temperatures on and around the machine. In general, machine process monitoring can be used for two main purposes: using process variables to predict various part quality output parameters and error compensation. The interesting thing to note here is that regardless of the method of monitoring, the overall goal is to improve or maintain quality in some capacity. This section briefly discusses various techniques of machine process monitoring found in the literature regarding all of the aforementioned process variable measurements and quality measurements. All of the reviewed articles use some kind of modeling technique with the bulk of them using artificial neural networks in some capacity.

Azouzi and Guillot (1996) used an artificial neural network (ANN) for predicting the surface finish and dimensional deviation in a turning operation using sensor fusion techniques. They illustrate how sensor fusion can be used to create a model for the estimation of desired quality parameters. In their experiments, they measured forces, vibrations, acoustic emissions and the speed/feed deviations. The goal here was to model various cutting parameters (feeds, speeds, depths of cut) and process parameters (cutting fluid variation, part diameter, tool wear, material properties). Combinations of tests were designed using orthogonal arrays and each set of tests was performed multiple times to build the sensor fusion model. After the model was built using the training set data, a data set used to check the model was used with cutting parameters that varied slightly from those in the training set. Furthermore, signal conditioning was performed such that the data was taking during steady state cutting only and is shown in Figure 2.5.

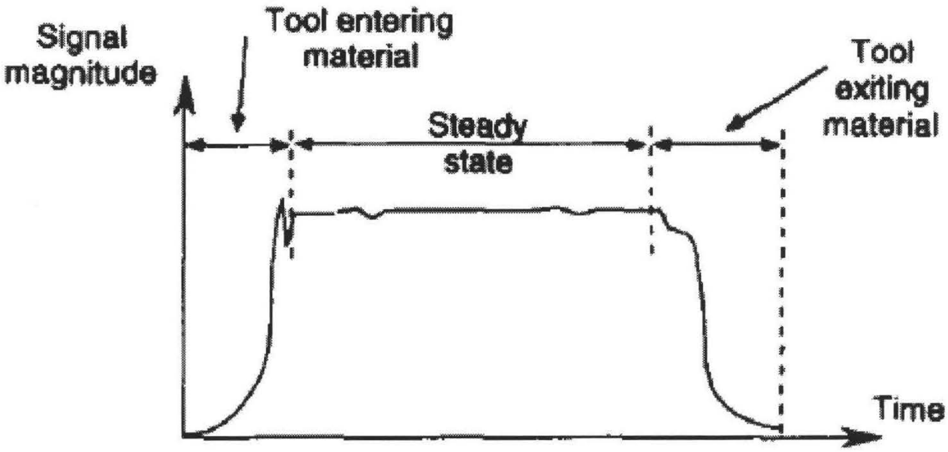

Figure 2.5: Signal conditioning for cutting tests (Azouzi & Guillot, 1996).

A multilayered feed-forward neural network was used for building a model to relate process data to quality data. A total of thirty models were designed using different combinations of sensors as inputs and neural network architectures. In the end, the model that gave the best performance (lowest total squared error from both quality parameters) consisted of feed, depth of cut, radial force and feed force to predict the dimensional deviation and surface finish (a.k.a 4x3x2 neural network). The surface finish was predicted with an error ranging from 2 to 25% with dimensional deviations were predicted with an average error of 6μm. An interesting feature of these models is the use of the known process parameters such as feed and speed. Including this type of data in a set of experiments is useful only when these parameters are changing, as in the tests performed. In the case of a high volume manufacturing, however, these parameters are often static.

Chen, Yuan and Ni (1996) developed a real-time compensation strategy for modeling thermal errors in machine tools. In this study, they used two different types of modeling techniques: multiple regression analysis (MRA) and ANN's. It should be noted that a discussion of the theory and methods behind additional modeling techniques are beyond the scope of this report and are left to the reader for future investigation. Eight thermocouples were placed about the machine in various locations with an additional thermocouple measuring the ambient "environmental" temperature. Thermal drift of the spindle in all three directions (x, y, and z) was measured at various speeds ranging from 600 – 2,600 RPM. Both methods provided models with good fits and an example of this is shown in Figure 2.6. As machine shops can be very noisy environments, a 0.4°C noise level was added to simulate this effect and Figure 2.7 shows how well both models are able to predict the thermal drift with the noisy data.

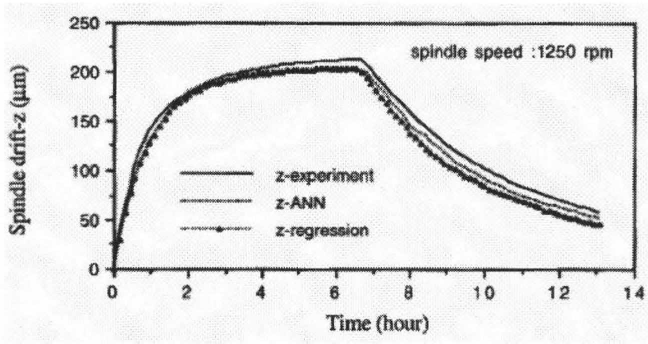

Figure 2.6: Spindle drift in z-axis – models vs. experimentally acquired data (Chen, Yuan, & Ni, 1996).

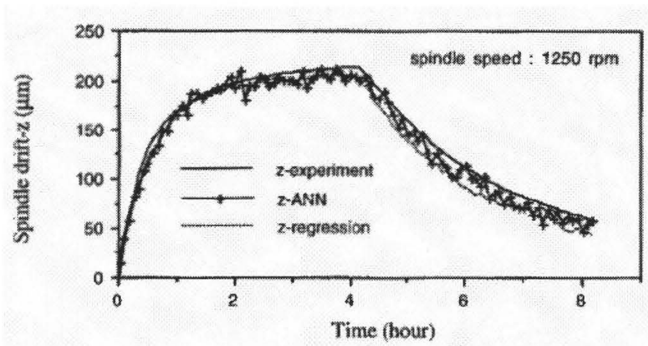

Figure 2.7: Prediction of spindle drift with 0.4°C noise (Chen, Yuan, & Ni, 1996).

The techniques used in this study were implemented on a 3-axis machine and reported a reduction in y-axis and z-axis errors from 92.4µm to 7.2µm and 196µm to 8µm, respectively.

Process monitoring for machine tools has also been applied to the monitoring of tool condition. Chen and Jen (2000) investigated a data fusion method using neural networks for the assessment of tool condition during milling. In this investigation, a data fusion model was created using signals from a dynamometer, placed under the machine table, and an accelerometer, placed on the spindle shaft. A combination of four feed rates, ranging from 28 - 70mm/min, and four spindle speeds, ranging from 900-1,800 RPM, was used totaling 16 different tests. Since cutting was performed in the x-y plane, the z-axis was ignored and signals from the x and y directions of the dynamometer were used with the accelerometer signal. For signal preprocessing the average value, variance in amplitude, and local fluctuation in frequency were all computed and combined into various data fusion combinations. Furthermore, the tool condition, for which the models were trained, was categorized into four groups ranging from light wear to tool breakage. In the end, the data fusion ANN model that provided the best results come from the use of a five layer ANN which used the “Index Multiplication Group” data fusion type. Data from each signal were combined via multiplication from each preprocessing type yielding three fusion indices. This model yielded an overall error of 1.35% with a standard deviation of the measurements of 0.015% in the prediction of tool wear.

Another example of machine process monitoring was done by Mathews and Shunmugam (1999) where they used neural networks for prediction of hole quality in reaming. In this study, they acquired acoustic emission (AE), forces and vibration signals and trained their ANN to predict surface finish (including roughness average, R_a, and residual stresses) and roundness error of the holes. Here acoustic signals are categorized as two different types; continuous type caused by plastic deformation during and burst type caused by fractures in the material. Mathews and Shunmugam (1999) also used sensor fusion claiming its ability to “improve the performance and reliability of manufacturing process monitoring” due to “insufficient sensitivity of a sensor to a specific phenomenon of interest.” ANN Models were built using each signal type individually and then with the signals combined in a sensor-fused model. In all tests, the multisensor (or fused) data created more accurate models than in the single sensor models, further illustrating the power of using multisensory data for machine process monitoring.

Veldhuis and Elbestawi (1995) proposed a strategy for the compensation of thermal errors in five-axis machining. This study used ANN's to model the non-linear behavior of the machine. In addition, a kinematic model of the machine was developed and simulation data from this model was used to train the ANN. Another interesting feature of this work was the strategy for determining the optimal number of thermocouples placed on a machine for model accuracy. Basically, an excessive amount of thermocouples were installed on the machine and a model was built using these inputs and then they were removed from the model. If removing the input did not significantly affect the model performance that it was deemed unnecessary. Overall, the error in the z-axis was reduced from 0.060mm to 0.020mm and the angular error in the x-axis rotation direction was reduced from 0.008° to 0.002°. Furthermore, the ANN was shown to provide reliable results when tested against actual cutting conditions.

Ramesh *et al.* (2003) noted, in their discussion of thermal error measurement and modeling in machine tools, how "commercially viable system capable of providing an effective solution to the needs of a production-class machine tool is still to be realized" and attempted to develop a thermal error compensation system which can be implemented in a production machine. An interesting finding in this study was that a simple mapping of measured temperatures to thermal errors did not give an accurate model when different machining conditions were used. An example of this is shown in Figure 2.8 as temperatures on the X-ballscrew nut were measured under four different machining conditions where the variation in the X direction changes quite differently under the 4 conditions.

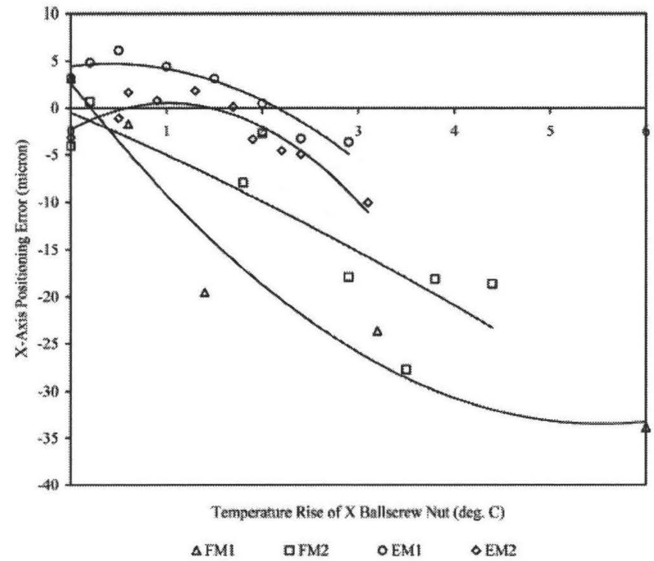

Figure 2.8: Differences in X-axis positioning error caused by thermal effects under various machining conditions (Ramesh, Mannan, & Poo, 2003).

While there has been much research on this topic, a review article addressing monitoring of tool wear using artificial neural networks over the past decade (Sick, 2002) discusses how and why "the development of tool wear monitoring systems is an on-going attempt." Sick describes the usage of ANN's and fuzzy systems for modeling the non-linear dynamics within the machine tool. Some of the problems mentioned include the requirement of many training cycles, the restriction to specific trained cutting conditions and limiting the machine tool to operate within the trained performance range. In total

138 articles were reviewed for tool condition monitoring of turning and it was reported that the general consensus, regardless of all of the research, is there still remains little industrial implementation these methods.

Using multivariate techniques relevant to those used in the methods described in this thesis, Hussein (2007) presented some techniques using latent variable techniques of principal component analysis (PCA), projection to latent structures-discriminant analysis (PLS-DA) and projection to latent structures (PLS). Hussein's work had several objectives which included identifying work done by a particular machine via PLS-DA; predicting surface finish from tests performed on three different machines; using model inversion techniques to identify which machine would be best suited to obtain desired quality parameters; and, a case study using plant data from a manufacturing process from General Motors. Overall, the multivariate modeling techniques proved to be successful in accurately predicting surface finish and the model inversion was shown to be useful in the prediction of which machine would provide the best quality parameters with verification by experimental results. Hussein also provides a comparison to these modeling techniques with more traditionally used techniques like ANN's. It was found that while all modeling techniques provided reasonable fits to the data, it was noted for a process monitoring system, however, "there is a need for more than a good predicted value." Using the tools available with PCA and PLS (described later in this chapter), it is possible to gain insight into what is actually happening during the process via contribution plots and score plots, for example.

While researching machine process monitoring an interesting thing to note is that no tools were found that are capable of easily conveying the process information into simple control charts such as those described by (Nomikos & MacGregor, 1995) and (Kourti & MacGregor, Multivariate SPC Methods for Process Monitoring and Product Monitoring, 1996) that had been developed for chemical engineering applications, for example. While SPC methods have been developed for tracking quality; e.g. (Bering, 2003), (Automotive Industrial Action Group, 2005), all of these techniques which rely on tracking quality parameters only and altering the process based on what is observed in the final part quality. Again, it is important to note that the process monitoring techniques described here are for a very specific set of tasks, which limits the applicability of these techniques to industry. Furthermore, it was also found that few studies involved the use industrial case studies to validate their methods with practical applications.

2.4 Multivariate Data Analysis

In any type of statistical process control (SPC), the main idea is to keep the process within operating conditions that are statistically 'in control.' Traditionally in the manufacturing industry, quality parameters are measured and individually monitored using SPC charts like Shewhart, Exponentially Weighted Moving Average (EWMA), Cumulative Sum (CUSUM) and these types of charts are available in commercial software such as Mitutoyo's MeasurLink package. However, the monitoring of a few quality variables has been noted as being inadequate for the diagnosis of a process

(Kourti & MacGregor, 1995). Using Hotelling's T^2 and squared prediction error control charts (as described in section 2.4.3), it is possible to monitor all of the measured process and quality variables at once, as opposed to individually as is done by the, previously mentioned, traditional control charts. As processes become complex with many different variables affecting the outcome of a process, it becomes difficult to assess the state of the process using traditional univariate techniques. Figure 2.9 illustrates the case where two arbitrary parameters, $y1$ and $y2$, are shown to be individually in-control; but when multivariate analysis techniques are applied, an observation can be shown to be out-of-control when the analyzed together. Multivariate analysis takes this lower dimensional example further by explaining what is happening in a process with 10-20 variables, for example, in as few as only 2-3 latent variables. In the case of machining, the process variables can include information from vibrations, forces, temperatures, etc. When looking at many variables there are often a few underlying effects causing a process to move a certain way (called multicollinearity) and multivariate data analysis is the only way to look at all the data simultaneously (Eriksson *et al.,* 2001). As previously described, there are many different types of measurements in machining and the most common method of analysis has been ANN's.

The methods of multivariate data analysis described here include principal component analysis (PCA) and partial least squares or projection to latent structures (PLS). PCA is the method of determining the underlying structure of multivariable data of process data only (**X**). PLS is the method of projecting the process data (**X**) onto the quality data (**Y**) in order to determine the covariance between the two data structures.

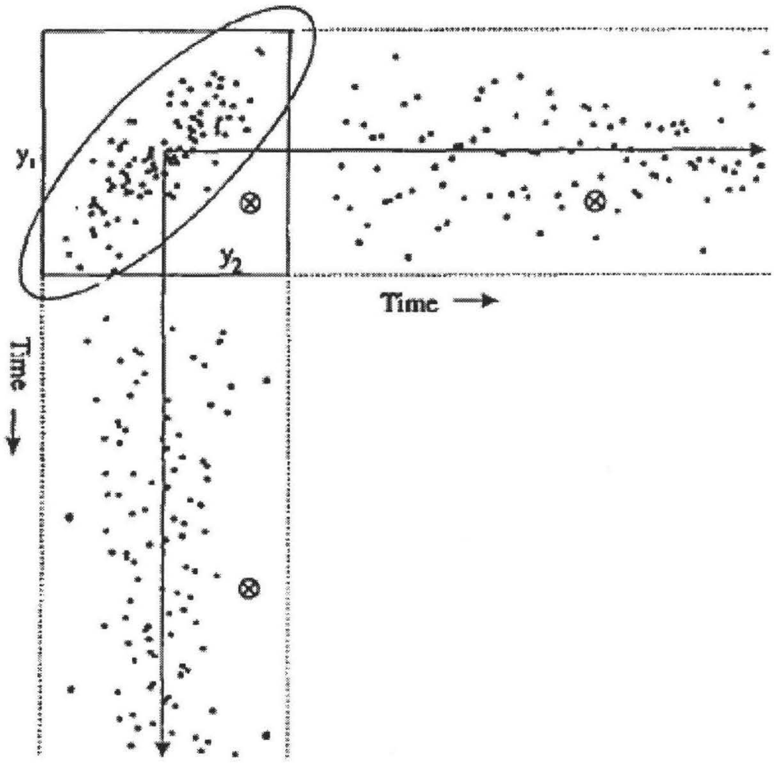

Figure 2.9: Illustration of how univariate style control charts can be misleading. Note how *y1* and *y2* are both in control, but together they lead to a data point outside of acceptable quality (Kourti & MacGregor, 1995).

2.4.1 Principal Component Analysis (PCA)

When working with data sets containing large amounts of variables, a common practice for reducing the dimensionality of the system is by way of using PCA (Jackson, 1991; Kourti & MacGregor, 1995; Eriksson *et al*, 2001).

In a data set, the first principal component (PC) can be found by identifying the direction with the most variance in a multidimensional space. The second principal component is the direction with the second most variance, and so on (see Figure 2.10). This method can be described mathematically as follows (Kourti & MacGregor, 1995):

- The first principal component, t_1, of dataset X is a linear combination such that:

$$t_1 = Xp_1 \tag{2.1}$$

which has the maximum variance with $|p_1| = 1$.

- The second component, t_2, of X is defined similarly as:

$$t_2 = Xp_2 \tag{2.2}$$

where t_2 is orthogonal to t_1 and is also subject to $|p_2| = 1$.

- This method continues as follows and can be summarized with:

$$X = \sum_{i=1}^{A} t_i p_i^T + E \tag{2.3}$$

where X is the matrix of process data with columns representing process variables and the rows are the observations, A is the number of PC's computed and E is the residual matrix.

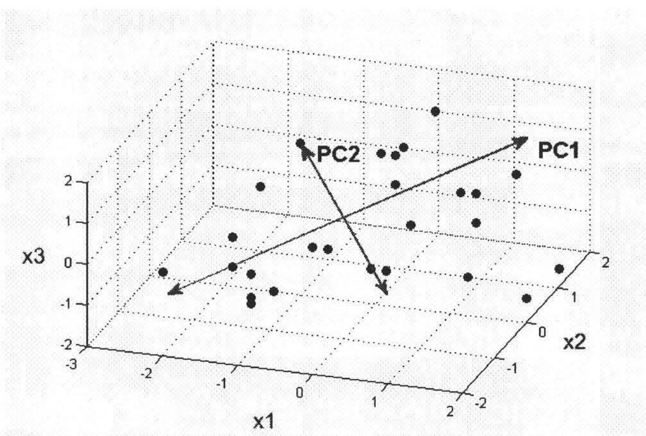

Figure 2.10: The geometric interpretation of PCA on three arbitrary process variables illustrating the first two principal components (adapted from Kresta, J.V. *et al*, 1991; Eriksson *et al*, 2001).

It should be noted that **X** consists of *N* observations and *K* variables (*N*x*K*) and the corresponding score (*t*) and loading (*p*) vectors are of *N*x*A* and *K*x*A* dimensions, respectively.

One of the methods for computing the PC's is known as the NIPALS algorithm (*N*on-linear *I*terative *PA*rtial *L*east *S*quares). This algorithm, given in chapter 2.4.1.1, is ideal since it iteratively computes each PC, and typically only 2 or 3 components are needed to efficiently describe the variation in a process (Kourti & MacGregor, 1995). Principal component models are generally trained on historical reference data that contains information from successful process conditions so that new observations can be compared to what has been identified as 'in-control' (Kourti & MacGregor, 1995; Nomikos & MacGregor, 1995). These historical data bases often contain missing information and so the NIPALS algorithm has been widely accepted by commercial software (e.g. SIMCA-P) due to its ability to handle missing data (Grunge & Manne, 1998).

2.4.1.1 PCA NIPALS Algorithm

Before using PCA some data preprocessing needs to be performed. Since a wide variety of values from different types of measurements are being used, it is necessary to scale all of the data by its standard deviation and mean center the data (Kourti & MacGregor, 1995; Eriksson *et al*, 2001). In a comparison of several different expanded methods of PCA and PLS, Westerhuis, Kourti & MacGregor (1998) present the NIPALS algorithm used for PCA:

1. Select a column of X as the first PC score vector, t
2. Loading vector: $p=X^Tt/(t^Tt)$
3. Normalize the loading vector: $p=p/|p|$
4. Score vector: $t=Xp/(p^Tp)$
5. Check t for convergence:
    a. If t has converged, move on to step 6
    b. If t has not converged, go back to step 2
6. Compute residual matrix $E = X - tp^T$
7. Go to step 1, and repeat with $X=E$, to extract the next PC if desired.

Finally, a graphical representation of the NIPALS algorithm is presented in Figure 2.11.

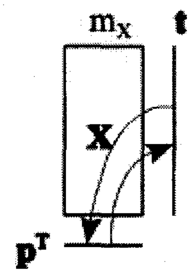

Figure 2.11: Graphical illustration of PCA NIPALS algorithm (Westerhuis, Kourti, & MacGregor, 1998).

2.4.1.2 Predictions Using PCA

With a model built using the NIPALS algorithm, with A principal components, on process data (the **X** matrix) where the t-scores and p-loading vectors are computed, the loading vectors can be used to compute the new t-scores on newly acquired process data. For a matrix of new observations, X_{new}, having the same number of columns the matrix for which the model was built, the new scores, t_{new}, can be computed as:

$$t_{new} = X_{new}p \tag{2.4}$$

With the new scores computed, the predictions of the new observations can be computed as:

$$\hat{X}_{new} = t_{new} p^T \tag{2.5}$$

where $\hat{X}$ represents the predicted data points. The predicted data becomes useful when computing the squared prediction error for multivariate control charts in chapter 2.4.3.

2.4.2 Partial Least Squares (PLS)

When only process variable data or product quality data is available one must use PCA. But, when measurements are also made on both it is possible to use PLS to relate the process data (**X**) to the quality data (**Y**). Using contribution plots, as described in 2.4.3.3, it then becomes possible to identify which process variable was the cause of an undesirable product (Kourti & MacGregor, 1995).

2.4.2.1 PLS NIPALS Algorithm

The NIPALS algorithm for PLS is very similar to the one presented for PCA. As done with PCA, before entering the algorithm, values in both **X** and **Y** data matrices are scaled to unit variance and mean centered to bring the data to the same level. As mentioned in 2.4.1.1, Westerhuis, Kourti & MacGregor (1998) present the NIPALS algorithm used for PLS:

1. Select column of Y to be the first score vector, u
2. X weighting vector: $w=X^Tu/(u^Tu)$
3. Normalize weighting vector: $w=w/|w|$
4. Score vector: $t=Xw/(w^Tw)$
5. Y weighting vector: $q=Y^Tt/(t^Tt)$
6. Y score vector: $u=Yq$
7. Check t for convergence:
    a. If t has converged, move on to step 8
    b. If t has not converged, go to step 2
8. X loading vector: $p=X^Tt/(t^Tt)$
9. Compute residual matrices: $E = X - tp^T$
   $F = Y - tq^T$
10. Go to step 1, and repeat with $X=E$ and $Y=F$, to extract the next component if desired.

A graphical representation of the PLS NIPALS algorithm, similar to that for PCA in Figure 2.11, is presented in Figure 2.12.

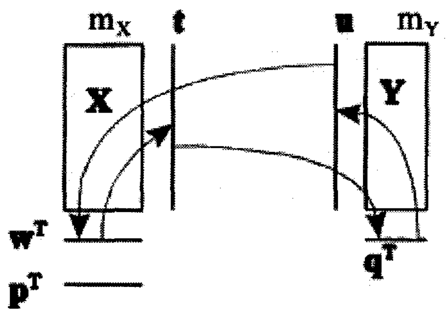

Figure 2.12: Graphical illustration of PLS NIPALS algorithm (Westerhuis, Kourti, & MacGregor, 1998).

2.4.2.2 Predictions Using PLS

With a PLS model, created via the NIPALS algorithm having A principal components, it can be very useful to predict the outcome of the process (**Y**), whether it be quality information or any other quantity (for example, thermal drift in the Z-axis in the case of machine tools), from the process data (**X**). With a model built with training data, it can then be possible to describe the model as a regression model as (Eriksson *et al*, 2001):

$$Y = XB + F \tag{2.6}$$

Where Y is the matrix of response variables (or quality variables) X is the matrix of predictor variables (or process variables), B is the vector of PLS regression coefficients, and F is the residual (or error) matrix. The vector, B, of PLS regression coefficients is computed by:

$$B = w(p^T w)^{-1} q^T \tag{2.7}$$

where w is the matrix of weights describing the correlation between X and the u-scores, p is the matrix of loadings on the X matrix, and q is the matrix of weights that explain the correlation between Y and the t-scores, as illustrated in section 2.4.2.1.

With the regression coefficients, B, are computed and based on the training data, predictions of the quality variables from new process conditions can be simply performed by the following calculation:

$$\hat{Y}_{new} = X_{new} B \tag{2.8}$$

where $\hat{Y}$ is the matrix of predictions on the new observations, X_{new}. In the case of machining, for example, these predictions could be used for thermal error compensation.

2.4.3 Multivariate Control Charts

There has been much research in the development of control charts for assessing the state of a multivariable process (Kourti & MacGregor, 1995; MacGregor & Kourti, 1995; Nomikos & MacGregor, 1995; Kourti & MacGregor, 1996). These control charts not only provide a tool for determining if a process has gone 'out of control,' but they also provide some tools for diagnosing the process. Two of the control charts that are to be discussed here are the Hotelling's T^2 (T2) and Squared Prediction Error (SPE) charts. The T2 control chart is one that is specifically applicable to the monitoring of a machining process because it is noted in the Statistical Process Control guide for automotive SPC by the Automotive Industrial Action Group (2005) as an acceptable control chart. The T2 control chart, however, is noted as not being sufficient for monitoring the process since it is only capable of detecting variation in the plane of the PC's if it is greater than what can be explained by noise or 'common cause.' If a new event is occurring then the observation will tend to move off the plane (or hyperplane) and these events can be detected by SPE (Kresta, MacGregor, & Marlin, 1991). Furthermore, contribution plots provide a method of diagnosing 'out-of-control' observations.

2.4.3.1 Hotelling's T^2 Statistic

Hotelling's T^2 statistic for the i^{th} observation from a model using A components is computed using equation (2.9):

$$T_i^2 = \sum_{a=1}^{A} \frac{t_{ia}^2}{s_{ta}^2} \tag{2.9}$$

where t is the score of the i^{th} observation from the a^{th} principal component and s^2 is the variance of the t-scores from the a^{th} principal component (Eriksson, Johansson, Kettaneh-Wold, & Wold, 2001; Kourti & MacGregor, 1995).

Since the T2 statistic is directly related to the F-distribution, the upper control limit (UCL) for these control limits is given equation (2.10) as:

$$T_{UCL}^2 = \frac{A(N^2-1)}{N(N-A)} F_\alpha(A, N-A) \tag{2.10}$$

where A is the number of components, N is the number of observations and α is the level of significance for the F-distribution with A and N-A degrees of freedom (Jackson, 1991; Eriksson, Johansson, Kettaneh-Wold, & Wold, 2001; Kourti & MacGregor, 1995).

2.4.3.2 Squared Prediction Error

Also known as the Q-statistic (Jackson, 1991) or DModX (*D*istance to the *M*odel *X*, (Eriksson, Johansson, Kettaneh-Wold, & Wold, 2001)), SPE is used as a complementary control chart to the T2 control chart. The SPE is often used in the Y space (Kourti & MacGregor, 1995) but can also be used on process data from the X space (MacGregor & Kourti, 1995). SPE for a new observation can be computed using equation (2.11):

$$SPE_x = \sum_{i=1}^{M} (x_{new,i} - \hat{x}_{new,i})^2 \tag{2.11}$$

Where M is the number of process variables (or quality variables for SPE_y) and $\hat{X}$ is the predicted observation. The upper control limit for this is computed according to Jackson and Mudholkar (1979) and has been used successfully in multiple studies (Kourti & MacGregor, 1995). To compute the UCL let:

$$\begin{aligned} \theta_1 &= \sum_{i=A+1}^{K} l_i \\ \theta_2 &= \sum_{i=A+1}^{K} l_i^2 \\ \theta_3 &= \sum_{i=A+1}^{K} l_i^3 \end{aligned} \tag{2.12}$$

Where l is the vector of eigenvalues which form the sample covariance matrix of the data matrix X with K variables and A is the number of components in the model. Then, let:

$$h_0 = 1 - \frac{2\theta_1\theta_3}{3\theta_2^2} \tag{2.13}$$

and the UCL for the SPE can be computed using:

$$SPE_{UCL} = \theta_1 \left[\frac{c_\alpha \sqrt{2\theta_2 h_0^2}}{\theta_1} + \frac{\theta_2 h_0 (h_0 - 1)}{\theta_1^2} + 1 \right]^{1/h_0} \tag{2.14}$$

Where the c_α is the value of from the Normal distribution "cutting off the area of α under the upper tail of the distribution if h_0 is positive and under the lower tail if h_0 is negative (Jackson, 1991)."

2.4.3.3 Contribution Plots

One of the powerful tools for diagnosing a multivariable process is through the use of variable contribution plots. When trying to find the cause of an 'out-of-control' observation, contribution plots sum up the weighting of each variable in a simple bar-chart to show which variables caused the observation to go awry. Methods for finding the contribution are described by Kourti and MacGregor (1996) and in (Yoon & MacGregor, 2001). The contribution of the i^{th} variable in X to the large value of the j^{th} t-score of the a^{th} principal component is given by:

$$cont_{a,i} = \frac{t_{a,j}}{s_a^2} p_{a,i} \left(x_i - \mu_i \right) \tag{2.15}$$

where μ is the mean and s^2 is the variance of the t-scores of component a. It should be noted that if the data is mean centered than μ is simply zero. In order to find the total contribution of the variable in the model across A principal components, all which is required is to simply sum equation (2.15) across all components in the model. This is given by:

$$CONT_i = \sum_{a=1}^{A} (cont_{a,i}) \tag{2.16}$$

A graphical illustration of how contribution plots can be used to diagnose an 'out-of-control' observation from a process is shown in Figure 2.13.

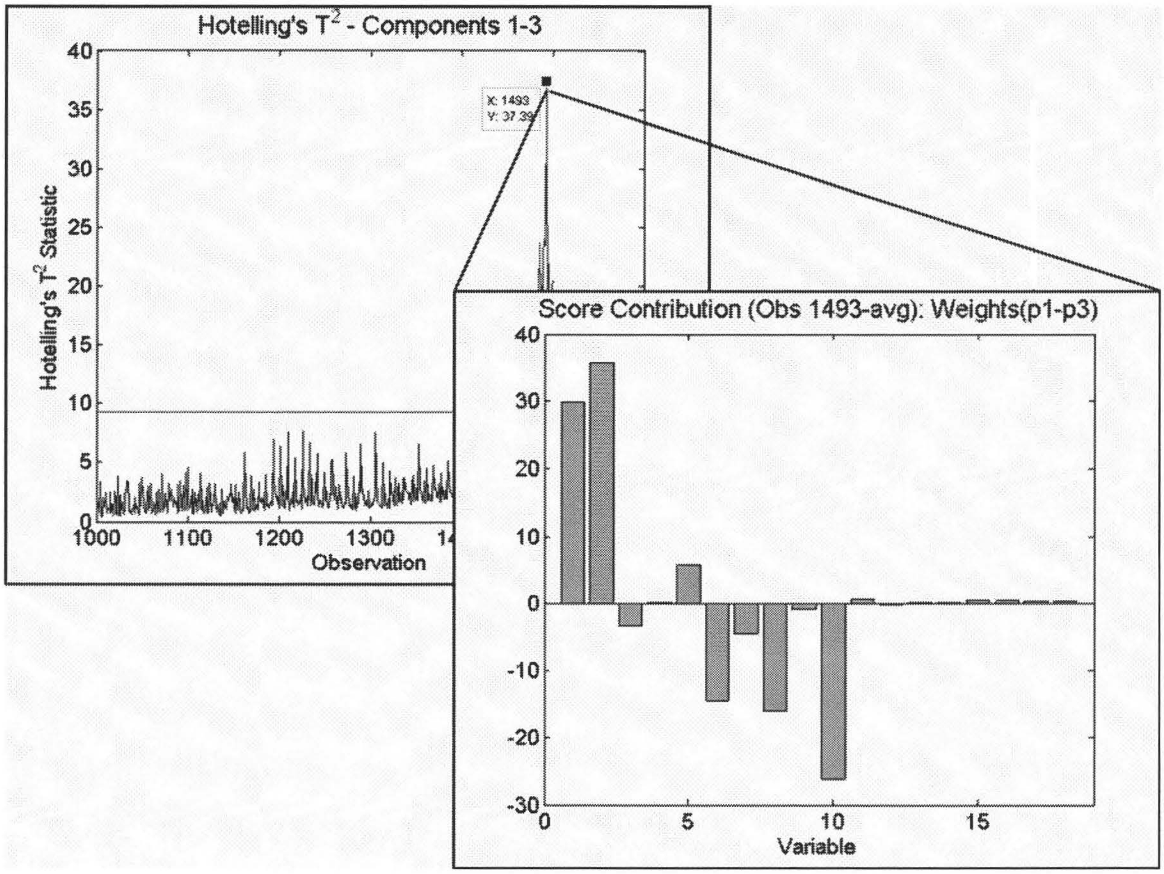

Figure 2.13: Contribution plot illustration for 'out of control' observation #1493 as detected by the Hotelling's T2 control chart.

2.5 Summary

Presented in this literature review are various works that illustrate techniques for process monitoring. With any type of monitoring system, sensor selection is crucial to capturing the features of the process that can help indicate when something might have gone 'out-of-control.' Due to the fact that table force dynamometers or tool shank mounted dynamometers are difficult to implement in practice (due to fixturing and tool changes) a review was performed on alternatives to measuring forces during cutting. From this review, current sensors and accelerometers are noted as being indirect indicators of forces during cutting. Using the data analysis tools (e.g. PCA, PLS), however, it is not necessary to initially model the forces because the data is mean centered and scaled to unit variance before analysis. Furthermore, review on thermal measurements and modeling on machine tools was performed so that the thermal errors can be monitored. Finally, control charts based on Hotelling's T^2 statistic and Squared Prediction Error of the multivariate models have been shown to be powerful tools in the diagnosis of a process in many chemical engineering applications and are to be implemented for process monitoring of machining.

Chapter 3 – Experimental Methods

One of the main goals of this work was to work through the issues associated with a practical implementation of a multivariate approach in an industrial environment. All of the experimental setup and work described was performed at Nixon Integrated Machining Designs Ltd. (Nixon), located in Burlington, Ontario. Because of the industrial implementation, all of the sensor selection was done on the basis that it needed to be seamlessly integrated into their current machining process with no interference to normal operation; with the final goal being the implementation of a fully functional process monitoring system.

3.1 Description of Process

The machining process used for the manufacturing of "widgets" is relatively simple consisting of two features that are machined: a bore and a boss. The machine used is a Daewoo DMV-400 vertical machining center with a rotary table. The rotary table system, with two fixture tables, enables the operator to inspect and load new parts during a machining cycle with each table holding 8 parts. Since there are two features that are machined, one tool machines the bore feature (boring tool) and one tool machines the boss feature (boss tool). The parts are machined in the order shown in Figure 3.1 and is repeated after a tool change to machine the second feature. To save time in a machining cycle there is only one tool change per cycle and each cycle starts with the opposite tool. This means that it is necessary to know which tool is being used in order to properly preprocess data for analysis.

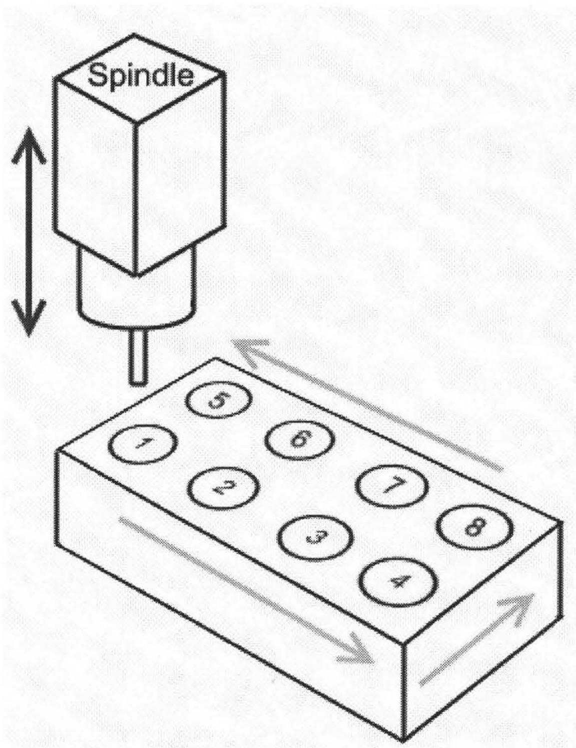

Figure 3.1: Illustration of machining cycle.

For the machining of the widgets, the bore tool was operated at 7,000 RPM and the boss tool was operated at 5,000 RPM. The boring tool also has another single tooth at its base so that when it plunges through the bore it also faces the surface around the bore.

Figure 3.2 shows a generic dimensionless sketch of the part to illustrate the machined features.

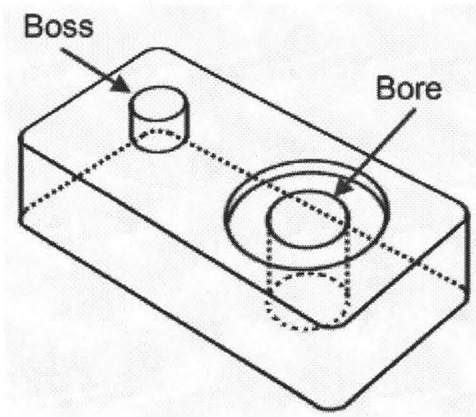

Figure 3.2: Sketch of part to illustrate machined features.

3.2 Machine Thermal Expansion Modeling

It is well known that machine error is induced by a change in temperature during a machining operation and there has been much research into the compensation of these types of errors (Ramesh, Mannan, & Poo, 2000a). Of the two features that are machined on the part shown in Figure 3.2, the dimension of most concern was in the Z-direction. In order to model the expansion of the Z-axis, first an initial test was carried out to observe the behaviour of this system. One of the goals of the initial test was to measure the temperatures until a maximum expansion was captured. If a model with reasonable fit and predictive ability could be created with the data from this initial test then it would be possible to model the system during production. It was important to try to capture the behaviour of the system during production since there were other factors that can contribute to the thermal expansion; for example, during cutting the load can increase on both the spindle motor and the axis motor which will affect the thermal profile of the machine (Ramesh, Mannan, & Poo, 2003). For this reason, experiments were later carried out during production in an attempt to model the thermal behaviour of the machine. It should be noted that sensor noise was expected during the production experiments due to the fact that only one surface of the cast part was machined.

3.2.1 Initial Measurement of Z-Axis Expansion

The initial measurement was carried out in a similar method as performed by Statham, Martin, & Blackshaw (1997). In this experiment proximity sensors are placed in a fixture that was designed to hold them in the directions of the X, Y, and Z axes. This method of measuring thermal distortion only considering the case where it is caused by spindle rotation and does not take into account other factors causing thermal distortion of the part during machining. This experimental work follows standards described in ASME B5.54-2005 and ISO 230-3. While the ASME standard has this experimental method in the section describing methods for measuring tilt error motion, the main sensor of interest was the one in the Z-direction. The experimental set up is illustrated in Figure 3.3.

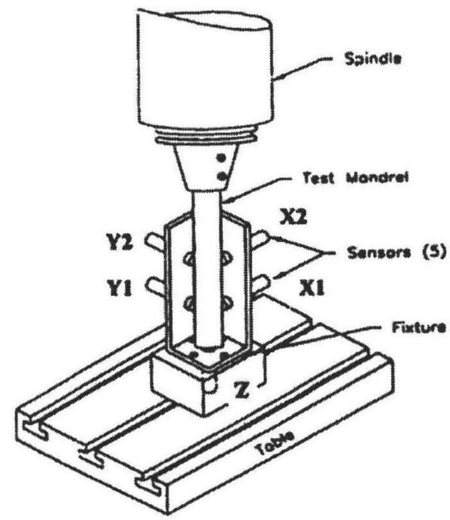

Figure 3.3: Sensor fixture design for measuring thermal distortion and expansions (The American Society of Mechanical Engineers, 2005).

At the time of performing this experiment, only three sensors were used, one for Z and two for the X and Y directions. In this case only the Z axis direction was considered as it was the direction with the tightest tolerance and was consistently measured by the operators and the CMM.

3.2.1.1 Sensors and Equipment

For this experiment, E-type thermocouples manufactured by Omega were used to measure the surface temperatures around the spindle. These thermocouples were chosen as per the literature review in section 2.2.3. While the temperatures to be measured during machining do not come near to the extremes of the temperature that the thermocouple is capable of measuring (-200°C to 900°C), Figure 3.4 from OMEGA, shows that the E-type thermocouples are the most sensitive of the common types of thermocouples. This type of thermocouple uses a Nickel-Chromium vs. Copper-Nickel junction. Furthermore, the error limits for these thermocouples are listed as 1.7°C or 0.5% (whichever is greater) above 0°C.

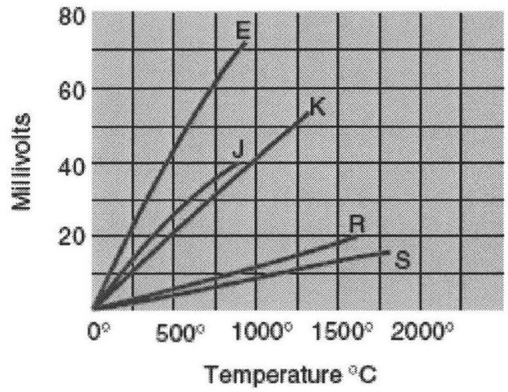

Type	Metals + –
E	Chromel vs. Constantan
J	Iron vs. Constantan
K	Chromel vs. Alumel
R	Platinum vs. Platinum 13% Rhodium
S	Platinum vs. Platinum 10% Rhodium
T	Copper vs. Constantan

Figure 3.4: Millivolts vs. Temperature for various types of thermocouples (OMEGA).

While the ASME standard for measuring effects due to environmental temperature variation lists only one spindle surface temperature measurement and one ambient temperature measurement, four surface measurements were taken up the front of the spindle structure with one ambient temperature measurement. Figure 3.5 shows the placement of the thermocouples on the front of the spindle.

In order to measure the movement of the axes, Bently-Nevada 3300 series eddy-current type proximity sensors were used. These sensors are capable of measuring over a range of 80 mil (2mm) with a sensitivity of 200 mV/mil (7.87V/mm or 7.87mV/μm). It is also recommended that the proximity sensor be placed 50 mil (1.27mm) away from the target at the start to ensure the change can be measured in either direction. The output voltage of the proximity sensors ranges from -1V to -17V. Furthermore, the sensors were placed at least 43mm from each other to ensure there was no cross-talk between the sensors, as suggested by the data sheet. The experimental setup using the proximity sensors and the fixture to hold them from Figure 3.3 is shown in Figure 3.6. Since the datasheet states that the sensors are calibrated with an AISI 4140 steel target, the sensors were recalibrated using an external dial indicator with 10.62 V/mm, 9.96V/mm and 11.20 V/mm for the X, Y, and Z sensors, respectively, for the stainless steel shaft target shown in Figure 3.6 .

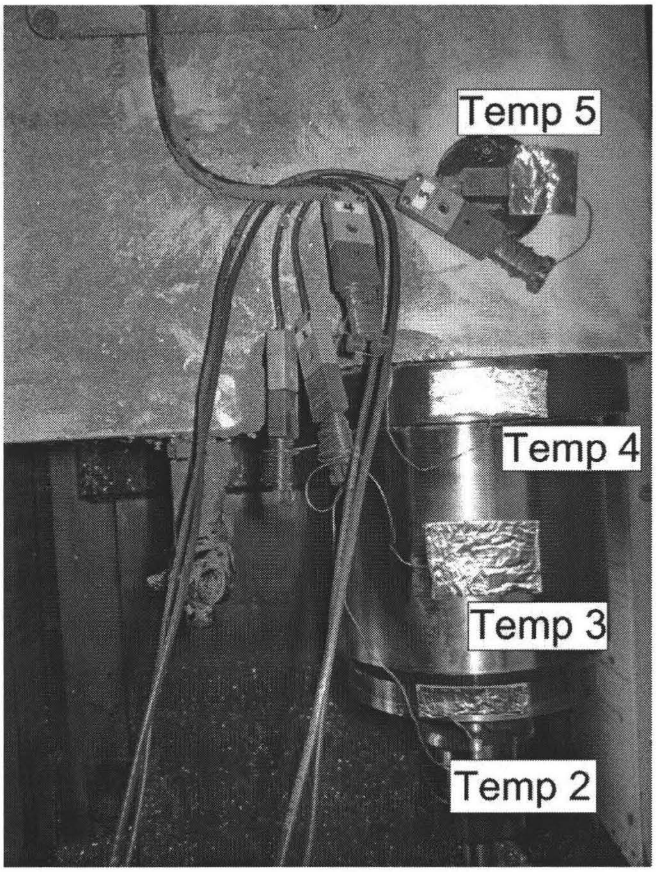

Figure 3.5: Placement of four thermocouples during initial thermal experiment.

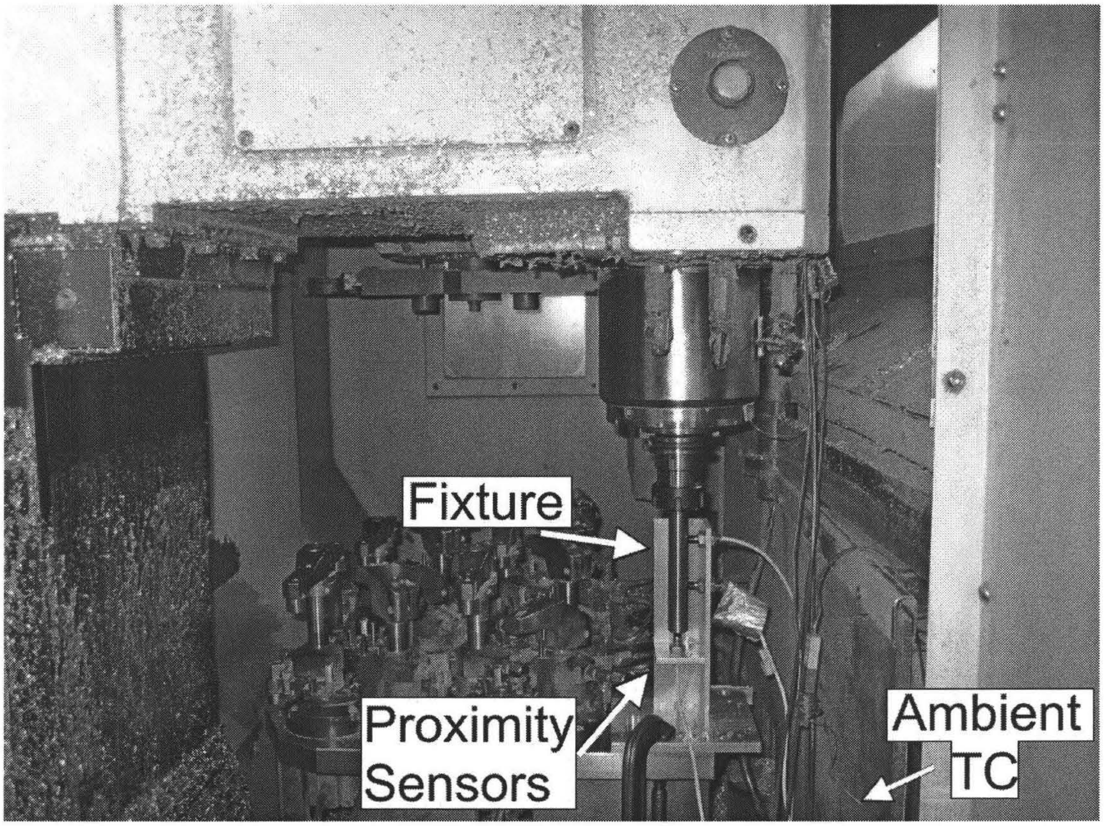

Figure 3.6: Measurement of z-axis movement carried out in similar fashion to Statham, Martin & Blackshaw, (1997) and ASME B5.54-2005.

The acquisition system consisted of a PC with two National Instruments (NI) PCI-6023E data acquisition (DAQ) cards. These DAQ cards are capable of measuring 16 analog inputs with a total sampling rate of 200kHz and 12-bit resolution across a ±10V range. One card was used for measuring the thermocouple inputs was connected to an SC-2345 connector block and one card was used for measuring the proximity sensor inputs which are connected to a BNC-2110 standard connector block using BNC cables. Since the input range of the card is ±10V but the sensor output range is -1V to -17V, the distance from the target to the sensor was set to fall within a range of -1V to -10V. To convert the voltage signals from the thermocouples to temperatures, the thermocouples were connected to the SC-2345 connector block via a SCC-TC02 connector block modules. These thermocouple modules have built in cold-junction-compensation to accurately convert the thermocouple signals to temperatures. The method used to compute thermocouple signals using the NIST – ITS 90 standard polynomial coefficients and the cold-junction-sensor signal from the modules is illustrated in a Matlab code function that is presented in Appendix A.

Thermocouple and proximity sensor signals were acquired using the Data Acquisition toolbox in Matlab. The decision to use the Matlab as the acquisition software was made because it is compatible with NI hardware (including the PCI-6023E) and could thus be used later for programming an online monitoring system.

3.2.1.2 Experimental Conditions

The experimental conditions for this section were set simply to capture the maximum amount of thermal distortion using spindle speeds that are typically used during production. At the time of testing, the maximum spindle speed used during the machining was 7,000 RPM. While not typical of the machining cycle where the axes are moving and there are spindle starts and stops during tool changes, the spindle was set to run constantly at 7,000 RPM for 3 hours in an attempt to capture the maximum distortion while it was expected that the measured temperatures would level off over this period of operation.

The data for the proximity sensors was acquired at 10kHz for 1 second at 30 second intervals. The thermocouple data was acquired at 100 Hz for 1 second at 30 second intervals, for a total of 360 samples. While many samples were acquired, for the purpose of this analysis only the signal means across the 1 second sample were taken.

3.2.1.3 Analysis

Often before any in depth analysis is performed, PCA is performed on the data to ensure there is good correlation between all of the variables, both process and quality (Burnham, MacGregor, & Viveros, 1999). Demonstrating a good model fit using PCA ensures the data is coherent and has structure. In general, a model with a goodness of fit, R^2, and goodness of prediction, Q^2, greater than 0.5 is considered as acceptable. It should be noted that Q^2 cannot exceed R^2, as it is not possible to predict with better accuracy than the model is able to fit (Eriksson, Johansson, Kettaneh-Wold, & Wold, 2001).

The next step for analysis of the data is to use PLS to model the Z-axis proximity sensor measurements by the thermocouple temperature measurements. The rules and guidelines describing goodness of fit in PCA are also applicable to PLS analysis.

Analysis will initially be carried out using the commercial software package SIMCA-P+ v.11 (UMETRICS, 2005) for multivariate analysis.

3.2.2 Measurement of Z-axis Expansion During Production

While measurement of the Z-axis expansion during the test described in section 3.2.1 may be effective in determining the behaviour of a machine under certain conditions; however, the specific conditions involving only spindle rotation cannot be representative of the machine's performance during a production machining cycle involving changing spindle speeds, movement of the axes, etc. For this reason, an indirect method of measuring the change in the Z-axis position induced by thermal effects was required.

The main quality parameter of the two machined features of the part shown in Figure 3.2 was the height of those features as machined in the Z-direction. At the operator's station there was a custom gage with a dial indicator fixed on the unit so that the operator can check the heights of these features and manually adjust offsets in the controller to maintain this quality parameter within tolerance. Using this measurement it was possible to indirectly track the change in the in the Z-axis over time as the machine was being used throughout the day.

3.2.2.1 Sensor Locations and Operating Conditions

The placement of the thermocouples used in the previous section, while in accordance with some methods described in the ASME standard and using some additional thermocouples, does not account for some additional major heat sources. In past research, major sources of heat have been shown to include axis motors, spindles, ball screws, and guideways (Ramesh, Mannan, & Poo, 2003). A study by Lo *et al.* (1995) for the real-time error compensation (RTEC) on a turning center showed that the number of temperature sensors can be reduced from 80 to 16. In this case they used an optimization strategy which maintained the desired prediction accuracy using just a few temperature locations. It should also be noted that the thermal error of the machine tool was closely related to its operating conditions (Ramesh, Mannan, & Poo, 2003). While studies like Lo *et al.* (1995) optimize the number of thermocouples used after some empirical testing, the case where sensors need to be placed on a production machine within a limited time frame has resulted in the placement of thermocouples on some major heat sources. The placement of the thermocouples used in this research is summarized in Table 3.1 and their physical location is shown in Figure 3.7. It should also be noted that the DMV-400 machining center is outfitted with a third-party spindle chiller unit which attempts to remove heat from the spindle region. Since the SC-2345 is only capable of handling eight thermocouple inputs, only this many were used during the experiments and modeling. If the experimental work had shown inadequate modeling additional sensors would have been implemented.

As previously mentioned, the operator used a custom gage with a dial indicator to track the heights of the part for occasional offset updates. Typically, the operator would measure a part at the start of the shift then set the offsets to account for the cold-start state of the machine. Approximately an hour later another offset change would be made and another after lunch break. Assuming normal operation throughout the day, there would be anywhere from three to six offset changes in a day, depending on the operator. This "human-factor" was another reason for this work so that a real-time thermal error compensation system making adjustments at scheduled intervals could maintain quality that is within the specified tolerance. While the resolution of the machine was 0.001mm, offsets in the Z axis are only ever made with a resolution of 0.01mm due to the tolerance requirements of the parts as well as the repeatability of the machine and the repeatability of the castings. Furthermore, the resolution of the dial indicator on the gage is 0.01mm.

Table 3.1: List of thermocouples and locations

Thermocouple #	Description of location
1	Ambient – placed approximately mid-way through total Z-axis travel
2	Spindle – Front
3	Spindle Chiller Tubing
4	Spindle Motor - Base
5	Spindle Housing Structure/Z column – Near back of the machine adjacent to where the housing structure is connected to the Z-column guideways.
6	Z Motor – Base
7	X Motor – Base
8	Y Motor - Base

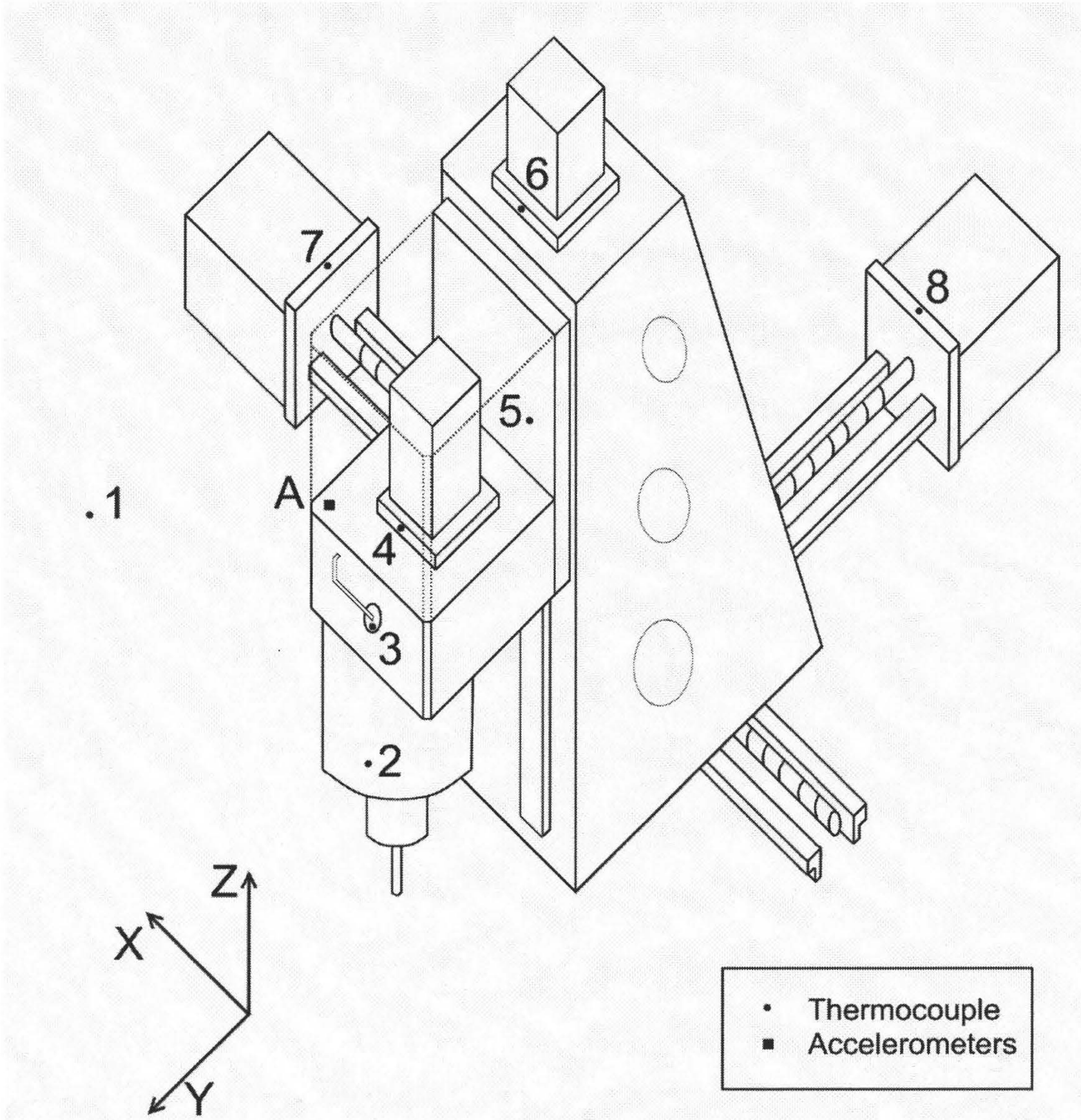

Figure 3.7: Thermocouple and accelerometer locations on the machine.

3.2.2.2 Analysis

As performed in section 3.2.1, a PLS model was built to relate the measured heights (i.e. change in Z-axis) to the temperatures on the machine. An initial trial of measuring the parts showed the data to be very noisy due to the imprecise nature of the cast aluminum parts. Because of this noise, simple smoothing techniques were investigated with the intention of improving the predictability of the model. Since the temperatures of the machine do not increase or vary in a fashion similar to the discrete measurements taken on the custom gage, the smoothing techniques were used to capture the general trend of the quality measurements.

3.3 Machine Production Process Monitoring

In general, it is known that in a production environment, whether manually or automatically operated, process faults will occur. It is very rare for a company to perform 100% quality inspection simply due to the time required to do a CMM inspection. Most SPC is performed, however, using a few measured quality parameters on a small number of parts on an infrequent schedule (Kourti & MacGregor, 1996). It is possible, however, to mount sensors on the machine to monitor what is happening while a part is being produced. Since many parts are being produced all the time it is possible to collect process data on every part that is created. The main finding of this research was that with massive amounts of process data composed of multiple variables it is possible to create an effective multivariate SPC system to identify good and poor process conditions related to specific quality outcomes.

One of the main criteria of developing this system, as mentioned in section 3.1, was that it cannot interfere with the part manufacturing process. Sensors such as table dynamometers, often used in laboratory experimental work (Yan, El-Wardany, & Elbestawi, 1994), cannot be used in this case because of the use of both the multiple rotating tables and the custom fixtures. As mentioned in chapter 2, there has been research involving the indirect measurement of forces either through vibrations, spindle power measurements, or feed-drive current measurements. Also, the studies that have modeled forces on these other parameters have originally measured the cutting forces directly with a dynamometer. Because of the status of the machine and the fixture tables it was never possible to model the forces on the machine during production conditions. However, due to the preprocessing used in PCA, namely mean-centering and unit-variance scaling, it should not be necessary to first model the forces. Instead, simply using the sensors that have been shown to adequately model forces in the literature should be sufficient for process monitoring where variation in these measurements would be the key indicator and not the exceeding of specific threshold values.

For sensor selection, two types of sensors are capable of measuring critical machine process conditions without interference: accelerometers and current sensors. Accelerometers mounted on the spindle structure will be capable of measuring vibrations during cutting while not being restricted to the table movement. Current sensors are fixed to the motor power leads in the back of the machine far removed from the cutting fluids and metal chips. Using these sensors satisfies the conditions specified in section 3.1 as they will not interfere with the process or structure of the machine. Furthermore, the boring and bossing operations consist of a plunging in the Z direction and the monitoring of process conditions in this direction was of primary concern. Therefore, applying a single axis accelerometer in the Z direction and a current sensor on the Z feed-drive motor should be sufficient for observing the process in its primary dimension. The actual removal of material using both tools occurs in the X/Y plane as well; hence, the use of single axis accelerometers in the X and Y directions was also employed.

Furthermore, since temperatures also have a great influence on quality (especially geometric parameters), thermocouple measurements will also be recorded during the machine production process monitoring.

3.3.1 Sensors and Equipment

The thermocouples used in the general machine process monitoring are of the same setup as those used in section 3.2.2.1. As mentioned in the previous section, three Kistler 8702B50 accelerometers were used mounted within the spindle structure behind the covering panel of the machine. A one-inch cube was created with 10-32 tapped holes on the center of the cube faces for mounting the accelerometers in the directions of the three axes. These accelerometers are capable of measuring a maximum range of ±50g, have a sensitivity of 100mV/g, and have a frequency response of 0.5 – 10,000 Hz. The accelerometers were connected to a Kistler 5134 power coupler and then connected to the BNC-2110 connector block of the acquisition system. The coupler was setup to filter the signals with the low-pass filter setting at 1 kHz and, after some initial test recording of the machining cycle, a gain of 100 was required due to the relatively low sensitivity of the accelerometers and the strength of the signal in this location on the machine for this application. The location of the accelerometers on the machine is presented in Figure 3.7, and is denoted as 'A'.

As previously mentioned current sensors are to be used on the Z-axis feed motor and the spindle motor. On the DMV-400 both motors are three-phase A.C. motors; however, since each phase will contain the same motor signal separated by a phase angle of 120°, only one phase on each motor will be monitored. On the Z-axis motor a Sypris (F.W. Bell) IHA-150 open loop hall-effect current sensor was used which had a sensitivity of 33mV/A and an AC bandwidth of 50 kHz. The current sensor used on the spindle motor was a clamp-type current sensor with a sensitivity of 5mV/A.

The acquisition equipment setup was very similar to that of section 3.2.1.1 except in this case 5 channels are used on the BNC-2110. Each channel on the BNC-2110 was initially sampled at a rate of 10kHz, however, after it was established that only the magnitude of the spindle RPM peaks was going to be used the sample rate was reduced to 2kHz. Acquisition software was again written using the Data Acquisition toolbox in Matlab 7 so that data could be saved in MAT files for easy processing and compatibility with other Matlab programs written for the online-process monitoring software. The acquisition and process monitoring system followed a standard configuration with the sensors all connected to a central acquisition system PC and a monitor setup to provide feedback to the operators.

3.3.2 Operating Conditions

For this machining operation, the spindle speeds were 7,000 RPM and 5,000 RPM for the boring tool and bossing tool, respectively. The cycle length when eight parts were being manufactured is 70 seconds and the acquisition was triggered off the X-axis accelerometer since the first movement was in the X direction.

3.3.2.1 Inspection

Formal CMM inspection for the parts was generally carried out only once per day. Since the boring and bossing tool dimensions were fixed, this inspection is mainly used to provide a formal measurement of depth and verification of tool setup. During the inspection one cycle from each table was taken to the CMM for manual inspection, for a total of 16 parts from each machine were measured. Inspection on the CMM, however, takes a long time (approximately 2 minutes per part versus 70 seconds to machine eight parts) which was one reason why constant inspection cannot be performed. Furthermore, the long inspection time was also caused by the fact the inspection includes all of the features of the parts, including the cast features which are not machined and Nixon is not responsible for.

Due to the long inspection time of the parts, it was not plausible to inspect representative samples of the parts as they were manufactured throughout the day if all eight parts are to be inspected. For this reason, a sample part from the first nest location on each table was taken approximately every 15 minutes during two days. This sampling of parts provided an adequate amount of data to model the quality data with the process data while still providing some additional data to test against the model.

Throughout the time spent monitoring this machining process, many machining cycles have been inspected and modeling of these parts were also investigated.

For the inspection of these parts, there are multiple quality parameters that are affected by machining. Table 3.2 shows a list of the quality parameters that are affected by machining. These parameters will be investigated using PLS.

Table 3.2: List of quality parameters affected by machining operations.

Quality Parameter	Description
Item 34	Boss Diameter (Tol. 16.744→16.896)
Item 37	Squareness of Boss (Tol. 0→0.08)
Item 38	Height from base of part to bored/faced surface (Tol. 41.48→41.58, Nom. 41.50mm)
Item 53	Height of boss face to bore face (Tol. 12.4→12.54, Nom. 12.47)
Item 56	Squareness of bore (Tol. 0→0.1).
Item 57	Bore Diameter (Tol 21.176→ 21.226, Nom. 22.201)

3.3.2.2 Simulation of Process Faults

Multivariate statistical models are generally built on historical data from processes that have resulted in good quality product while experiencing common-cause variation (Yoon & MacGregor, 2001). In this study, however, there was no readily available historical process data. Furthermore, there exists no historical data that can represent events containing process faults. In the machining process examined here, there were two main types of process faults not related to thermal errors: catastrophic and minor. During the catastrophic process fault, the operator completely miss-loaded the part so that it was sitting crooked and both tools entered the part at such an angle that in some cases machined completely through the wall of the bore hole. An example of a minor process fault was when the operator had not removed the chips from the previous machining cycle, and the parts were resting on these chips while the fixture clamps them down. Since the case of the catastrophic fault results in shut down and retooling of the machine, only the minor fault was investigated. If a process monitoring scheme is to be implemented and provide appropriate feedback to the operator, it is important that it is able to differentiate between a good process and a bad process.

As described, the major cause of process faults in this machining process was operator miss-loads. Since the catastrophic case was not feasible to simulate and results in broken tools and down-time, a simulation of the minor process faults was investigated here. In order to simulate minor process faults, shims under were placed the parts in three locations where they rest on the fixture nest. This was an attempt to recreate the case where the part was sitting slightly crooked due to residual chips. With these minor process faults, it was possible that the parts may pass the initial quality check from the custom gages. Furthermore, the operators do not routinely perform 100% inspection. Here it would be useful to detect these minor process faults from process data to inform the operator of a possible problem. The shim was placed on three different locations under the part where it sits on the fixture nest. Different combinations of thicknesses and locations were used in an attempt to capture some different process faults. Because of the limited time available to perform these experiments only three sets of tests were completed and, because of the similar results from each test, only one is presented. To prevent damage to the tool, a maximum shim thickness of 0.008" (~0.2mm) was used. The shim placement of the process fault simulation trials are summarized in Table 3.3. The 'NestID' refers to its location on the fixture, as shown in Figure 3.1.

Table 3.3: Shim thicknesses and locations used in experimentation.

Nest ID	Location 1 Thickness	Location 2 Thickness	Location 3 Thickness
1 (Control)	-	-	-
2	0.008"	0.008"	-
3	-	-	0.006"
4	0.008"	0.008"	-
5	-	0.006"	-
6	0.008"	-	-
7	-	0.006"	0.006"
8	0.006"	-	0.006"

3.3.3 Analysis

The preprocessing of this data was performed in a manner similar to that used in (Huessin, 2007) and is summarized in Table 3.4. The analysis for this experimental work can be broken up into two categories: process data and quality data. In the event that only process data can be made available to monitor the machine, PCA models can be built on data which is known to produce good parts while experiencing common-cause variation. Once a model with sufficient fit and predictive ability can be created, the use of simple control charts can be investigated. Hotelling's T^2 and Squared Prediction Error charts could be used together to determine if a part was good or if it required further inspection. Next, a process monitoring system employing these simple control charts could be used and presented to the operator. These techniques will be investigated and discussed in the following chapter. For a PCA model, the structure of the **X** matrix is shown in Figure 3.8. For shorter notation in this figure, the Boss and Bore tool measurements are labeled as **A** and **B**, respectively.

In the case where there is an automated CMM inspection site with lots of quality data, PLS models can be created which will relate the quality data to the process data. This action can be used to associate trends in process data to the outcome of various quality parameters and also provide predictive monitoring of these parameters. Identifying process trends, either good or bad, is a crucial step in quality improvement. This method of modeling will also be investigated.

Table 3.4: Signal preprocessing techniques.

Signal	Preprocessing
Spindle Current	Mean
Z-Axis Current	Mean
Accelerometers (X,Y,Z)	Magnitude of FFT @ Tooth passing frequency
Temperatures (8)	Average temperature over entire cycle.

ID	SpinCurr A	SpinCurr B	ZAxis A	ZAxis B	MagX A	MagX B	MagY A	MagY B	MagZ A	MagZ B	T1	...	T8
041907-1602-51													
...													
...													
041907-1608-62													

Figure 3.8: Illustration of X-matrix structure.

Chapter 4 Results and Discussion

4.1 Machine Thermal Expansion Modeling Results

This section is devoted to the investigation of modeling the thermal expansion of the DMV-400 under operating conditions experienced during production.

4.1.1 Initial Measurements of Z-axis Expansion

As previously stated, the goal of this measurement was to capture the maximum expansion of the Z-axis to both ensure that a maximum was achieved and to see if it was possible to model this behaviour with temperature measurements.

The measured data from the proximity sensors during the three hour test is shown in Figure 4.1. The convention used in this figure is at time zero there has been no movement so this will also be the starting point at a distance of zero. It can be seen that as time progresses with the spindle spinning at 7,000 RPM, the Z-axis moves downward as temperatures increase. The arrow in Figure 4.1 denotes the time which the external spindle chiller unit has turned on. It can be seen that this unit operates in a cyclical control fashion (similar to a thermostat controlling a furnace) in an attempt to provide thermal compensation. After about 75 minutes trajectory of the Z-axis starts to reverse direction, however, this test does show the large deviation of the Z-axis over a course of three hours. It is important to note that this test does not encompass any distortion that may be caused by the movement of the machine while running a production cycle. While the case here does not reach an equilibrium point, this kind of behaviour from the spindle chiller unit is to be expected (due to its on-off style control) and result in some fluctuation over long periods of time. Furthermore, the spindle chiller unit has a temperature indicator which displays the temperature of the coolant. The temperatures on the chiller started at 15.5°C, peaked at 19°C after 1.5 hours, then dropped to 17°C in the next half hour, and ended up showing 18°C at the end of the test.

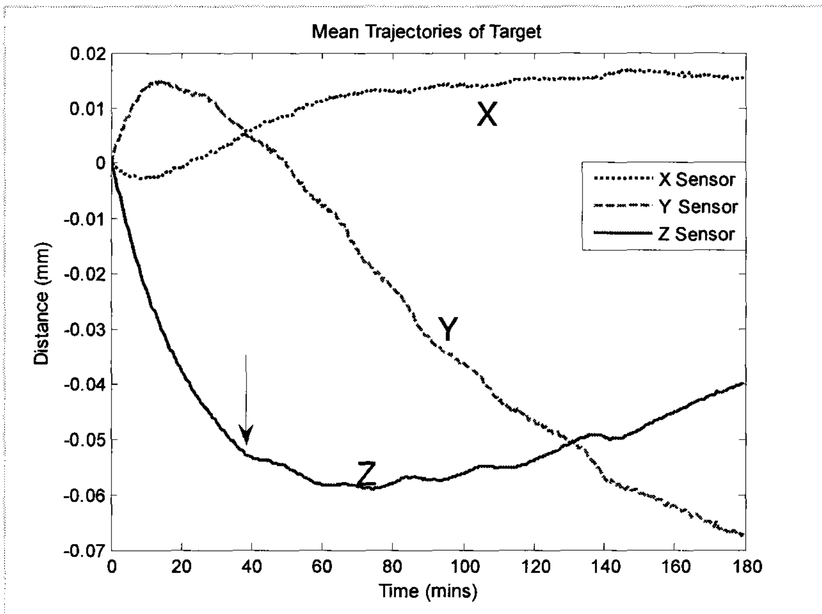

Figure 4.1: Mean trajectories of the target shaft. The time at which the spindle chiller is suspected to have turned on is denoted by the arrow.

The measured temperatures, which correspond to the thermocouple placements in Figure 3.5, are shown Figure 4.2. All of the temperatures, including *Ambient*, appear to follow a general trend of slow increase over the time period. While the temperature measured at location *Temp 3* has the lowest overall measured value, it also appears to mimic the action of the spindle chiller the closest as recorded and best matches the Z-axis proximity sensor. Furthermore, the temperatures appear to reach an equilibrium point after approximately 140 minutes which was contrary to the measurement of the Z-axis trajectory.

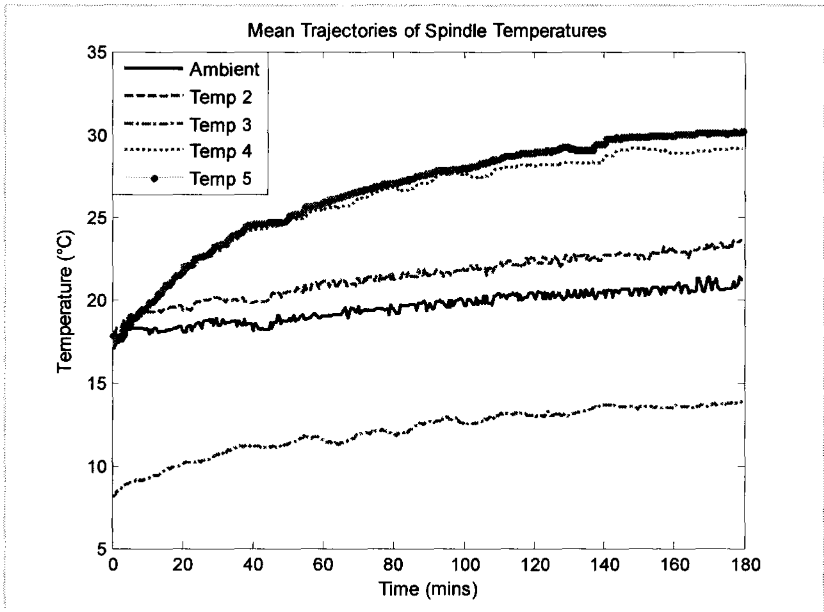

Figure 4.2: Mean trajectories of spindle temperatures.

While the plot in Figure 4.1 indicates the movement of all three axes, this setup only employed the use of three sensors and their values were only recorded for the sake of interest. That being said, there is drastic movement in the Y-axis suggesting tilt of the spindle support arm as illustrated in Figure 2.3. The modeling and investigation of these measurements was not explicitly performed in this study, however, they are noteworthy and may affect quality parameters such as squareness and location of the bore and boss.

4.1.1.1 Modeling of Initial Measurements

In this case, the **X** matrix consists of the measured temperatures from Figure 3.5 and the **Y** matrix contained the Z-axis thermal drift. For the analysis of these measurements, PCA on the **XY** space was performed to ensure coherent data correlation between the process and quality data. Using the SIMCA-P+ software, a PCA model was created with two components and the results are shown in Figure 4.3. After two principal components (PCs) were identified, a cumulative R^2 value of 0.989 and a cumulative Q^2 value of 0.936 indicate a very good model. A quick investigation into the structure of this model via score and loading plots was done, and is shown in Figure 4.4 and Figure 4.5, respectively.

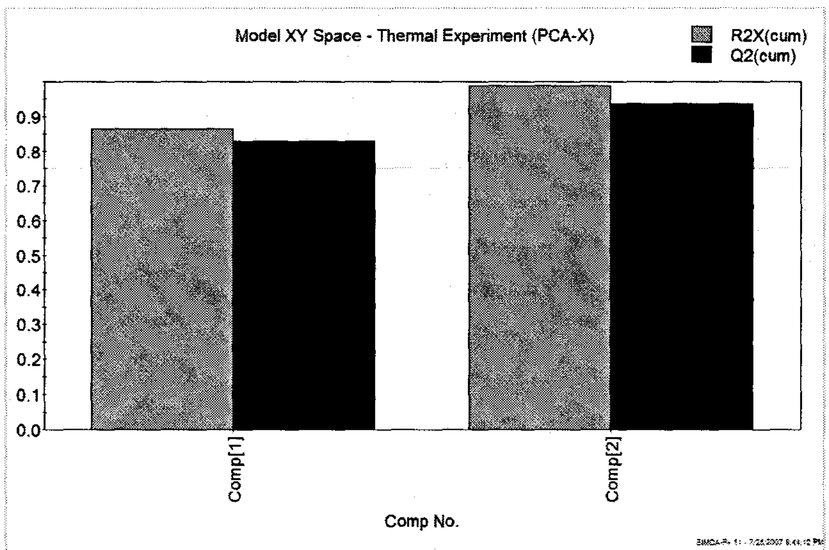

Figure 4.3: Model overview of XY space for thermal experiment.

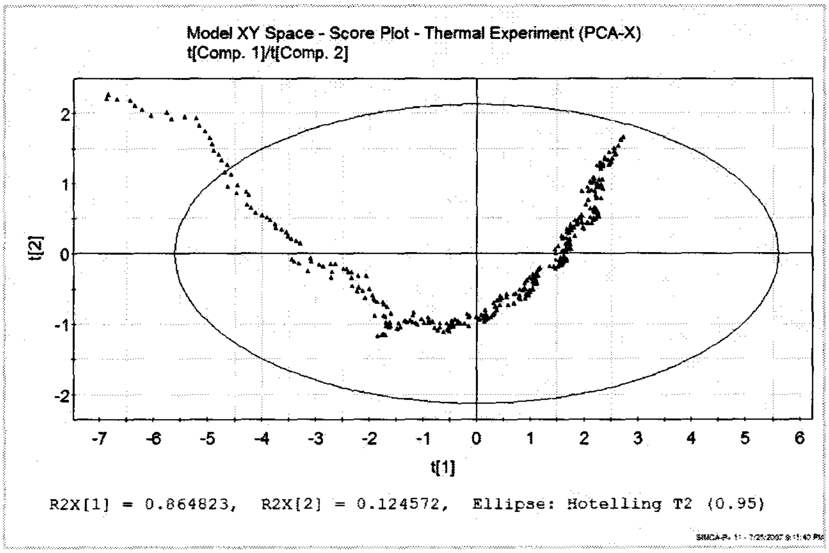

Figure 4.4: Score plot showing the two principal components in model.

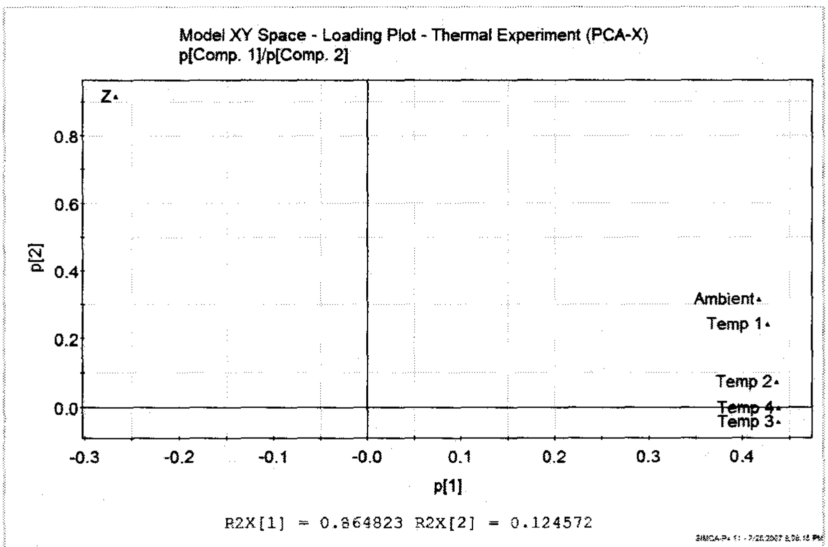

Figure 4.5: Loading plot showing the variable weightings on the model.

Looking at the score plot in Figure 4.4, it is clear to see that the main factor affecting this model is the Z axis measurement as the general trend of this model follows the trajectory of the Z-axis from Figure 4.1. Furthermore, a look at the loading plot shows the Z variable almost completely opposite of the temperature variables; which are clustered together, indicating strong correlation between these variables. The opposing location of the temperature variables and Z variable makes sense considering the Z-axis values decrease while the temperatures are increasing, which can be observed in Figure 4.1 and Figure 4.2. The loading plot makes it clear that the first PC mostly explains inverse relationship between the Z-axis and the temperatures, while the second PC explains the movement in the Z-direction. It was clear from this quick investigation that the data was strongly correlated yet with multivariate techniques still capable of producing a good model.

Modeling the data using PLS on the **X** and **Y** data was performed using the SIMCA-P+ software as well. The model relating the temperature measurements to the Z-axis trajectory yielded a three component model with cumulative R^2_Y of 0.824 and cumulative Q^2 of 0.822. A plot showing the trend of the Z-axis trajectory with the trend of the model predictions is shown in Figure 4.6. Over the first 5 minutes of predictions, the model was not capable of describing the change in the Z-axis with the change in temperatures. Excluding the first 5 minutes worth of measurements, this model provided an RMS error (RMSEE) of 0.0041 mm with a maximum deviation of 0.013 mm.

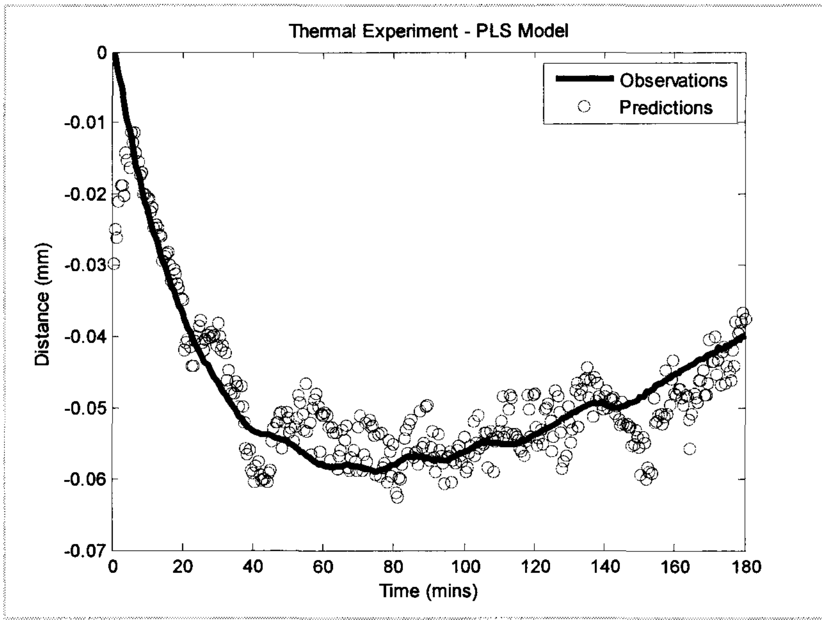

Figure 4.6: Plot showing model predictions vs. observations over the 3 hour test.

Looking closer at Figure 4.6, it can be seen that the model predictions tend to lag behind the observation. At the time of 40 minutes, where it was previously noted that the spindle chiller turns on, the model continues to predict that the Z-axis should still be moving down. This model behaviour suggests there was some time lag between the surface temperatures and the internal spindle temperatures that were actually affecting the thermal expansion of this axis.

Possible causes for this poor modeling ability during the first 5 minutes can be investigated using contribution plots. Figure 4.7 shows the contribution to the score of the first observation from the weights of all three components. It is clear that the temperatures are much lower than the average, with *Temp 3* being more than three standard deviations lower. This, again, suggests a temperature measurement time lag between the measured temperatures and the actual internal temperatures of the spindle, since there was a measureable change in the Z-axis.

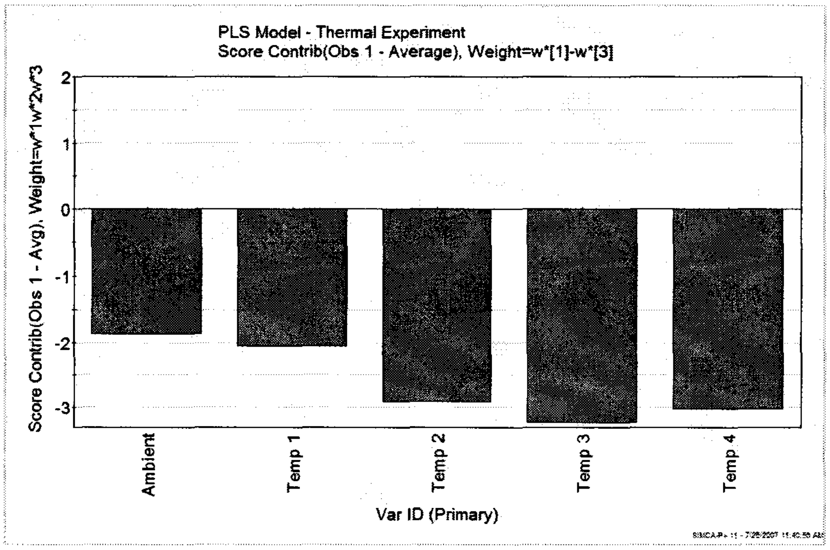

Figure 4.7: Score contribution plot showing the temperatures for the first measurement.

The modeling of time-lags in PLS time series models is described by Eriksson *et al.* (2001). Using the SIMCA-P+ software package, it was possible to introduce time lags into a PLS time series analysis model. Using this feature, lags were introduced into the Z-axis for the first 5 minutes of observations (or 10 samples). The model built using this feature had a fit with $R^2_Y = 0.998$ and $Q^2 = 0.998$ (rounded up to the third decimal) with two components. The observed vs. predicted plot in Figure 4.8 showed a very good model fit to the data with a RMSEE of 0.00044 and a maximum deviation of 0.0013 mm, and order of magnitude improvement.

This investigation clearly states that it is possible to model behaviour of the Z-axis while experiencing thermal distortion using only a few temperature measurements on the machine. It should be noted again, that this analysis does not encompass the behaviour of the machine while it was running a production machining cycle. The next section attempts to investigate the behaviour of the machine under full production operation.

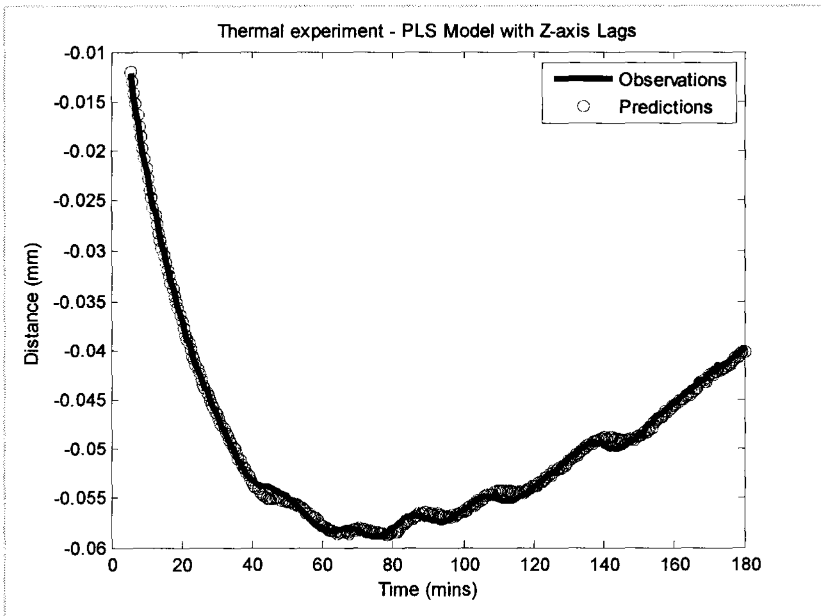

Figure 4.8: Plot showing model predictions vs. observations with Z measurement lags of 5 minutes introduced.

4.1.2 Indirect Measurements of Z-axis Expansion

To capture the true nature of this system's response to thermal distortion, the Z-axis needed to be measured during production. This was done by measuring the value of the heights of the part on the custom gage that was set up next to the operator. This gage is set up so that the nominal reading was set as 0mm and has a resolution of 0.01mm. Furthermore, while not shown on the plots, the standard error for all measurements was

±0.005mm. These quantities were measured over two days. The measured heights and temperature profile for day one are shown in Figure 4.9 and Figure 4.10, respectively. The same quantities for day two are shown in Figure 4.11 and Figure 4.12, respectively. A comparison of the two plots shows some slightly different behaviour between the two days, which was to be expected because of different ambient temperatures in the building as well as changes in the operator's behaviour throughout the two days. The employee morning and lunch breaks are clearly visible on the plots of the temperature profiles. Also, the first measurement of the corrected heights indicates the first measurement taken that day. The heights are 'corrected' by subtracting the original machine offset from the new offsets, as they are changed throughout the day, and adding the difference to the measured height. This will give an approximate profile of the Z-axis distortion throughout the day.

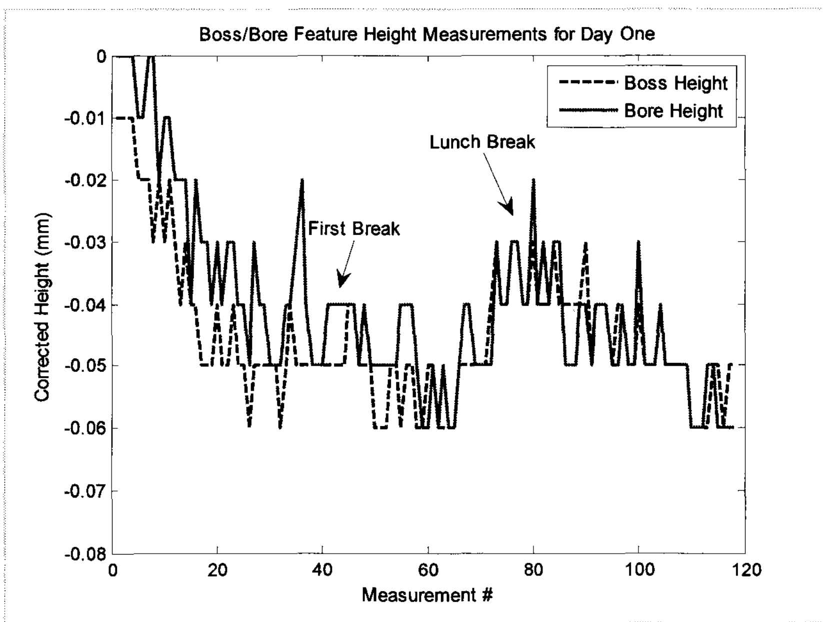

Figure 4.9: Boss and Bore heights measured throughout day one from ~7:30AM to ~3PM.

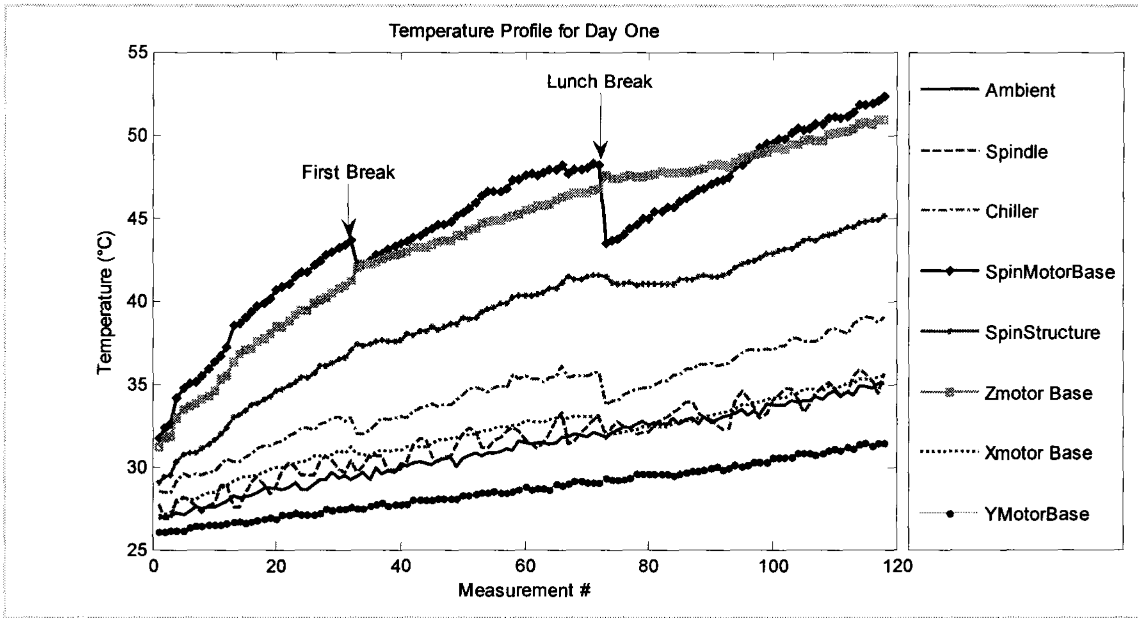

Figure 4.10: Temperature profile for machine on day one from ~7:30AM to ~3PM.

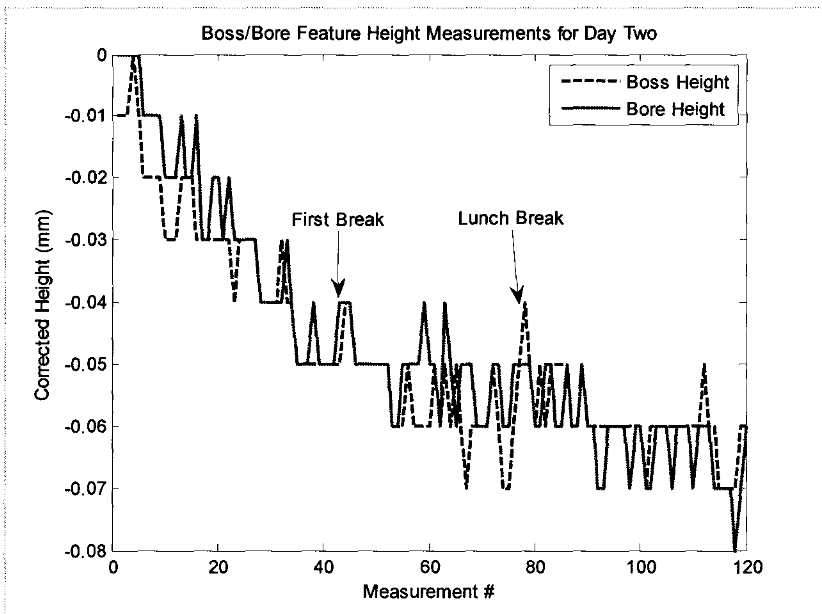

Figure 4.11: Boss and Bore heights measured throughout day two from ~7:30AM to ~3PM.

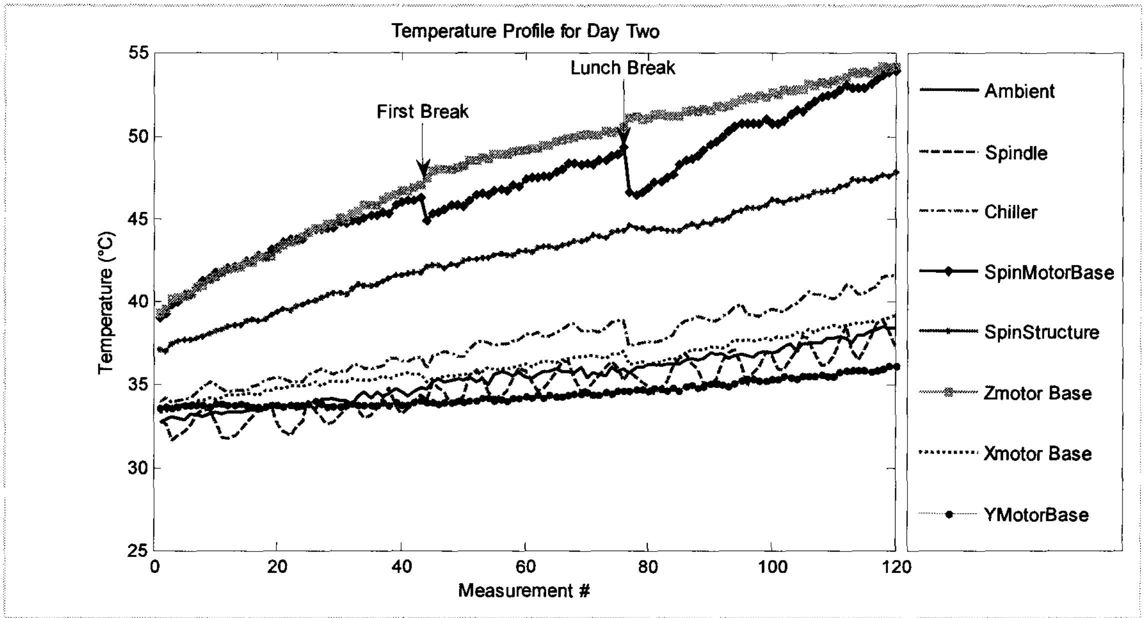

Figure 4.12: Temperature profile of machine for day two from ~7:30AM to ~3PM.

While the data in Figure 4.9 and Figure 4.11 reveal the general trend of the machine, these data sources are very noisy as only one side of the part was machined. Thus, the height was measured with a cleanly machined face on the top side, but the bottom side of the part was from the original casting of the component; and, the large variation in the casting process was seen in these plots. Smoothing the data using a simple 5-point moving average was carried out and the result was shown in Figure 4.13 and Figure 4.14. With the smoothing applied to these data points, much of the dimensional variation from the casting surface was removed and the overall trend of the machine becomes more apparent. Based on this, it was expected that the smoothed data will yield a better model. Since PCA and PLS are noted for their ability to filter through noisy data, both cases will be investigated in the following section.

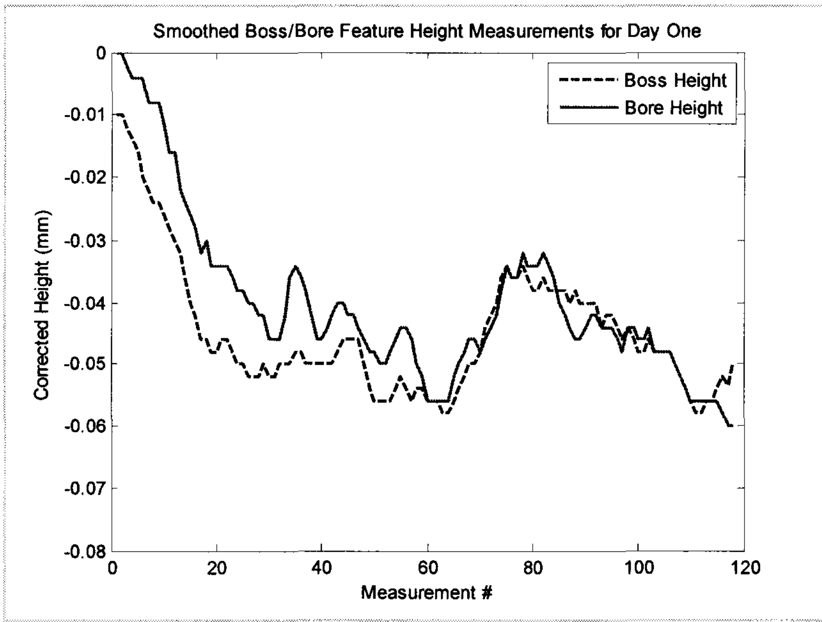

Figure 4.13: Height measurements from day one smoothed using 5-point moving average.

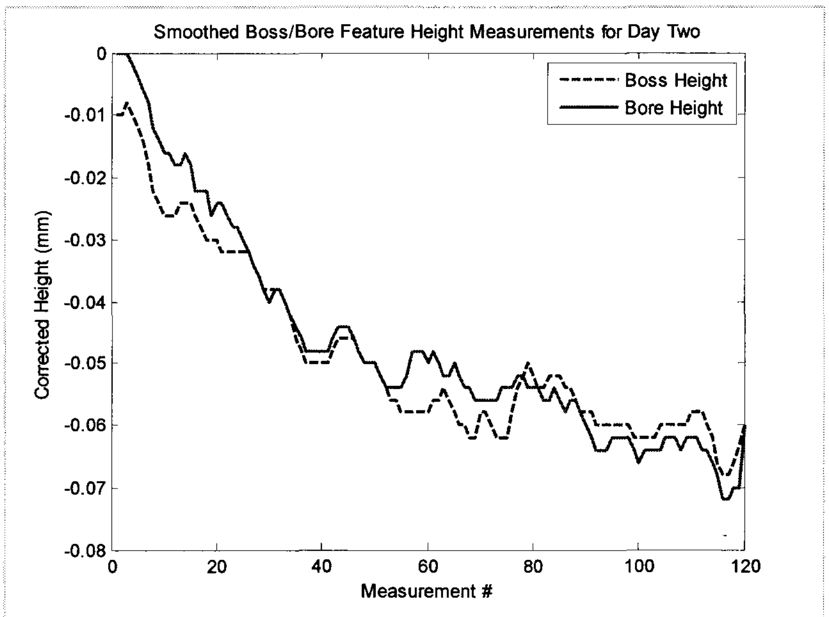

Figure 4.14: Height measurements from day two smoothed using 5-point moving average.

4.1.2.1 Modeling of Indirect Measurements

The analysis of these measurements taken during production will be comprised of several modeling investigations. Since the data from the two different days shows distinctly different behaviour, consideration was taken to model both days together because incorporating more data will improve the predictive ability of the model. This day-to-day variation is expected due to ambient temperature variation within the shop and how much the machine is run during the day. Furthermore, various models are created which will investigate the cases in the previous section, including those with the smoothed data. The overall goal of modeling these data was to predict the thermal expansion of the Z-axis and be able to then feedback this information to the machine to automatically update the machine's offsets for improved quality control. This section will investigate several cases and model types. In depth analysis, however, will only be performed on the model with the best overall fit.

The first data set to be investigated was the measured heights of day one from Figure 4.9. The modeled data gave an R^2_Y fit of 0.775 with a Q^2 of 0.768 using two components. While the fit of this model maybe considered acceptable, a closer look at this data while comparing showed that the model was really only able to predict the trend of the machine and the discreteness of the measurements, due to the resolution of the dial indicator, there seems to be a natural filtering process involved with the predicted data. Note that the predictions are all made on data for which the model was built. While the entire model has a R^2_Y of 0.775, the fit of the individual Y-variables are R^2_{Boss}=0.751 and

R^2_{Bore}= 0.798 and are shown in Figure 4.15. The RMSEE for the Boss and Bore heights are 0.006 and 0.007, respectively.

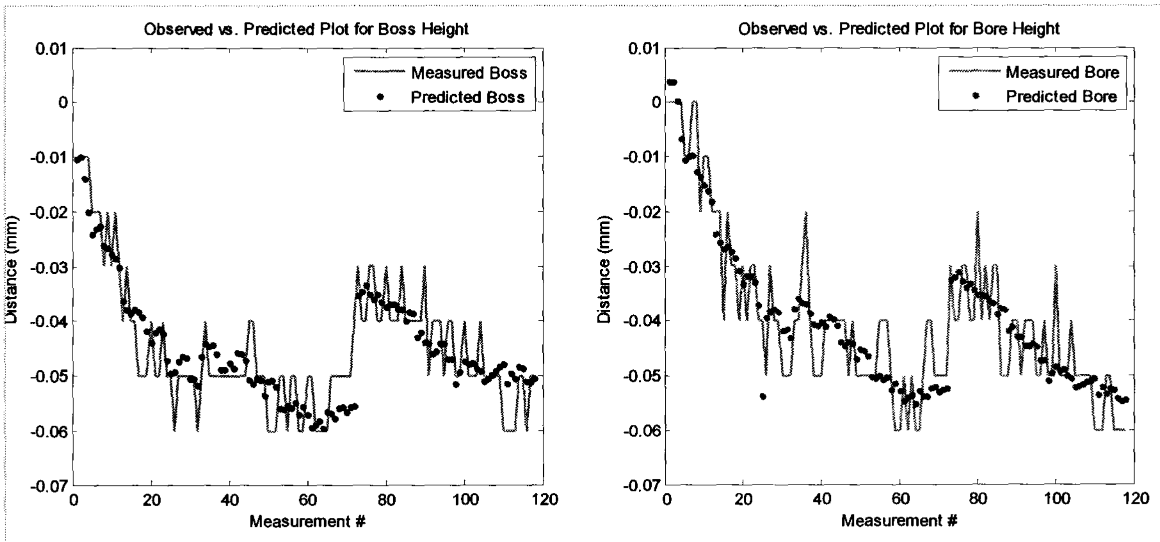

Figure 4.15: Day One - Observed vs. Predicted plots for Boss height (left) and Bore height (right).

Similar results are presented for *Day Two* in Figure 4.16. This model fit was noticeably better than the model for *Day One* with an R^2_Y of 0.900 with a Q^2 of 0.894. In both cases, however, the Q^2 value was within 0.01 of the R^2_Y indicating good predictive ability. For *Day Two*, the fit of the variables was R^2_{Boss}=0.751 and R^2_{Bore}= 0.798 and the RMSEE was 0.005 and 0.006 for the Boss and Bore, respectively.

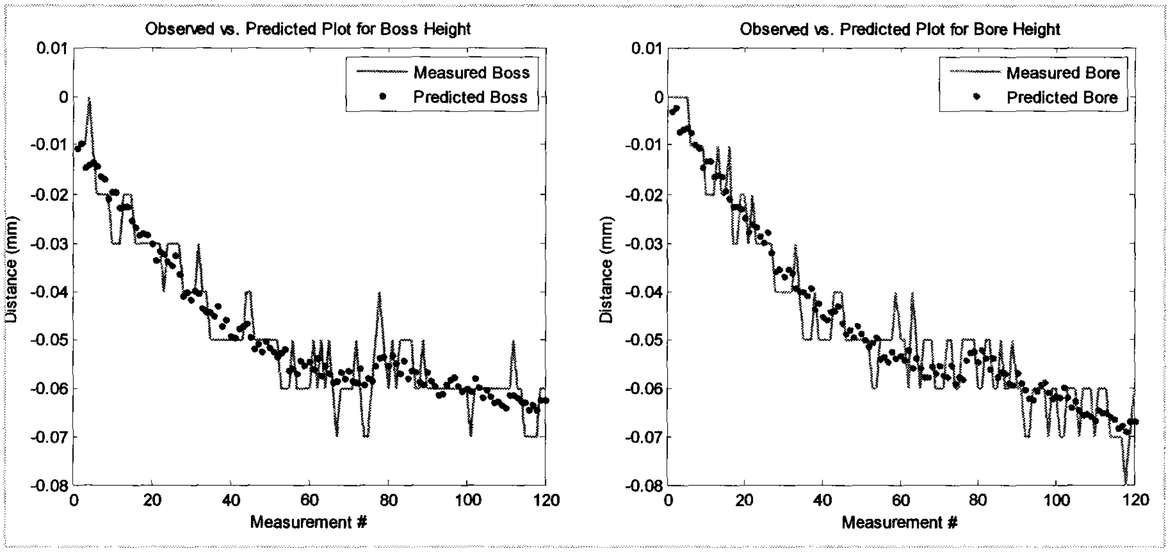

Figure 4.16: Day Two - Observed vs. Predicted plots for Boss height (left) and Bore height (right).

Since the variability of the measurements was reduced by smoothing the data, it is to be expected that the predicted data will fit the smoothed data much better if they are both describing the trend of the thermal distortion. Shown in Figure 4.17 is the observed vs. predicted plots for both the Boss and the Bore heights after the data had been smoothed. This model yielded an R^2_Y of 0.889 and a Q^2 of 0.884 in two components, which corresponds to an improvement to the model's fit of approximately 15%. The interesting thing to note is that smoothing the data did not provide predictions that differed substantially from those of the model built on the measured data.

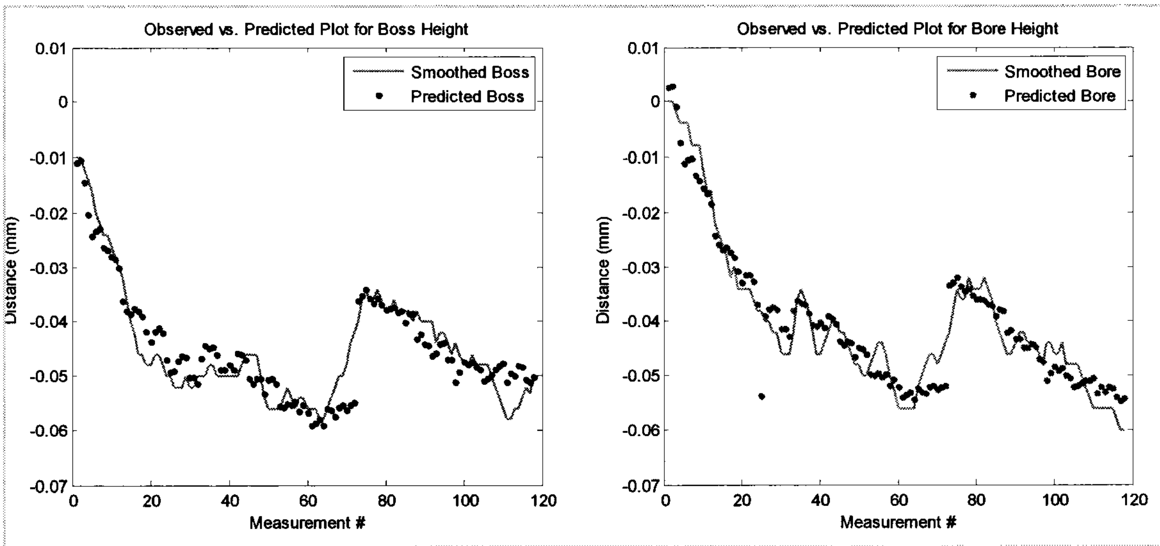

Figure 4.17: Day One - Observed vs. Predicted plot for smoothed Boss (left) and Bore (right) measurements.

Figure 4.18 shows a comparison of the model types by plotting the predictions from the measured data model against the predictions from the smoothed data model. As suspected, PLS has filtered out the dimensional measurement variability of the measured data and predicted the general trend of the machine. While this does not give a model with as good of fit as the smoothed data, this illustrates that the predictions for the machine are as good as possible using the measured data.

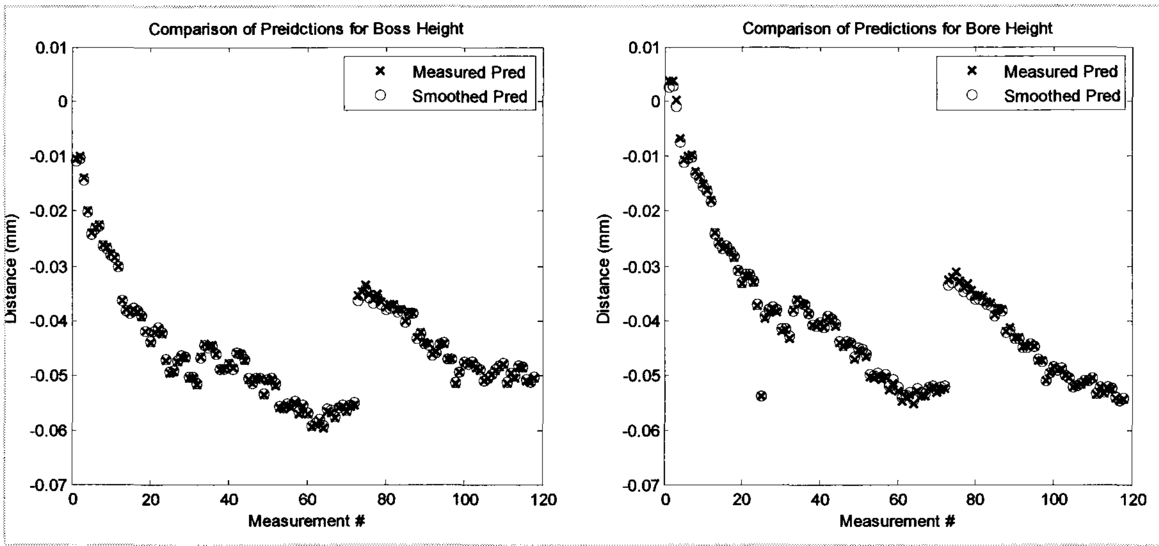

Figure 4.18: Comparison of predictions for models built from measured and smoothed data for Day One.

Next, there was the case where time-lags were introduced in the model to account for the delay, where by the temperature inside the machine structure/component does not reach the surface until a certain lag in time has occurred. As shown in Figure 4.8, lags accounting for 5 minutes seem to be adequate in modeling. When measuring parts, approximately three of the measurements would account for 5 minutes. This approximation was based on the times when production was continuous and did account for morning or lunch breaks. Shown in Figure 4.19 is the case where three time lags are introduced into the model built from measured data on *Day One*. In this model, the fit was not as good as the original model built on this data with R^2_Y of 0.72, Q^2 of 0.685, R^2_{Boss}=0.706, and R^2_{Bore}= 0.741; however, the RMSEE of the Boss and Bore was 0.006 and 0.007, respectively; the same as the original *Day One* model.

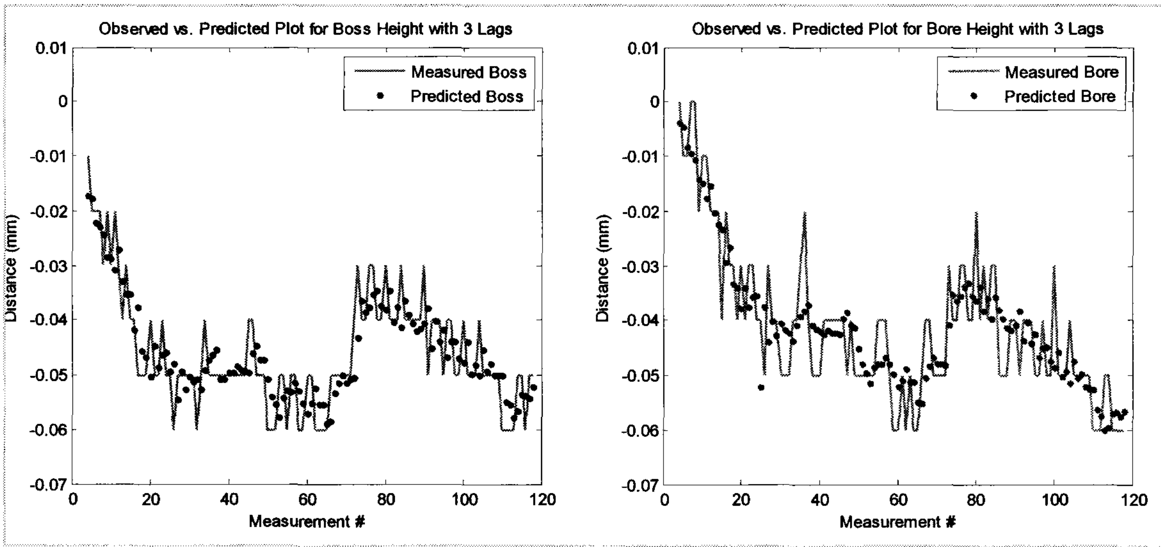

Figure 4.19: Day One - Observed vs. Predicted plot showing the effect of using three time-lags.

The true test of a model, however, is its ability to accurately predict data that was not included in the original work set used to establish the model. Three test cases will be examined to identify the capabilities of this data. The first will test a model built on *Day One* with the data from *Day Two*. The second will test the model built on *Day One* with the time-lags with the data from *Day Two*. The third will try to create a model built on half of the data from each day (odd observations only) and then test it on the remaining data (even observations). The effect in the third case was to capture information from multiple days and test the model against known similar temperature days. This idea promoted the use of seasonal models that could be beneficial to a shop that is not temperature controlled.

In the case where *Day One* data was tested against *Day Two* data, the plots in Figure 4.20 show how the original model was tested against new data. It was clear to see from this figure that, while the model was very capable of predicting the trend of the data, however it was not capable of accurately predicting the magnitude of this data. Further investigation via contribution plots would yield the underlying cause of the overall increase in the predictions, however, simply comparing Figure 4.12 to Figure 4.10 showed that the general temperature of the machine was higher and that the *Ambient* temperature was on average 4.24°C hotter on *Day Two*.

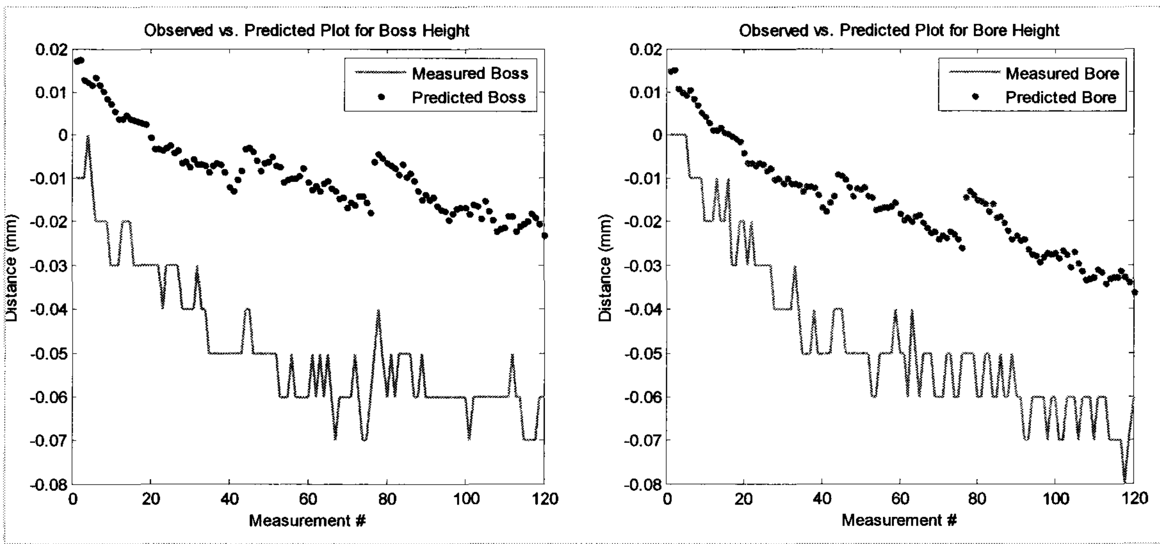

Figure 4.20: Data from Day Two tested against the Day One model (without time lags).

In the case where the *Day One* model was created with lags, the plot in Figure 4.21 showed the effect of the addition of time – lags into the model. It can be seen on the plot that the first few measurements yield poor fit to the actual data, however, the cause of this was due to the fact that the additional **X** variables from the lags were missing since there is no information on the Boss or Bore measurements on the prediction set. Since the use of three time lags will take that number of units to catch up to the current conditions, it was clear that after the first three predictions, the model was up-to-date and was predicting appropriate conditions, as the error is visibly reduced.

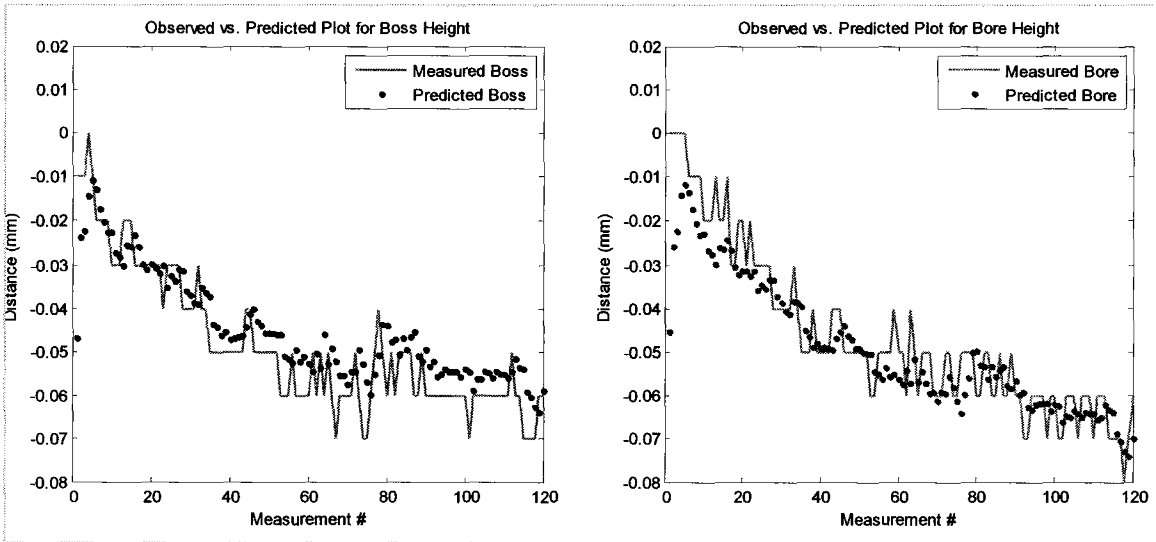

Figure 4.21: Data from Day Two tested against the Day One model with three time lags.

It is clear from Figure 4.21 that this method provides excellent predictivity of new data, even when the temperature trends differ from those for which the model was built. The Boss predictions fit the actual data with $R^2_{Boss} = 0.843$ and RMSEE of 0.008, and the Bore predictions fit the actual data with $R^2_{Bore} = 0.872$ and RMSEE of 0.008. It is worth noting that the fit of the individual **Y** variables on the predicted data was better than the original data, as in Figure 4.19. Not including the first three measurements, this model yielded a maximum error of 0.0203mm for the Boss measurement and 0.0184mm for the Bore measurement.

The final model illustrated the case where a model was to be built on multiple days' worth of data. This was done by including the odd numbered observations from both days in the model, and predicting the even numbered observations against it. The assumption made here was that the even numbered observations are from days where the machine is operating under 'similar' temperature conditions. The data from these *new* days will be referred to as *Day Three* and *Day Four*.

The model created using the odd numbered observations from *Day One* and *Day Two* had six components and $R^2_Y = 0.849$ and $Q^2=0.812$. The predictions for *Day Three* and *Day Four* were shown in Figure 4.22. In general, this model showed relatively good predictive ability for data from similar days. The model had an $R^2_{Boss}=0.710$ and an $R^2_{Bore}=0.814$ with a maximum error of 0.0203 and 0.0259 for the Boss and Bore Heights, respectively, and both prediction sets have an RMSEE of 0.008.

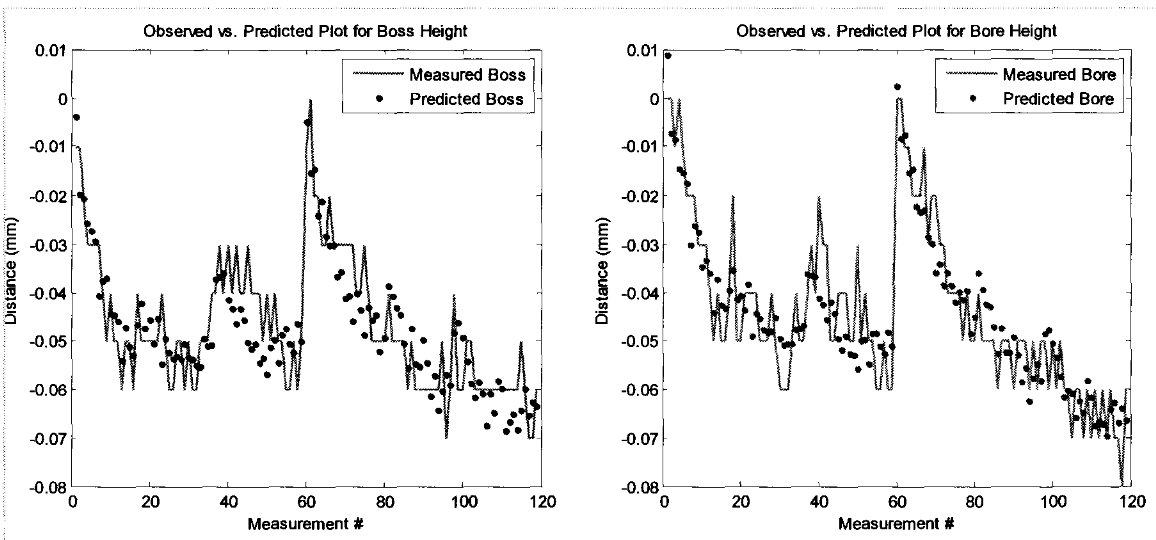

Figure 4.22: Day Three/Day Four observed vs. predicted data.

While both of the last two models gave similar results and both were built using the same number of data points, the *DayThree/DayFour* predictions were based on a model that incorporated machine trends from days where the ambient temperature in the shop varied significantly. The other reason why this type of model would be preferred is that it contains information from days where process conditions change.

Now that possible models have been investigated and narrowed down to two choices, the next step would be to look at how this would perform under a real-time thermal error compensation strategy.

4.1.2.2 Real Time Thermal Error Compensation

The two model types selected in the previous section show that overall performance can be judged by how well compensation via the model held the heights to zero. In order to comply with both the resolution of the dial indicator and the resolution that the operators must use when entering offset values, all of the values estimated by the model were rounded to the nearest 0.01mm. The measurements were then subtracted from adjusted prediction values to see how well the compensation held the heights to a nominal value of 0 mm. It should also be noted that the tolerance of this part was ±0.05 of the nominal value.

For the case where data from Day Two was predicted using model of Day One, the compensation strategy, shown in Figure 4.23, yields a maximum deviation of -0.03mm on the first measurement and held the heights of the two dimensions to within ±0.02mm; well within the tolerance limits.

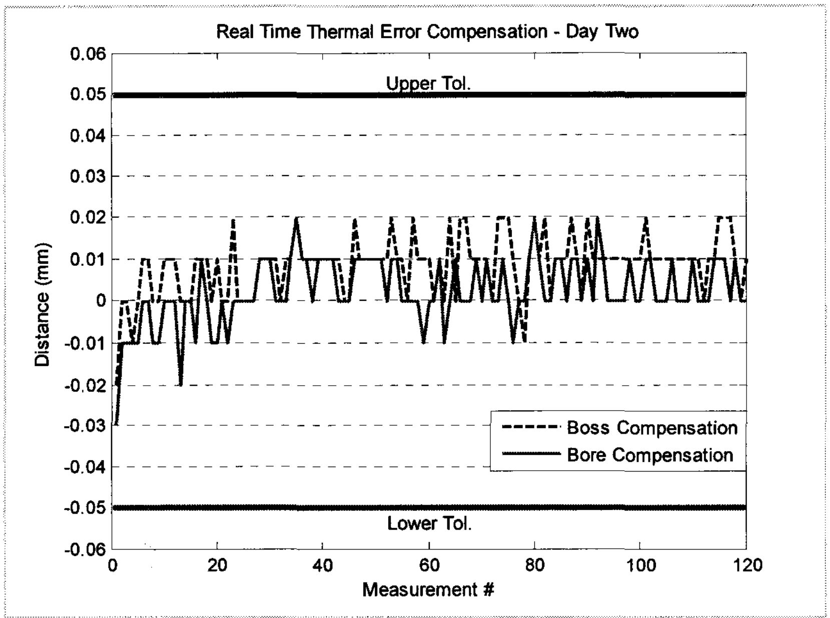

Figure 4.23: Real time thermal error compensation for Day Two data/predictions.

In the second case where the data from the *DayThree/DayFour* was tested against the *DayOne/DayTwo* model, a similar result was achieved using the compensation strategy for the Z-offsets. Figure 4.24 showed the compensation holding the heights of the parts to ±0.02mm; also, well within the tolerance limits.

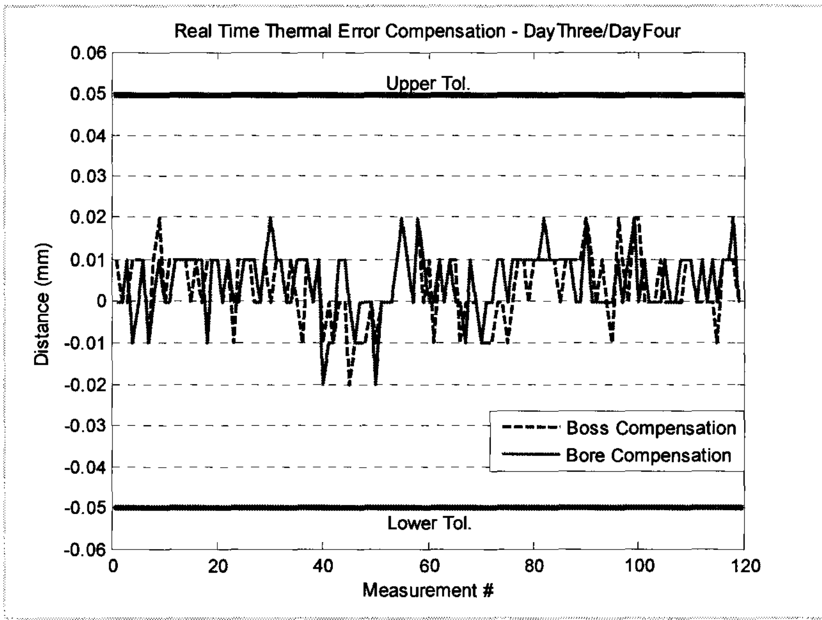

Figure 4.24: Real time thermal error compensation for DayThree/DayFour predictions.

A compensation strategy was shown to give good results from two different PLS models on the thermal error of a machine tool in a production environment. Even though the measured heights of the parts provided very noisy data, the PLS model was able to eliminate most of the variability and determine the general trend of the thermal distortion of the machine that enabled a reasonably accurate compensation strategy to be deployed.

4.2 Machine Process Data

The machine process data was acquired as one long time signal of data and before preprocessing of the signals for the individual parts could be done, this time signal for the entire machining cycle was first broken up into the eight sections where machining was taking place and eliminated additional time signals from when the machine was simply moving. This windowing was performed by looking at the Z-axis current signal to determine when machining was taking place. An example of this window for the first tool of the first part in a cycle was shown in Figure 4.25, where the "Start" and "Finish" labels indicate when the tool enters and exits the part, respectively. Once the time-indices were determined for each part and both tools, the signal was split up and the data was preprocessed as discrete parts. Also, since the common practice of mean-centering/unit variance scaling of the data prior to PCA/PLS was performed here, the signals were left in their original voltage signal state and not converted to their physical units.

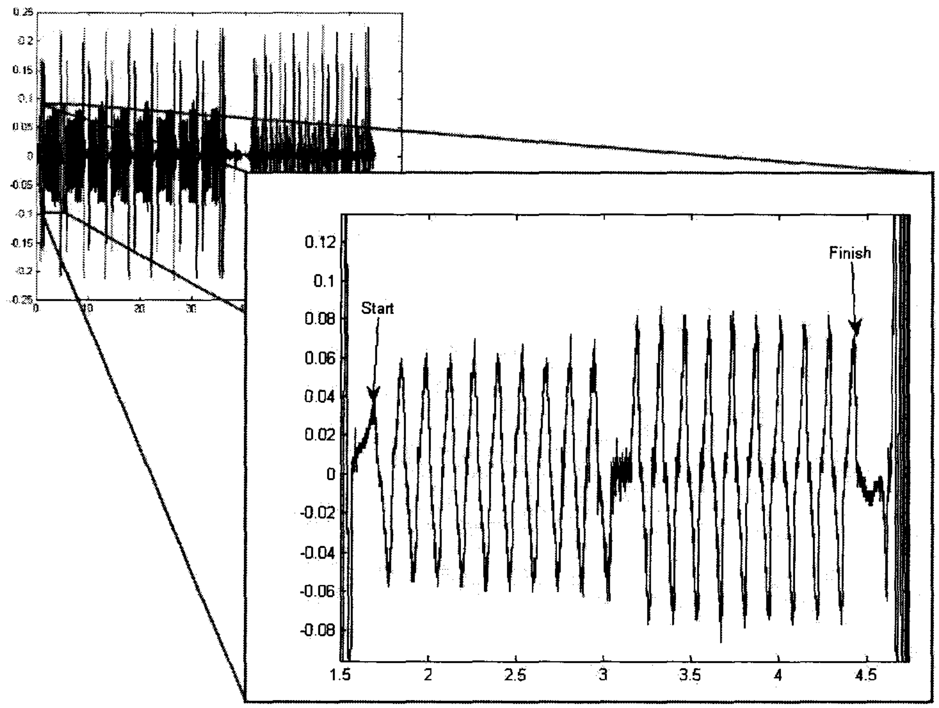

Figure 4.25: Signal windowing example for the first tool of the first part.

4.2.1 Machine Process Modeling

In order to create a model of the process run on the machine, data representing common-cause operation must be used. This was easily done by selecting process data from known good parts throughout a day. As can be seen from the previous section, the parts were known to experience variation throughout the day and since many parts were made during production throughout the day, it can be as simple as building a model from the process data of one day. The process data was analyzed using PCA and when quality data is available PLS can be used to model the quality data using process data.

4.2.1.1 PCA on Process Data

Throughout experimentation and data collection, process information on more than 20,000 parts was acquired. To simplify this discussion, models built on representative set of data were presented and described using score plots and loading plots. There were several test cases for these models, which included: testing the model against known good process data from the same day; testing it against known good process data from a different day; and testing the model using the simulated process fault experiments as described in section 3.3.2.2

A process based model was built using PCA on data from the day of the first set of simulated process experiments. The data matrix was of the same structure as illustrated in Figure 3.8. This model consisted of two components with R^2_X=0.652 and Q^2=0.581 and was made using 1,500 observations. The plot in Figure 4.26 showed a score plot illustrating the data was well correlated and the number of parts outside the 95% Hotelling's T^2 ellipse was insignificant and there were no parts outside of the 99% Hotelling's T^2 ellipse, which indicated a good model. Furthermore, the loading plot shown in Figure 4.27 illustrates the relationship between the variables and the components. All of the temperature variables were clustered together and were very close to the P1 axis, indicating the first component explained the temperature variation. The parts that had low T1 scores represent those that were made in the morning, or when the machine temperatures were cooler. The variables listed in Figure 4.27 have either the suffix *A* or *B* indicating the Boss tool or the Bore tool, respectively. When the data from the simulated experiments, as listed in Table 3.3, is applied to this model, these simulated process faults did not provide enough variation in the measurements to have these data points significantly jump out of the model. Figure 4.28 showed the experimental parts sitting in the middle of the plot. This location corresponds mostly to the temperatures as the experiments took place during the lunch break in the middle of the day.

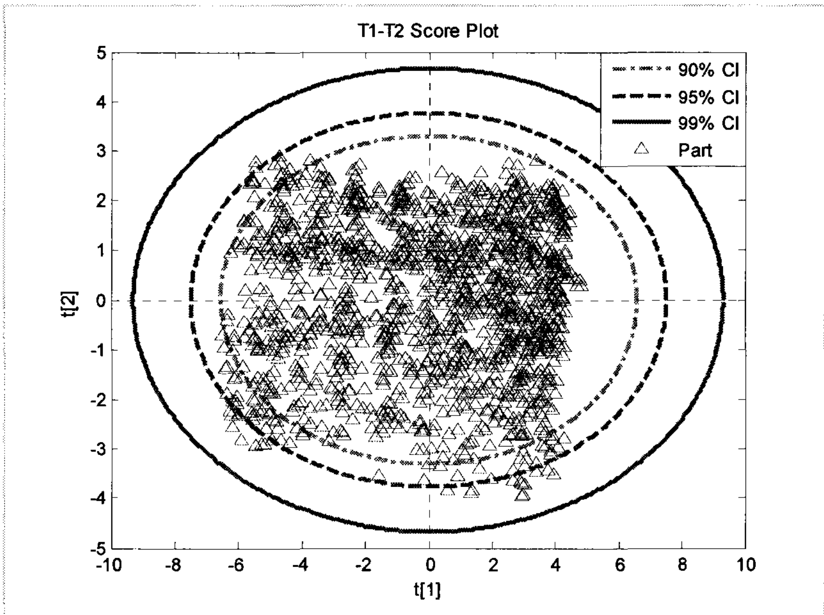

Figure 4.26: Score plot showing T1-T2 scores for 1500 parts.

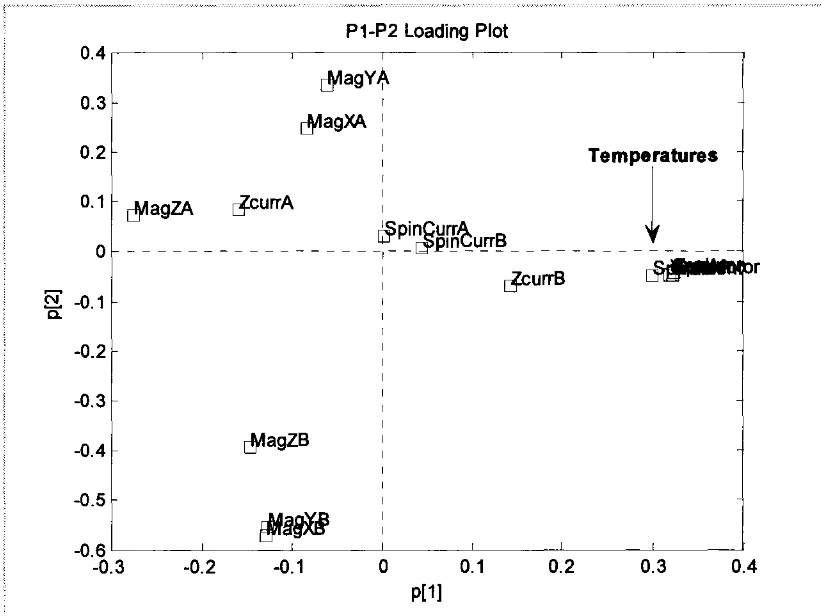

Figure 4.27: Loading plot showing p1-p2 weights for 1500 parts.

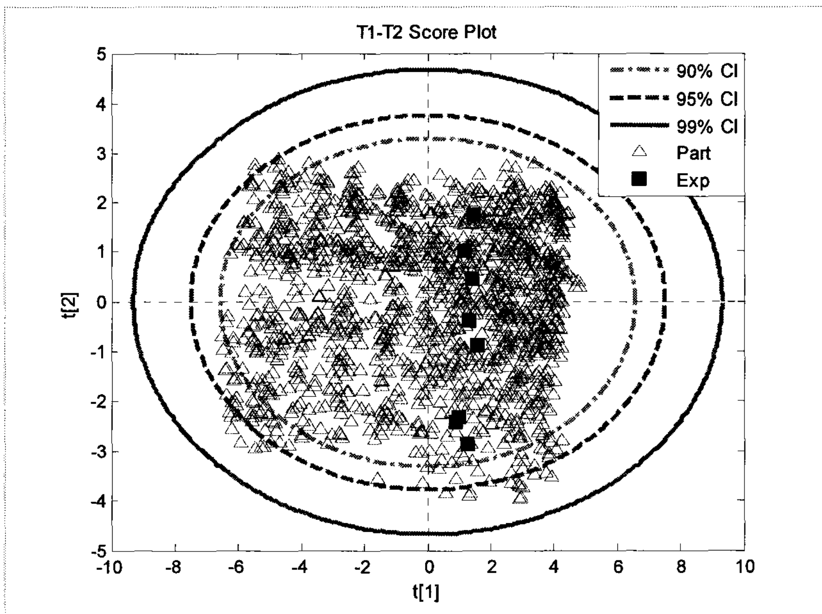

Figure 4.28: Score plot showing T1-T2 scores from experimental process fault simulation.

Since the temperature variables explained a large source of variation in the first component, a model was built that did not include the temperature variables. This model consisted of two components with $R^2_X=0.457$ and $Q^2=0.152$ and was made using the same 1,500 observations. The score plot shown in Figure 4.29 shows the parts used in the model. Here the '*NewPart*' observations indicated a few measurements from parts on the same day and a few from the next day, just to illustrate how the new observations fit in with this model. In this example, the experimental process fault simulation parts also lay within the 90% confidence ellipse, further indicating that this sensor fusion system is incapable of detecting process faults with this small magnitude. As mentioned before, the tests outlined in Table 3.3 used the maximum allowable deviations to prevent possible tooling or fixture damage. While process faults do happen, the ones that would stand out of this data analysis are often catastrophic and the machine is stopped before the cycle is complete, thus interrupting the signal.

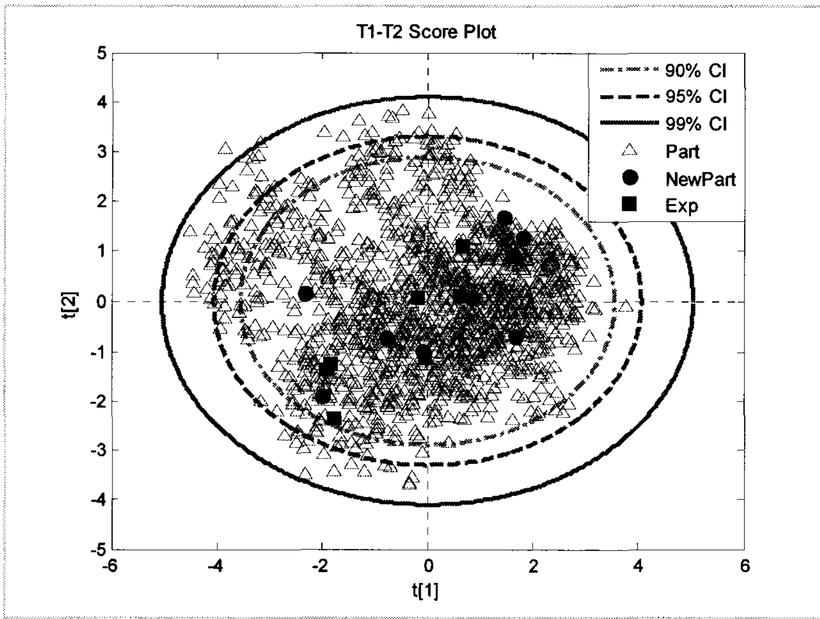

Figure 4.29: Score plot showing T1-T2 scores of process data (not including temperatures). Also shown are the scores for new parts and process fault experiment parts.

Throughout all of the experimentation and data acquisition performed, there was only one part that was loaded in such a way that the outcome was not catastrophic but the part was of noticeable poor quality. For comparison purposes, the machined features of two parts showing a good part and a miss-loaded part were given in Figure 4.30 and Figure 4.31, respectively. It should be noted, however, that the following data was acquired during at a later date, and in the mean time the spindle speed of the Bore tool was increased from 7,000RPM to 8,000RPM. For this reason, the previous model cannot be used for the newer data and a new model was built for this purpose.

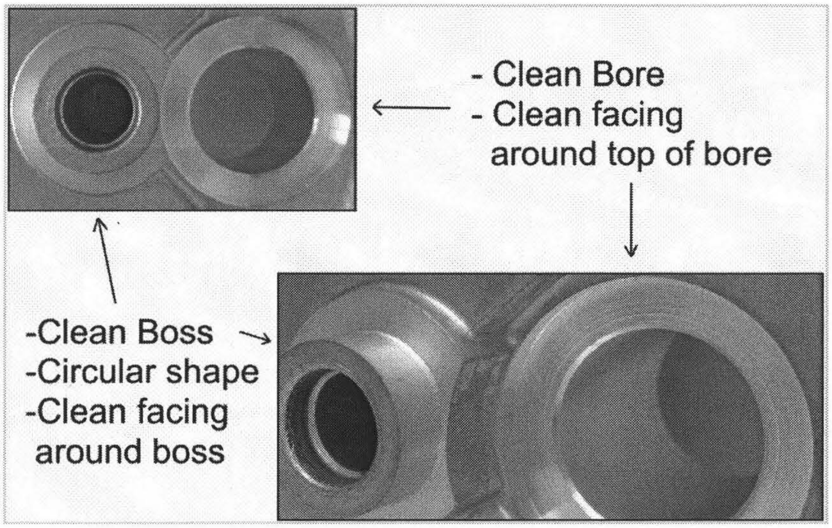

Figure 4.30: Picture showing machined features of a good part.

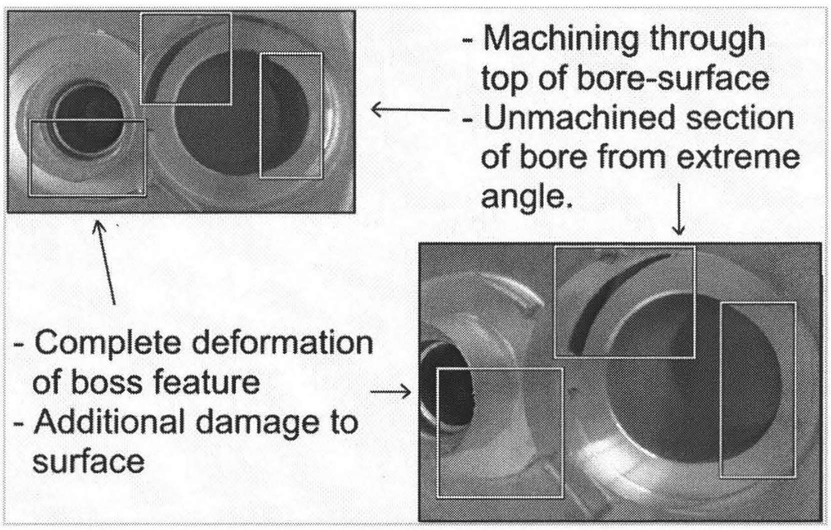

Figure 4.31: Picture showing miss-loaded part with catastrophic failure.

The model built on this new data from 544 parts (not including the temperature variables) consisted of two components with R^2_X=0.547 and Q^2=0.266. Temperature variables were not included in this model to simply illustrate the expected increased vibrations in the model. The bad part was machined in the 141st cycle of the day and was located in nest #2 of fixture 50 (141-52) and occurred in the middle of the day. Process data for this cycle and another cycle were tested against the model to ensure that it is correctly predicting the status of the parts. The plot in Figure 4.32 showed the T1-T2 scores for this model. There were several parts outside of the 99% confidence ellipse, however, these observations account for approximately 1.5% out of the 544 and were not investigated further as it was expected that they were the result of common-cause variation and were not bad quality parts. When the extra data containing the aforementioned bad part was applied to the model, the score plot in Figure 4.33 clearly illustrates how the process information from part 141-52 indicates that there was a problem with this observation as it was located far outside of the 99% confidence ellipse. However, the other three parts shown from this cycle are well within the 99% confidence.

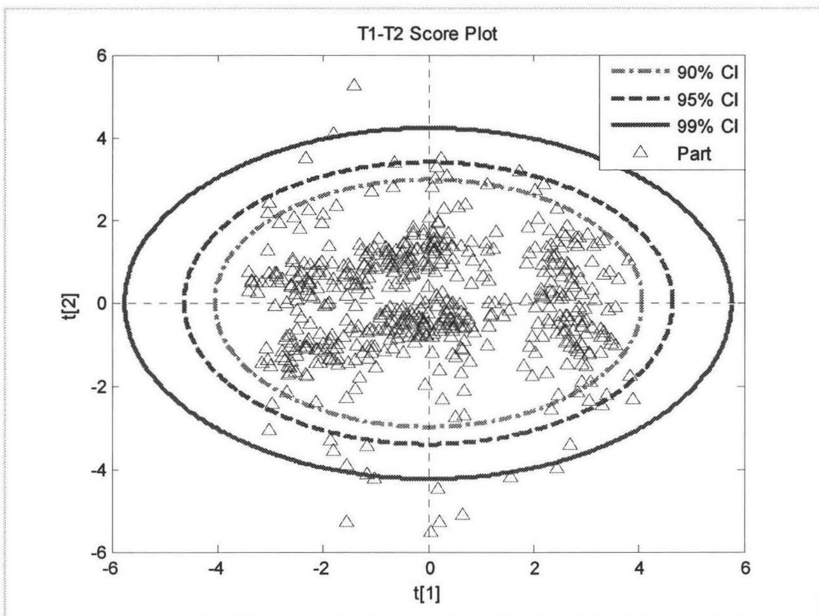

Figure 4.32: Score plot showing t1-t2 scores for 544 parts.

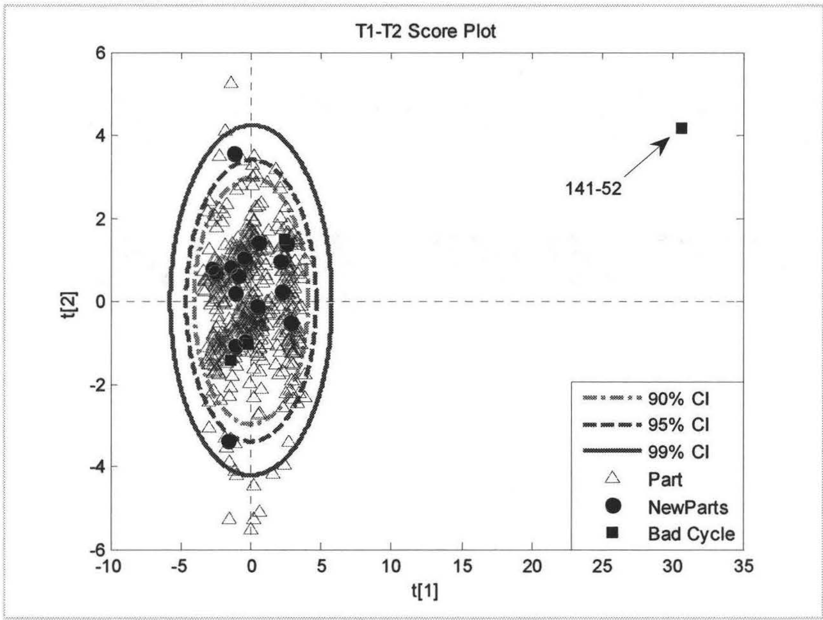

Figure 4.33: Score plot illustrating the known bad part (indicated as 141-52).

Further investigation of this part, using SIMCA software, yielded the contribution plot shown in Figure 4.34. It was clear that the vibrations measured at the spindle frequency have a significant contribution to this distance of the observation from the 99% confidence ellipse. Furthermore, the effects of these measured variables were seen in a picture of the part as shown in Figure 4.35. It is clear that this part was sitting slightly crooked in the fixture and resulted in increased vibrations due to the heavier load of machining extra material which caused the bad part. It should be noted that, this method is superior to using multiple control charts for each parameter as the operator would have to monitor multiple control charts. Furthermore, since the model is made with plant data from common cause variation, it is not possible to determine the individual limits for each parameter as no initial experimentation can be performed to identify these limits.

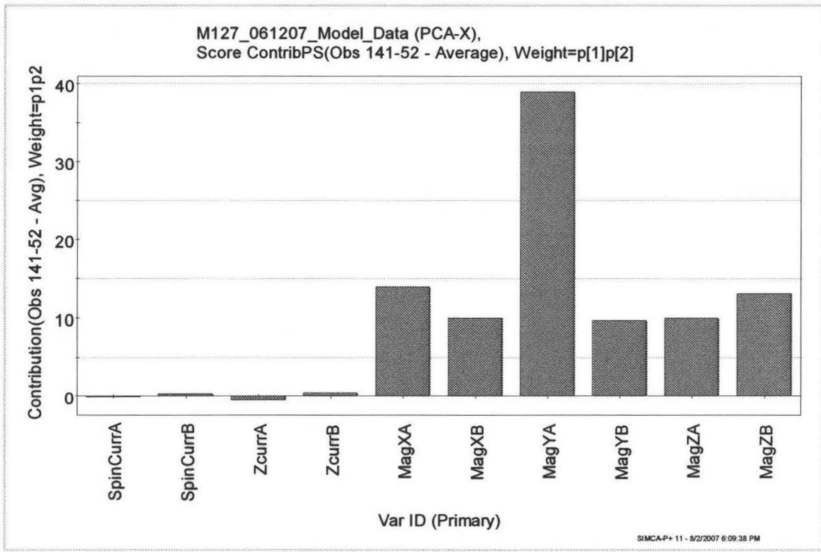

Figure 4.34: Contribution plot for part 141-52.

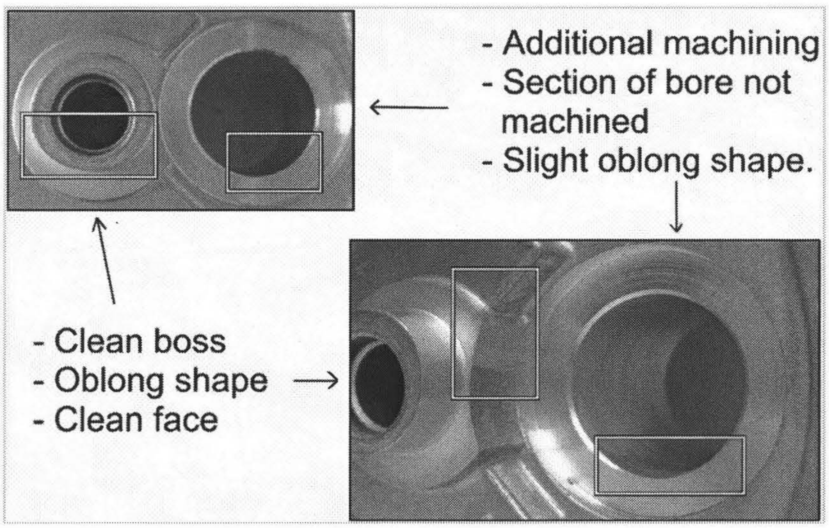

Figure 4.35: Picture showing machined features of part 141-52.

As process faults are generally known to occur, and since 100% inspection is rarely practiced in industry, it would normally be possible for part 141-52 to make it through an automated quality control system or even a manual quality control system.

The described process monitoring system was capable of detecting non-catastrophic process faults; however, its sensitivity was limited as it could not detect the proposed experimentally simulated process faults as the allowable thickness of the shims was on the order of the variation of the cast parts.

4.2.1.2 Simple Control Charts

Simple control charts, whether presented to a human or computer, are an effective way of determining if a process is bad or at least that product requires further inspection. As described in section 2.4.3, two popular control charts, used in tandem, are the Hotelling's T^2 and Squared Prediction Error control charts. The upper control limits (UCLs) are computed using equations 2.5 and 2.9, respectively, where observations that exist below the UCL can be considered "good" and observations above the UCL can be considered "bad." Unlike the score plots shown in the previous section, only 95% and 99% confidence intervals will be shown. Two examples of these control charts are shown in figures 4.37 and 4.38 and illustrate the case where good process was observed and where bad process was observed. As in the score plot of Figure 4.32, there are several observations that appear over the 99% UCL. While Hotelling's T^2 statistic indicates the distance of the observation from the origin model plane, the squared prediction error indicates the perpendicular distance of the observation from the model plane indicating a new type of event not included in the model (Kresta, MacGregor, & Marlin, 1991), part 141-52 was both far from the origin of the model plane and high off the plane which further showed how this observation did not belong with the model. It was shown that simple multivariate control charts were effective at illustrating the state of the process.

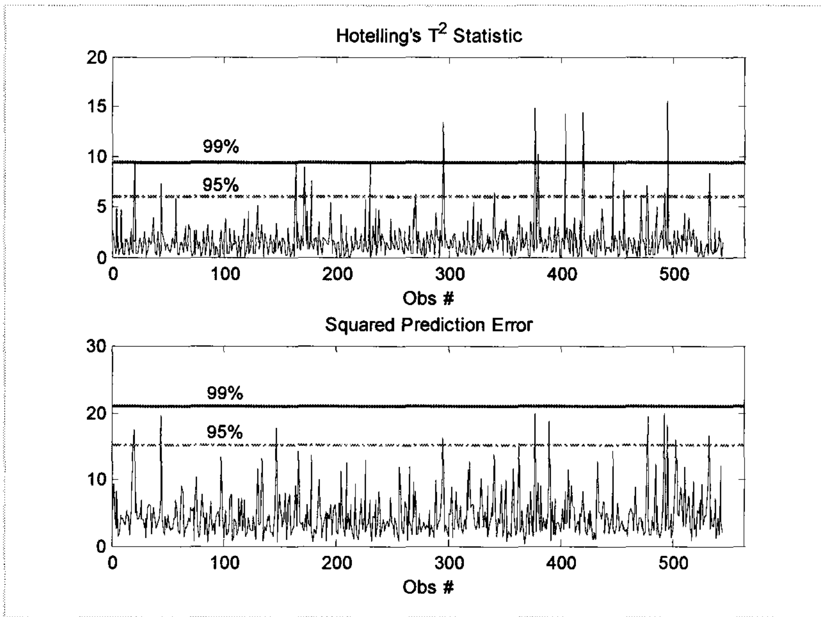

Figure 4.36: Simple control charts illustrating common cause variation.

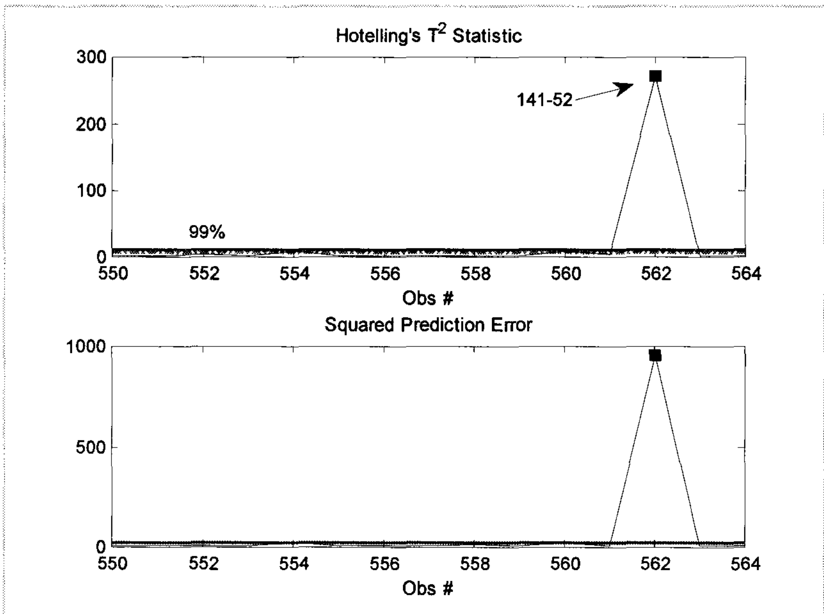

Figure 4.37: Simple control charts illustrating how bad part 141-52 is handled.

4.2.1.3 PLS on Process and Quality Data

It can be very useful to be able to predict quality data from the process data and many studies have performed this task in the laboratory. As previously mentioned, however, CMM inspection takes a lot of time when compared to machining and it was not possible to obtain a sample of parts that included all eight parts from each cycle over an entire day for two reasons: inspection would take a long time and parts need to be packaged for shipment.

The samples used in this investigation were acquired every 15 minutes across two days totaling 84 parts. The initial PCA performed on this data (not shown) set yielded a model with four components with R^2_X=0.663 and Q^2=0.358. While this did not provide as good of a model as the first PCA model of process data in the previous sections, fewer observations were used and now noise the process signal data and the variation in the quality data is being modeled. When PLS was applied to these data with the regular process data with 18 X-variables and the six Y-variables, a model with three components with overall fit R^2_Y=0.408 and Q^2=0.335. The relatively poor model fit indicates that there was much noise in the data and the low predictive ability indicated a poor model. The summary of the variable fits was shown in Figure 4.38 and all of the Y-variables had an R^2 that was below 0.5. To further illustrate the fit of these variables, the individual Observed vs. Predicted plots were shown in Figure 4.39.

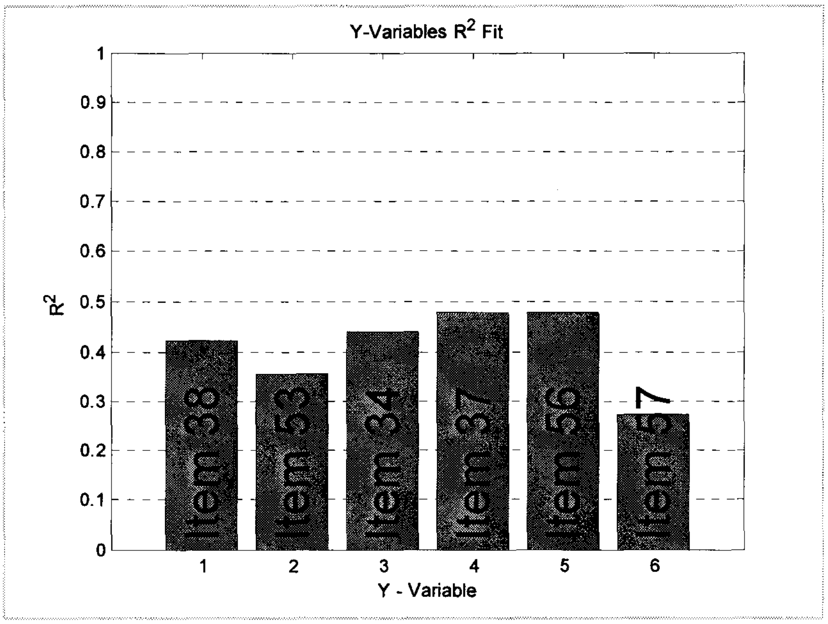

Figure 4.38: Summary of the fit of the individual Y-variables.

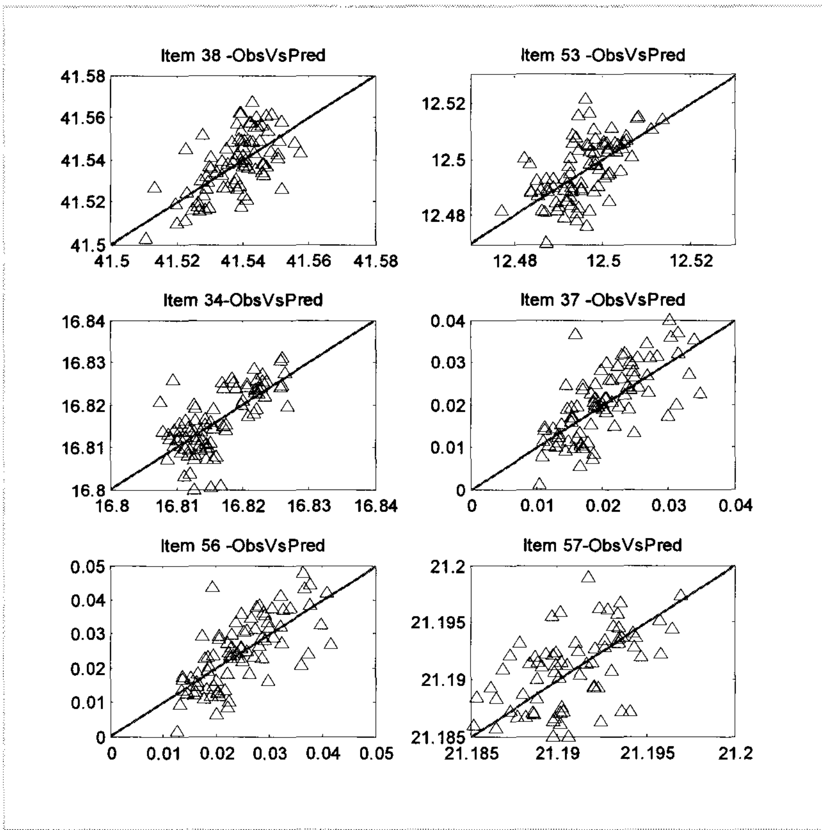

Figure 4.39: Observed vs. Predicted plots for all Y-variables.

One concern with this model was that temperatures were being modeled and had similar trends as in Figure 4.10, for example, but the quality parameters such as Item 38 and Item 53 are heights of the Boss and Bore features and were within tolerances. For this reason, the values of the corrected machine offsets (as used in section 4.1.2) are included in the same model which now contains 20 X-variables. This model also had three significant components with R^2_Y=0.422 and Q^2=0.347. The fit of the individual variables was shown in Figure 4.40 and when compared to the variable fits of Figure 4.38 it can be seen that this model was slightly better than the previous one; however, all variable fits are still below 0.5. Further investigation via Observed vs. Predicted plots illustrates how this model does not provide very good prediction accuracy.

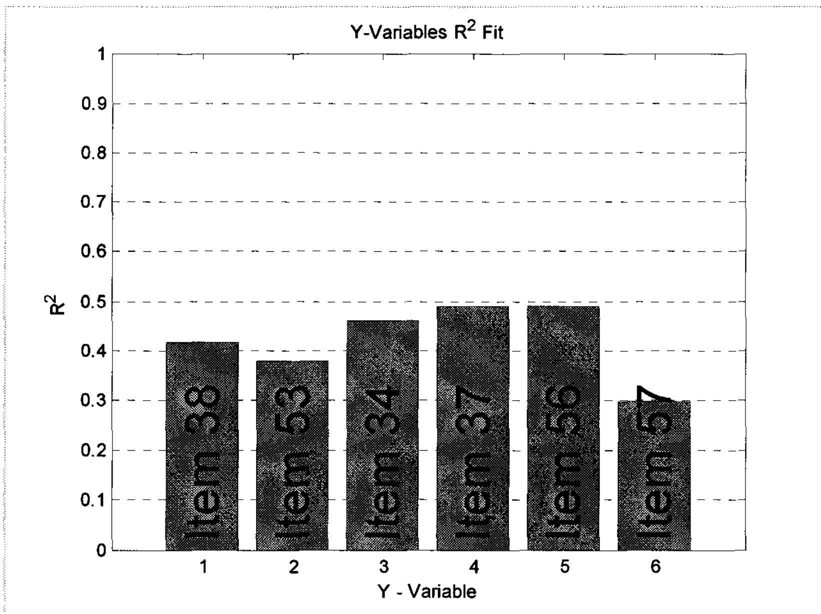

Figure 4.40: Summary of the fit of the individual Y-variables with offset information included in the model.

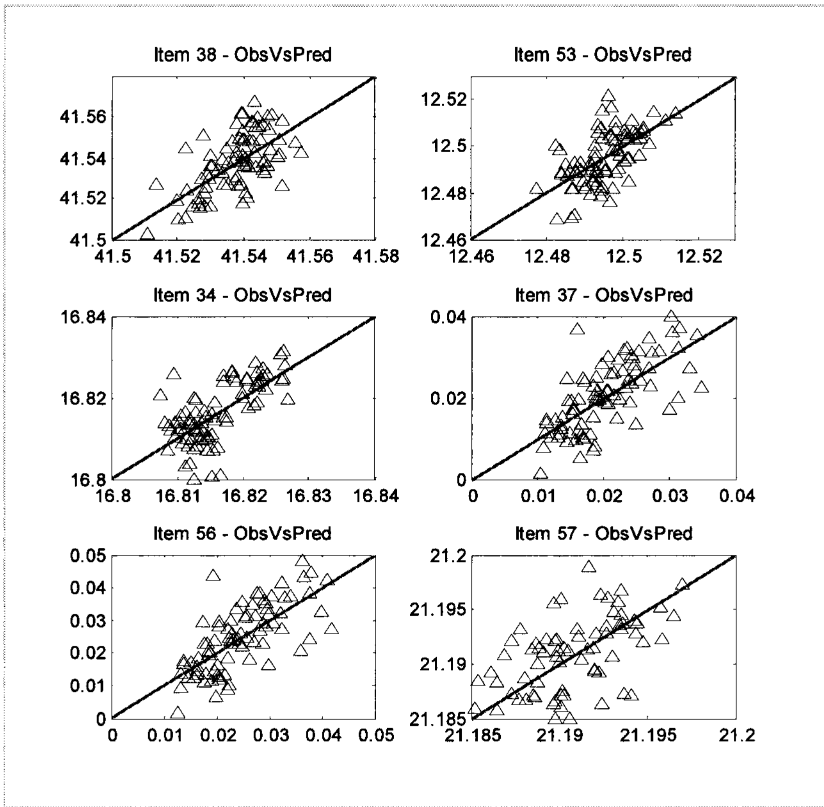

Figure 4.41: Observed vs. Predicted plots for all Y-variables with offset information in the model.

Using the Variable Importance for the Projection (VIP) plot as a diagnosis tool, it was be possible to see the variables that were most responsible for the fit of the model, with variables that were greater than 1 being strong predictors and variables that were less that 0.5 being unimportant (Eriksson, Johansson, Kettaneh-Wold, & Wold, 2001). The VIP plot in Figure 4.42, sorted in descending order of importance, showed the last four variables with little influence on the model. These variables were removed in an attempt to prune the model and create a better fit.

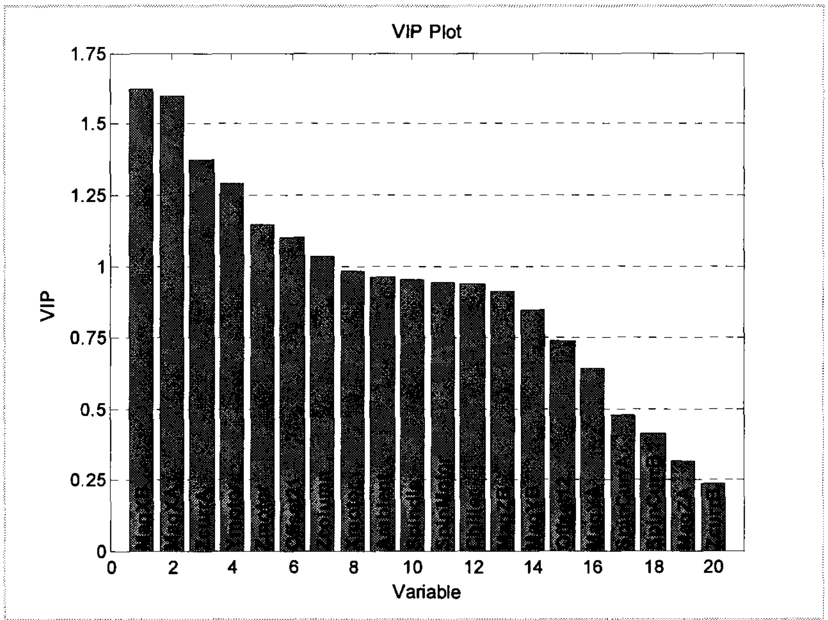

Figure 4.42: VIP Plot summarizing the importance of the variables when modeling this machining process.

With the variables *SpinCurrA*, *SpinCurrB*, *MagZA*, and *ZcurrB* removed, the model now consisted of six components R^2_Y=0.536 and Q^2=0.401 and an average 30% improvement in individual Y-variable fit, as shown in Figure 4.43. The new VIP plot, in Figure 4.44, showed all variables having a VIP value of at least 0.75 indicating they were all of importance to the model. Finally, the observed vs. predicted plots of all the quality parameters under the new model are shown in Figure 4.45 and a marginal improvement was obtained in the modeling of these parameters.

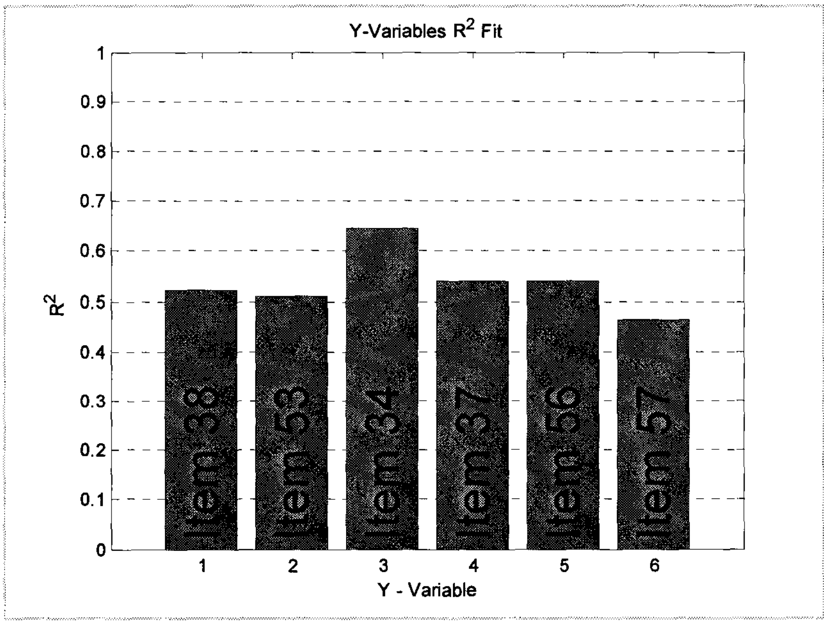

Figure 4.43: Summary of Y-variable fits after model pruning.

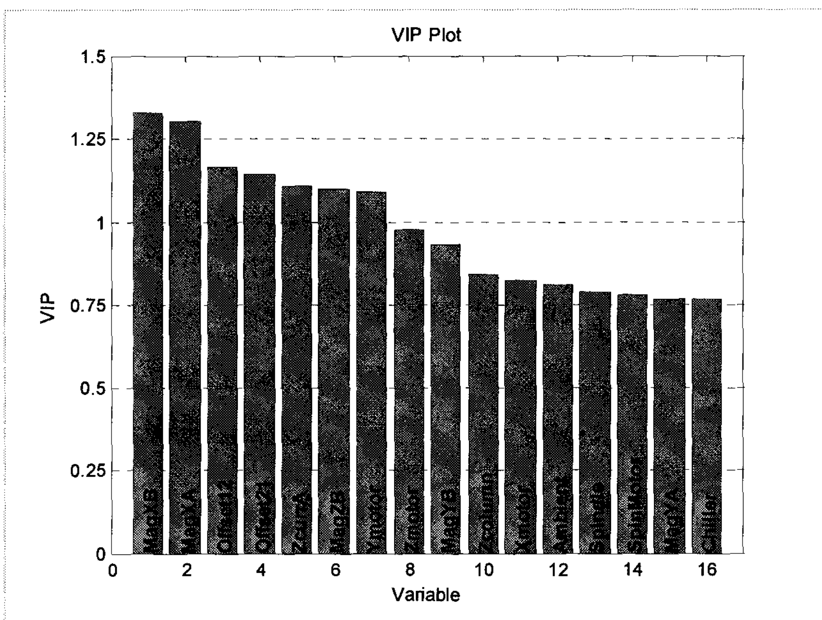

Figure 4.44: VIP plot after model pruning.

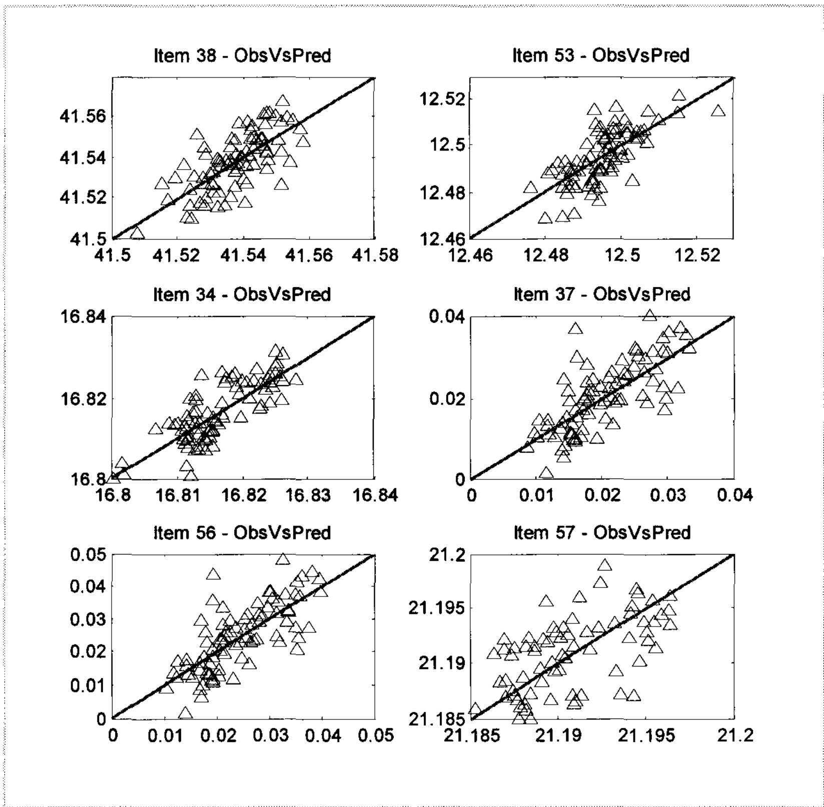

Figure 4.45: Observed vs. Predicted plots for quality parameters under new model.

While this sample of data represented only a small portion of the data acquired throughout experimentation, it provided an adequate picture of the ability of this sensor fusion system to predict the quality parameters of this part; therefore, further investigations into the modeling of additional data were not included here. Looking at Figure 4.41 and Figure 4.45 it is clear that there is a noticeable error in the modeling of these parameters; however, it should be noted that all of the predictions of quality parameters were within the specified tolerance limits as listed in Table 3.2.

4.3 Summary

Throughout the analysis in this section there have been several key contributions. Modeling of the thermal distortion of the machine was successful in holding the machine to within tolerance via real-time thermal error compensation. Furthermore, identification and modeling of the lag between the expansion of the Z-axis and the measured surface temperatures was significant for accurately predicting the behaviour of the machine. While the modeling of process parameters with the described sensor fusion system was not sensitive enough to capture simulated process faults, it was still capable of detecting more drastic process faults. This detection was important in preventing poor quality parts from shipping to the customer and was illustrated through the use of simple control charts. Finally, the modeling of quality parameters with the measured process data proved to have considerable prediction error. All of the predicted values, however, were within specified tolerances in this case.

Chapter 5 – Implementation

5.1 Structure of the Data Collection Environment

With the implementation of a process monitoring system in any high volume production environment, it was important to keep track of the parts in order to accurately associate process and quality information to the parts. This task becomes more demanding when multiple machines were being used to manufacture the same part. Nixon Integrated was an excellent site for beta testing the implementation of this process monitoring system because there are multiple machines manufacturing the same parts and it was a medium-high volume production environment. While the implementation described here was somewhat specific to the conventions used at Nixon, the principles can be generalized and applied to any site.

The parts at Nixon had several identification parameters that can be applied. The first was the machine number where the machines were identified by a three digit number. The next items that could used to identify the part were the date and time the part was made. A simple 24 hour clock and Month-Day-Year convention were used here.

As previously described in section 3.2, each machine has a rotary fixture enabling a cycle of parts to be machined while the operator is loading/unloading and inspecting parts. Each fixture is indentified by a single digit with each nest location being labeled from 1-8.

When the data from the parts are preprocessed the data was then saved in the following convention:

- M***-MMDDYY-HHMM-X#

where *** represents the machine number, in this case machine #127 was used; MMDDYY were the month/day/year; HHMM was the 24-hour clock format of hour and minutes; X represents the table #, in this case 5 or 6; and, # represents the nest number where the part was located on the fixture. The following is an example of the text file containing process information for a part:

- M127-061207-1421-53.txt

Files were stored in folders that were created daily and were named by the date in the same MMDDYY format. Data was stored in individual text files for each part, and each machining cycle was also stored in a Matlab MAT-file; however, since the entire cycle was stored in the MAT-file the # in the file name is simply left as zero (0). Once the data was processed and stored, the appropriate post-processing was completed in order to present the data in the control charts that were on a computer screen that is visible to the operator. This process was summarized in the flow chart that was presented in Figure

5.1. This process monitoring system still requires some manual intervention and all of the CMM inspection was also performed manually. Furthermore, it was up to the CMM operator to correctly identify the part as indicated on the control charts display, as there is no ID that is physically stamped on the part.

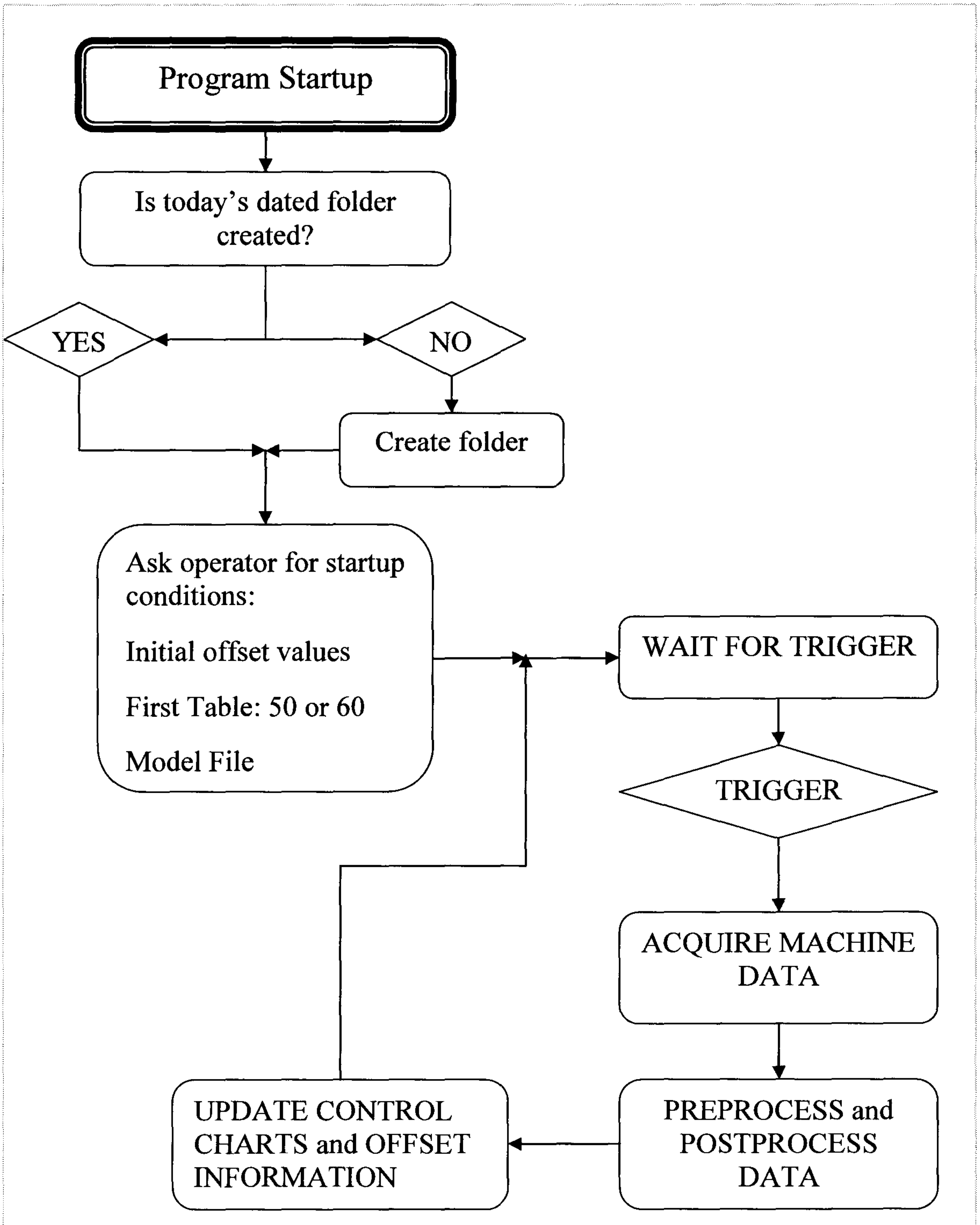

Figure 5.1: Process monitoring program flow chart.

5.1.1 Networking

In order for the data to be available to the CMM inspector and the Mitutoyo MCOSMOS CMM software, the acquisition must be connected to the company network. Through the use of Microsoft Windows networking, a network drive could be created on the CMM's PC which points to the location of the data folders on the process monitoring PC in the factory floor. The CMM program that was created in MCOSMOS pointed to this drive location when looking for data.

5.1.2 CMM software

Using the GEOPAK Part Program Editor, it was possible to perform a variety of additional functions that allow the input of information from text files, access to additional programs within Windows, and much more. Using these features, it is possible to extract the process information that is saved on a networked location of the process monitoring PC. One of the requirements of the CMM operator not previously mentioned is the need to input the cavity ID that is stamped in the part from the die of which the part was produced in the casting plant. As a form of quality control, only a certain range of cavities are allowed on one machine and this is used to determine which machine the parts were made. The current manual implementation of the CMM software involves the operator inputting some information as prompted by MCOSMOS, mainly:

- Cavity ID
- Nest ID
- Production Date/Time of part, as indicated by process monitoring system.

Using only these inputs, it was possible to uniquely create the file name of the text file holding the process information, as described in section 5.1. Furthermore, all of the data entered in the text file was input as strings and needed to be converted to numerical values using the '@' prefix. Finally, in order to get this information into the Mitutoyo MeasurLink statistical software package, each variable must be listed as a "Tolerance variable" and the option of inputting, nominal and upper/lower tolerance values is available. Setting a variable to have this property tells MCOSMOS to export these data to the statistical program; in this case, MeasurLink. The main goal here is that MeasurLink provides a tool for the 'warehousing' of the data. Once the database of process information was created, anyone could extract the data and perform multivariate analysis similar to what was done throughout this thesis. The MCOSMOS program used to illustrate this data acquisition technique was located in Appendix B.

5.1.3 Integration in an Automated Environment

While the previously mentioned system satisfied the requirements of the environment at Nixon Integrated, this process differs in a plant where a fully automated production/inspection system is implemented. In order for this system to function in this environment, the integration into the system's PLC will be required to keep track of the parts that are manufactured. While a full description of implementation in this type of setting was not performed, a simplified proposal of this system is presented here.

This system involves the use of a robot collecting parts from each machine and dispensing them to a centralized location. The parts would be placed in a queue as they await inspection. While in the queue, parts could be stamped with the serial number of the format that is presented in section 5.1. The PLC can communicate with the inspection system and provide it with the list of parts in the queue. As previously mentioned, the inspection of this part is time consuming, so parts can be inspected in time intervals. Furthermore, using the process monitoring system parts can be flagged for additional inspection if the process data analysis suggests a problem. This implementation is outlined in the flow chart located in Figure 5.2.

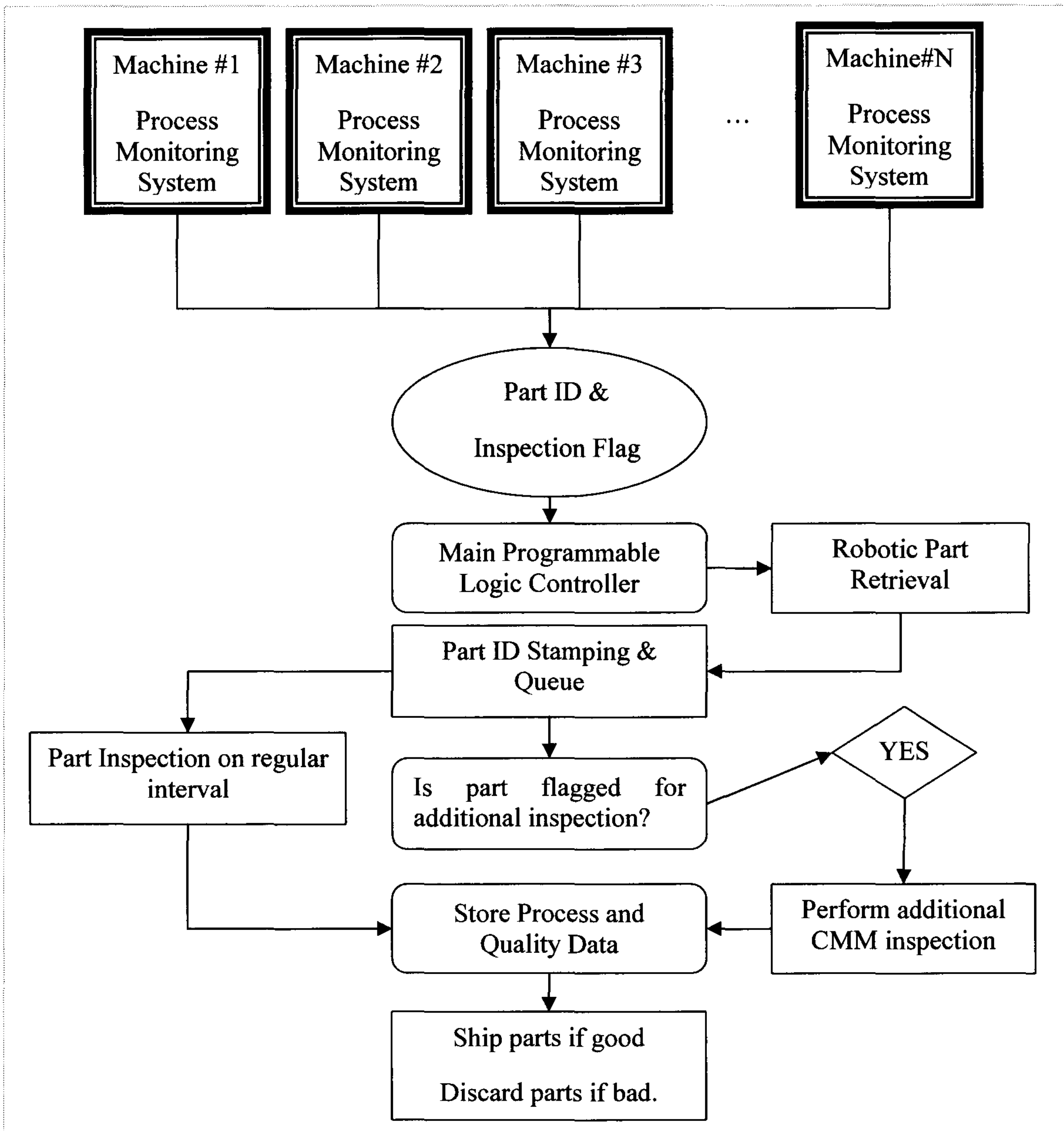

Figure 5.2 Proposed design for automated process monitoring and inspection system with process and quality data storage.

The proposed automated system would still use the same conventions for acquiring the data from each process monitoring system through the MCOSMOS CMM software as described in section 5.1.2.

5.2 Development of Process Monitoring System

The process monitoring system used information that was from a model created using offline historical data that was known to result in good parts and have experienced common-cause variation. Based on the results described in section 4.2, a process monitoring system developed on process data using PCA is presented here.

There are some key data requirements for the process monitoring system to represent the multivariable data in the simple control charts, such as Hotelling's T^2 and SPE charts. At the beginning of program start up, the operator was prompted to select a model file and the summary of model file contents are listed in Table 5.1.

Table 5.1: List and description of model file variables.

Variable Name	Description
xMean	Model Mean (for mean centering of data)
xStd	Model Standard Deviation (for scaling to unit variance
T2Crit	Vector of Hotelling's T^2 statistic critical confidence limits (e.g. 90%, 95%, and 99%)
SPECrit	Vector of SPE critical confidence limits (e.g. 90%, 95%, and 99%)
tVar	1 x A vector of t-score variances (A = model dimension, a.k.a. # of components)
p	K x A vector of model loadings (K = # of variables in model).

The new data was first mean centered and scaled to unit variance and then the new scores were computed using the following equation that is adapted from equation (2.3), previously given in equation (2.4) and is shown again as equation (5.1).

$$t_{new} = X_{new} p \tag{5.1}$$

Where t_{new} are the new scores and X is the new data that has been mean centered and scaled to unit variance. The new Hotelling's T^2 statistic can be computed similar to that in equation (2.9), as equation (5.2).

$$T_{new}^2 = \sum_{a=1}^{A} \frac{t_{new,a}^2}{s_{ta}^2} \tag{5.2}$$

where T^2_{new} is the Hotelling's T^2 statistic for the new part, s^2 is the variance of the *t*-scores as submitted by the model and A is the number of components in the model.

As indicated by equation (2.11), the computation of SPE involves the subtraction of the predicted values of the data, $\hat{X}$, from the actual values of X. The computation of the predicted values, previously given in equation (2.5), is again shown in equation (5.3).

$$\hat{X}_{new} = t_{new} p^T \tag{5.3}$$

Using the two control charts in tandem, the implemented process monitoring system looks similar to the charts shown in Figure 4.36. Also, on the display are the current Z-axis offset values and predictions. There is a button located on the screen labeled "Update Z-Offsets" which enables the operator to manually change the value of the offsets if a tool change or other manual adjustments are required. Note the green box around the latest machining cycle, indicating a good set of parts. An example of the process monitoring system is presented in Figure 5.3.

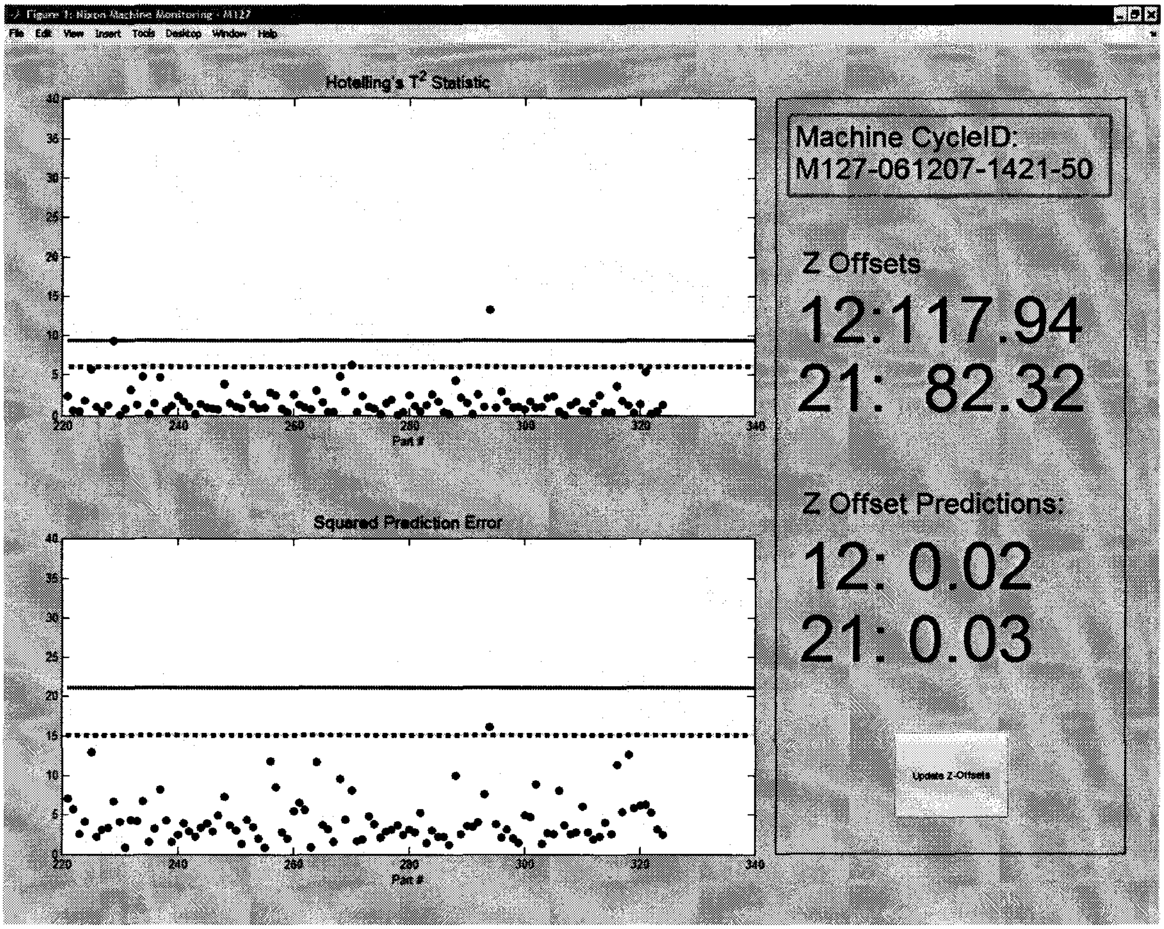

Figure 5.3: Typical process monitoring system display for the operator.

5.3 Multivariate Software

All of the code used in the implementation of this process monitoring system were developed using Matlab v2006a. Matlab provides an extensive set of tools for creating and manipulating user interfaces and is excellent for handling large matrices of data which are typical of these kinds of processes.

The codes for the various parameters and algorithms as discussed in section 2.4, including the NIPALS algorithm were implemented in Matlab with great success. As a metric for comparing the results of the codes used here, values of the scores are compared to those computed using SIMCA-P+ v11. Using the data from the example presented in section 4.2.1.1 with 544 data points and 10 variables, the score and loading vectors from one component are compared and presented in Table 5.2. It should be noted, however, that SIMCA only stores data holding six significant digits. These results are impressive as the NIPALS algorithm written in Matlab has a convergence limit set at $1x10^{-5}$ and all values are held in double precision floating point matrices. The precision of the variables and the NIPALS convergence limit used in SIMCA is not known.

Table 5.2: Comparison of PCA model from SIMCA and Matlab codes.

Error Type	T-score	P-loading
RMS	$1.837614x10^{-5}$	$4.250673x10^{-6}$
MEAN	$1.298382x10^{-7}$	$-2.494997x10^{-7}$
ACCURACY	99.99997%	99.995594%

For general analysis purposes, the codes completed for this thesis produce acceptable results, with the only drawback being a lack of user interface developed for them, which was not necessary at this stage and was thus beyond the scope of this project.

Chapter 6 – Conclusions

6.1 Overview

Presented in this thesis is the successful implementation of a fully featured machining process monitoring system based on multivariate statistical techniques. Concluding remarks on the individual key findings will be presented with some ideas for future work.

6.2 Thermal Error Compensation

The strategy that was presented for the compensation of thermal errors during production was both successful and practical. After the initial modeling of the thermal expansion of the Z-axis to characterize its behaviour, the modeling of this quantity during production through indirect measurements made on the parts proved to be successful regardless of the noise in the dimensional measurements arising due to the roughness of the casting surfaces. Furthermore, it was determined that the temperature measurements lag behind the thermal error by about 5-10 minutes in real time and the use of lagged error measurements are used to compensate for this behaviour.

Two cases that illustrated the performance of the modeling of thermal errors were presented. The first case where a model based on thermal measurements, all from one, day is applied to the data of the next day. In this case, the predicted data from the two measurements in the Z-axis for the second day fit the real data with an R^2 of 0.843 and 0.872, for the boss and bore measurements, respectively, and both of these quantities had an RMSEE of 0.008. The second case involved the use of half of the data from two different days to create a model. In this case, odd number data points were used in the model for the work set and even numbered data points were used in the test set for predictions. The idea of this model was to incorporate data from multiple days, and test it with data from days which experienced similar behaviour to assess performance. With the proposed automatic compensation strategy, both models were shown to hold the quality parameters to within ±0.02 while the tolerance for this part is ±0.05mm.

6.3 Machine Process Data Modeling

For the modeling of the machine process data, there were two main sections: modeling of process data with PCA and modeling quality data from process data with PLS. For the case where only the process data is modeled, PCA models were shown to be effective at capturing the main effects of the process. While the model was shown to not have the sensitivity required for detecting the minor faults performed during the experimental simulations, it was successful in detecting the one case where an actual non-catastrophic part miss-load occurred. The contribution plots identified the vibrations as being much higher than the nominal. Furthermore, when the process data from known good parts were applied to the model, the model made no false predictions as to their process state and they would all have been classified as "good parts." The use of the simple control charts is illustrated in the detection of poor process conditions for presentation to operators. Unfortunately, due to the fact that effort is placed on constantly making good parts, there were no other opportunities for detecting these major defects.

The modeling of the quality data, however, using PLS proved to be moderately successful. The first attempt at modeling the data proved to be challenging as both process and quality data contained noise from the common variation that was inherent in the process and the imprecise nature of aluminum cast parts. Investigation into this model led to its pruning which involved the removal of four process variables from the model; shown to be of little importance. This effectively improved the fit of the quality variables by an average of 30%; however, the variable with the best fit still only had an R^2 of 0.645. Although the plots showing observed vs. predicted values of the quality variables did not appear to be of the greatest accuracy, it should be noted that not one of the observations received a false prediction where the part is said to be out the tolerance specifications.

6.4 Implementation

While modeling of process data is an excellent tool for the investigation of machining processes, a plan for implementation must be developed which is compatible with medium to high production processes. The implementation software written in Matlab and a description was provided as to how it was integrated with commercially available software supplied by Mitutoyo for data storage. Process and quality data are associated to parts via simple part tagging conventions and a proposed plan for this implementation in an automated setting was provided. Furthermore, results obtained through the codes developed for this work were compared to commercially available multivariate software with excellent accuracy.

6.5 Future work

Although one of the challenges of this work was implementing a process monitoring system where the process and quality parameters are inherently noisy, better modeling results may be achieved if an industrial machining process where all of the quality parameters are machined is investigated. This will ensure that most of the noise associated with the quality of the parts is generated during machining and not by other processes which are outside of the control of the machining process such as aluminum die casting.

Another point of interest is the vast amount of data that is collected from the vibration signals. The analysis performed here only considered the magnitude of the frequency at the spindle speed because of the limitations on data storage capabilities. In the case where thousands of parts are made in a day, storing all of the vibration data for every part is not practical so, the selection of only a few important pieces of information was done. There is much more information, however, with regards to the state of the process within the entire frequency spectra. Handling this data could be performed using hierarchical multi-block PCA and PLS techniques that are presented by Westerhuis *et al.* (1998). Through this analysis, it is expected that the principal components would explain the variation in the frequencies that are causing the most variation, while ignoring those that provide no additional information.

References

Albrecht, A., Park, S. S., Altintas, Y., & Pritschow, G. (2005). High frequency bandwidth cutting force measurement in milling using capacitance displacement sensors. *International Journal of Machine Tools & manufacture*, *45*, 993-1008.

Attia, M., & Kops, L. (1993). Thermometric design considerations for themperature monitoring in machine tools and CMM structures. *International Journal of Advanced Manufacturing Technology*, *8*, 311-319.

Automotive Industrial Action Group. (2005). *Statistical Process Control - Second Edition.* Southfield, Michigan: AIAG.

Axinte, D., Gindy, N., Fox, K., & Unanue, I. (2004). Process monitoring to assist the workpiece surface quality in machining. *International Journal of Machine Tools & Manufacture*, *44* (10), 1091-1108.

Azouzi, R., & Guillot, M. (1996). On-line Predictionof Surface Finish and Dimensional Deviation in Turning Using Neural Network Based Sensor Fusion. *International Journal of Machine Tools and Manufacturing*, *37* (9), 1201-1217.

Bering, T. (2003). *SPC-Based Supervisory Controller for Closed Loop Machining.* Master of Engineering Dissertation, McMaster University.

Burnham, A. J., MacGregor, J. F., & Viveros, R. (1999). Latent variable multivariate regression modeling. *Chemometrics and Intelligent Laboratory Systems*, *48*, 167-180.

Byrne, G., Dornfeld, D., Inasaki, I., Ketteler, G., Konig, W., & Teti, R. (1995). *Annals of the CIRP*, *44*, 541-567.

Chen, J. (1996). Neural Network-based Modelling and Error Compensation of Thermally-induced Spindle Errors. *International Journal of Advanced Manufacturing Technology*, *12*, 303-308.

Chen, J., & Ling, C. (1996). Improving the Machine Accuracy Through Machine Tool Metrology and Error Correction. *International Journal of Advanced Manufacturing Technology*, *11*, 198-205.

Chen, J., Yuan, J., & Ni, J. (1996). Thermal Error Modelling for Real-Time Error Compensation. *The International Journal of Advanced Manufacturing Technology*, *12*, 266-275.

Chen, S.-L., & Jen, Y. (2000). Data fusion neural network for tool condition monitoring in CNC milling machining. *International Journal of Machine Tools & Manufacture*, *40*, 381-400.

Dimla, D., & Lister, P. (2000). On-line metal cutting tool condition monitoring. I: force and vibration analyses. *International Journal of Machine Tools & Manufacture*, *40* (5), 739-768.

Eriksson, L., Johansson, E., Kettaneh-Wold, N., & Wold, S. (2001). *Multi- and Megavariate Data Analysis.* Umeå, Sweden: Umetrics.

Grunge, B., & Manne, R. (1998). Missing values in principal component analysis. *Chemometrics and Intelligent Laboratory Systems*, *42*, 125-139.

Huessin, W. (2007). *Machining Process Monitoring Using Multivariate Latent Variables Methods.* Ph.D. Dissertation, McMaster University.

Inasaki, I., & Tönshoff, H. (2001). *Sensors Applications - Volume 1: Sensors in Manufacturing.* New York: Wiley-VCH Verlag GmbH.

Jackson, J. (1991). *A User's Guide To Principal Components*. New York: John Wiley & Sons, Inc.

Jackson, J., & Mudholkar, G. (1979). Control Procedures for residuals associated with principal component analysis. *Technometrics*, *21* (3), 341-349.

Jeong, Y.-H., & Cho, D.-W. (2002). Estimating cutting force from rotating and stationary feed motor currents on a milling machine. *International Journal of Machine Tools & Manufacture*, *42*, 1559-1566.

Kourti, T., & MacGregor, J. (1996). Multivariate SPC Methods for Process Monitoring and Product Monitoring. *Journal of Quality Technology*, *28* (4), 409-428.

Kourti, T., & MacGregor, J. (1995). Process analysis monitoring and diagnosis using multivariate projection methods. *Chemometrics and INtelligent Laboratory Systems*, *28*, 3-21.

Kresta, J., MacGregor, J., & Marlin, T. (1991). Multivariate Statistical Monitoring of Process Operating Performance. *The Canadian Journal of Chemcial Engineering, 69*, 35-47.

Li, W., Li, D., & Ni, J. (2003). Diagnosis of tapping process using spindle motor current. *International Journal of Machine Tools & Manufacture*, *43* (1), 73-79.

Liang, S. Y., Hecker, R. L., & Landers, R. G. (2004). Machining Process Monitoring and Control: The State-of-the-Art. *Journal of Manufacturing Science and Engineering, 28*, 297-310.

Lo, C.-H., Yuan, J., & Ni, J. (1995). center, An application of real-time error compensation on a turning. *International Journal of Machine Tools and Manufacture*, *35* (12), 1669-1682.

MacGregor, J., & Kourti, T. (1995). Statistical process control of multivariate processes. *Control Engineering Practice*, *3* (3), 403-414.

Mathews, P., & Shunmugam, M. (1999). Neural-network approach for predicting hole quality in reaming. *International Journal of Machine Tools & Manufacture*, *39*, 723-730.

Nomikos, P., & MacGregor, J. (1995). Multivariate SPC charts for monitoring batch processes. *Technometrics*, *37* (1), 41-59.

OMEGA. (n.d.). *OMEGA's Temperature Technical Reference Section.* Retrieved July 16, 2007, from Using Thermocouples: http://www.omega.com/temperature/Z/pdf/z021-032.pdf

Ramesh, R., Mannan, M., & Poo, A. (2000). Error Compensation in machine tools - a review Part I: geometric, cutting-force induced and fixture-dependent errors. *International Journal of Machine Tools & Manufacture*, *40*, 1235-1256.

Ramesh, R., Mannan, M., & Poo, A. (2000a). Error Compensation in machine tools - a review. Part II: thermal errors. *40*, 1257-1284.

Ramesh, R., Mannan, M., & Poo, A. (2003). Thermal error measurement and modeling in machine tools. Part I. Influence of varying operating conditions. *International Journal of Machine Tools & Manufacture*, *43*, 391-404.

Sick, B. (2002). On-line and indirect tool wear monitoring in turning with artificial neural networks: A review of more than a decade of research. *Mechanical Systems and Signal Processing*, *16* (4), 487-546.

Spiewak, S. (1995). Acceleration based indirect forcemeasurement in metal cutting processes. *International Journal of Machine Tools & Manufacture*, *35* (1), 1-17.

Statham, A., Martin, A., & Blackshaw, D. (1997). Assiessing the thermal distortion caused by spindle rotation of a machining centre using the draft standard ISO/DIS 230-3. *Transactions Engineering Sciences*, *16*, 101-111.

The American Society of Mechanical Engineers. (2005). *ASME B5.54-2005: Methods for Performance Evaluation of Computer Numerically Controlled Machining Sensors.* New York.

Tlusty, G. (2000). *Manufacturing Processes and Equipment.* Upper Saddle River, NJ: Prentice-Hall.

UMETRICS. (2005). *SIMCA-P+ v.11 Multivariate Analysis Software*. Umeå, Sweden.

Veldhuis, S. (1998). *Modelling and compensation of errors in five-axis machining.* McMaster University.

Veldhuis, S., & Elbastawi, M. (1995). A strategy for the compensation of thermal errors in five-axis machining. *Annals of the CIRP*, *44*, 373-377.

Westerhuis, J. A., Kourti, T., & MacGregor, J. (1998). Analysis of multiblock and hierarchical PCA and PLS models. *Journal of Chemometrics*, *12*, 301-321.

Yan, D., El-Wardany, T., & Elbestawi, M. (1994). A multi-sensor strategy for tool failure detection in milling. *International Journal of Machine Tools and Manufacture*, *35* (3), 383-398.

Yoon, S., & MacGregor, J. (2001). Fault diagnosis with multivariate statistical models part I: using steady state fault signatures. *Journal of Process Controll*, *11*, 387-400.

APPENDIX

Appendix A

When using the SCC-TC02 thermocouple modules in the SC-2345 connector block, from National Instruments (NI), the first eight channels contain the signal from the thermocouple voltage and the last eight channels contained the cold junction compensation (CJC) voltage; i.e. if the thermocouple channel is *X*, then the CJC is on channel *X*+8. The NIST ITS-90 coefficients and method suggested by NI for converting the thermocouple signals to temperatures is listed in the Matlab code provided below:

```
function tempOut = ThermoConvert (tempIn, CJC)
% tempOut = ThermoConvert (tempIn, CJC)
%
% tempOut is the output of the thermocouples in °C.
% For E-type thermocouples.
%
% This function will perform the necessary conversion from voltage
signals
% to temperature values for E-Type Thermocouples using the NIST ITS-
90
% coefficients for E-type thermocouples.  To be used with the NI SC-
2345
% connector box and SCC-TC02 thermocouple modules.
%
% tempIn - The signal voltages from the thermocouples
% CJC - The cold junction compensation values from the thermocouple
modules.
% Darryl Wallace - McMaster University - © 2007
% wallacdj@mcmaster.ca, wallacdj@gmail.com

% NIST ITS-90 Coefficients for thermocouples
% t90=d0+d1*E+d2*E^2+...+dn*E^n     E is in mV
% d0=0;
% d1=[17.057035;];
% d2=[-0.23301759;];
% d3=[0.0065435585;];
% d4=[-0.000073562749;];
% d5=[-0.0000017896001;];
% d6=[0.000000084036165;];
% d7=[-0.0000000013735879;];
% d8=1.0629823e-11;
% d9=-3.2447087e-14;
% Continued ...
```

```
d0=[0;
    17.057035;
    -0.23301759;
    0.0065435585;
    -0.000073562749;
    -0.0000017896001;
    0.000000084036165;
    -0.0000000013735879;
    1.0629823e-11;
    -3.2447087e-14];

%Nist Type E thermocouple Coefficients in mV.
% E90=c0+c1*t+c2*c^2+...+cn*t^n     t is in °C
% c0=0;
% c1=0.586655087100e-1;
% c2=0.450322755820e-4;
% c3=0.289084072120e-7;
% c4=-0.330568966520e-9;
% c5=0.650244032700e-12;
% c6=-0.191974955040e-15;
% c7=-0.12536607970e-17;
% c8=0.214892175360e-20;
% c9=-0.143880417820e-23;
% c10=0.359608994810e-27;
c0=[0;
    0.586655087100e-1;
    0.450322755820e-4;
    0.289084072120e-7;
    -0.330568966520e-9;
    0.650244032700e-12;
    -0.191974955040e-15;
    -0.12536607970e-17;
    0.214892175360e-20;
    -0.143880417820e-23;
    0.359608994810e-27];

%Convert CJC Voltage to temperature.  Then Convert temperature to
%thermocouple voltage.  See NI SCC-TC02 Thermocouple module
documentation.
%
% Coefficients for converting thermistor resistance to Temperature in
°K
% as provided by National Instruments
a=1.295361e-3;
b=2.343159e-4;
c=1.018703e-7;

% Continued …
```

```
% Resistance of thermistor in Ohms as calculated from CJC voltages
Rt=5000*(CJC./(2.5-CJC));
% Computation of CJC temperature in °K
Tk=1./(a+b*log(Rt)+c*log(Rt).^3);
% Conversion to °C
Tc=Tk-273.15;

% Conversion of CJC temperature to E-type thermocouple voltage
equivalent
% Using NIST polynomial coefficients 'c' 0-10
Ecjc=0;
for i=1:11
    Ecjc=Ecjc+c0(i).*Tc.^(i-1);
end

% Preprocess thermocouple voltages.
Vtc=tempIn./100;      % Remove gain from TC module
Vtc=Vtc.*1000;        % Convert to mV, 1000mv/V
Eth=Vtc+Ecjc;         % Add E-type CJC voltage to thermocouple voltage

% Convert thermocouple voltages to temperatures in °C using E-type
% thermocouple NIST polynomial coefficients 'd' 0-9
tempOut=0;
for i=1:10
    tempOut=tempOut+d0(i).*Eth.^(i-1);
end
% function complete
```

Appendix B

Listed here is an example of program code that could be used to implement data acquisition from process monitoring PC's that are already attached to the network. This program code was performed in the graphical environment of the Mitutoyo GeoPak Part Program Editor v3.0.R6. This program illustrates how the data could be acquired, however, from one machine only:

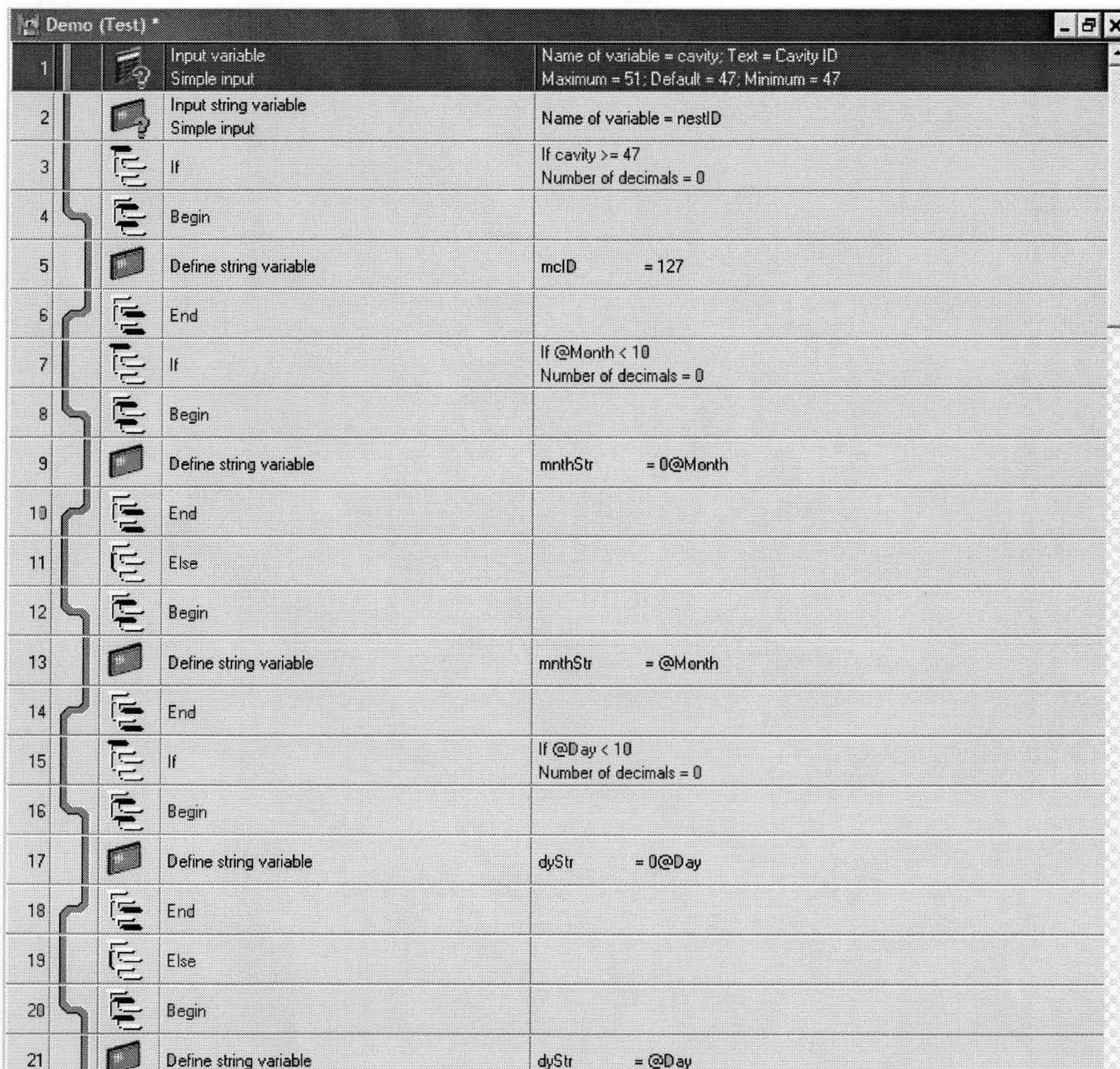

Demo (Test) *

1	Input variable Simple input	Name of variable = cavity; Text = Cavity ID Maximum = 51; Default = 47; Minimum = 47
2	Input string variable Simple input	Name of variable = nestID
3	If	If cavity >= 47 Number of decimals = 0
4	Begin	
5	Define string variable	mcID = 127
6	End	
7	If	If @Month < 10 Number of decimals = 0
8	Begin	
9	Define string variable	mnthStr = 0@Month
10	End	
11	Else	
12	Begin	
13	Define string variable	mnthStr = @Month
14	End	
15	If	If @Day < 10 Number of decimals = 0
16	Begin	
17	Define string variable	dyStr = 0@Day
18	End	
19	Else	
20	Begin	
21	Define string variable	dyStr = @Day

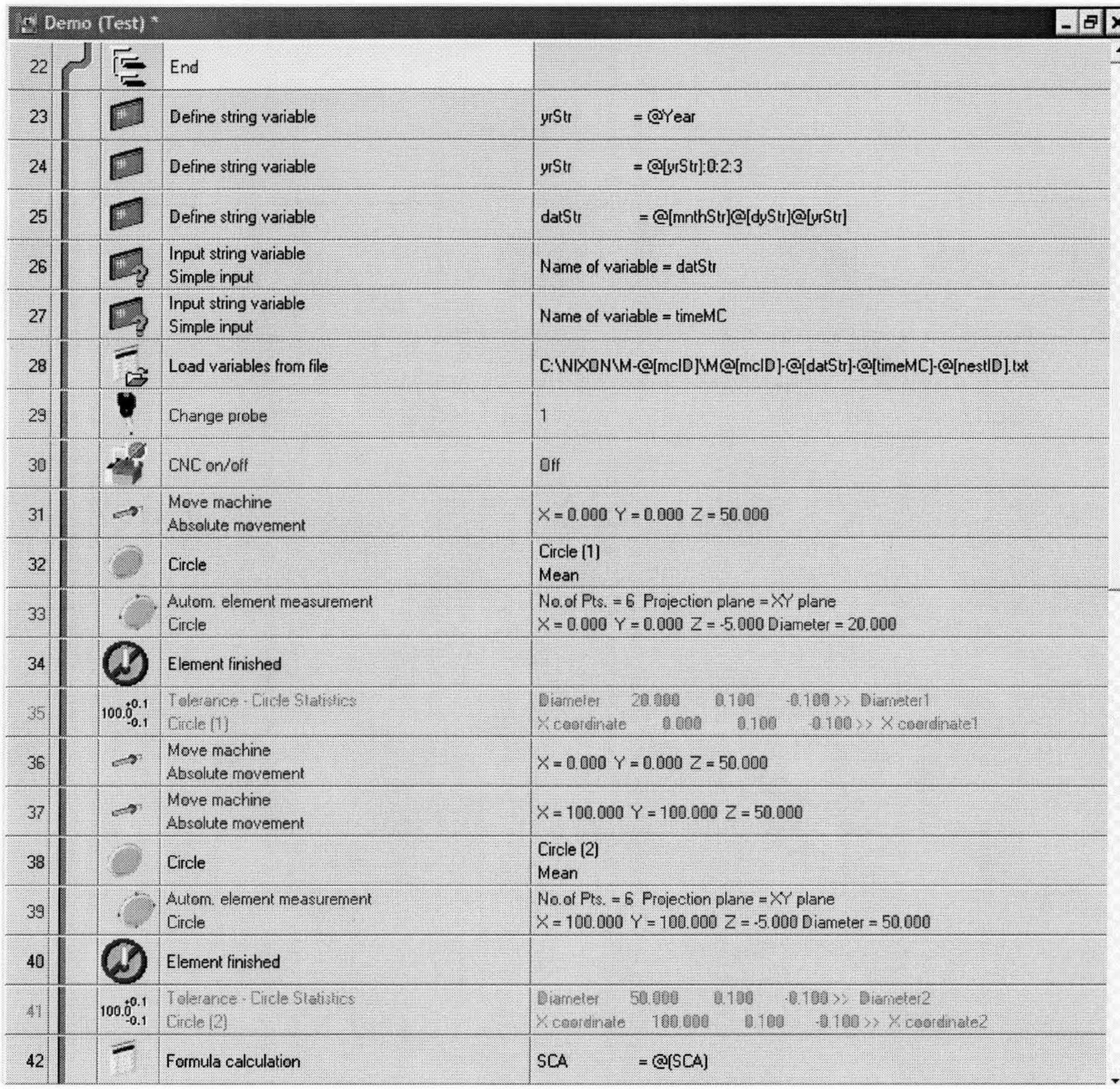

Demo (Test) *

22	End	
23	Define string variable	yrStr = @Year
24	Define string variable	yrStr = @[yrStr]:0:2:3
25	Define string variable	datStr = @[mnthStr]@[dyStr]@[yrStr]
26	Input string variable Simple input	Name of variable = datStr
27	Input string variable Simple input	Name of variable = timeMC
28	Load variables from file	C:\NIXON\M-@[mcID]\M@[mcID]-@[datStr]-@[timeMC]-@[nestID].txt
29	Change probe	1
30	CNC on/off	Off
31	Move machine Absolute movement	X = 0.000 Y = 0.000 Z = 50.000
32	Circle	Circle (1) Mean
33	Autom. element measurement Circle	No.of Pts. = 6 Projection plane = XY plane X = 0.000 Y = 0.000 Z = -5.000 Diameter = 20.000
34	Element finished	
35	Tolerance - Circle Statistics Circle (1)	Diameter 20.000 0.100 -0.100 >> Diameter1 X coordinate 0.000 0.100 -0.100 >> X coordinate1
36	Move machine Absolute movement	X = 0.000 Y = 0.000 Z = 50.000
37	Move machine Absolute movement	X = 100.000 Y = 100.000 Z = 50.000
38	Circle	Circle (2) Mean
39	Autom. element measurement Circle	No.of Pts. = 6 Projection plane = XY plane X = 100.000 Y = 100.000 Z = -5.000 Diameter = 50.000
40	Element finished	
41	Tolerance - Circle Statistics Circle (2)	Diameter 50.000 0.100 -0.100 >> Diameter2 X coordinate 100.000 0.100 -0.100 >> X coordinate2
42	Formula calculation	SCA = @(SCA)

Demo (Test) *

42		Formula calculation	SCA = @(SCA)
43		Formula calculation	SCB = @(SCB)
44		Formula calculation	ZCA = @(ZCA)
45		Formula calculation	ZCB = @(ZCB)
46		Formula calculation	MXA = @(MXA)
47		Formula calculation	MXB = @(MXB)
48		Formula calculation	MYA = @(MYA)
49		Formula calculation	MYB = @(MYB)
50		Formula calculation	MZA = @(MZA)
51		Formula calculation	MZB = @(MZB)
52		Formula calculation	TC1 = @(TC1)
53		Formula calculation	TC2 = @(TC2)
54		Formula calculation	TC3 = @(TC3)
55		Formula calculation	TC4 = @(TC4)
56		Formula calculation	TC5 = @(TC5)
57		Formula calculation	TC6 = @(TC6)
58		Formula calculation	TC7 = @(TC7)
59		Formula calculation	TC8 = @(TC8)
60	$100.0^{+0.1}_{-0.1}$	Tolerance Statistics Tolerance variable	SCA Nom. = 0.000 Upper tol. = 0.000 Lower tol. = 0.000
61	$100.0^{+0.1}_{-0.1}$	Tolerance Statistics Tolerance variable	SCB Nom. = 0.000 Upper tol. = 0.000 Lower tol. = 0.000
62	$100.0^{+0.1}_{-0.1}$	Tolerance Statistics Tolerance variable	ZCA Nom. = 0.000 Upper tol. = 0.000 Lower tol. = 0.000

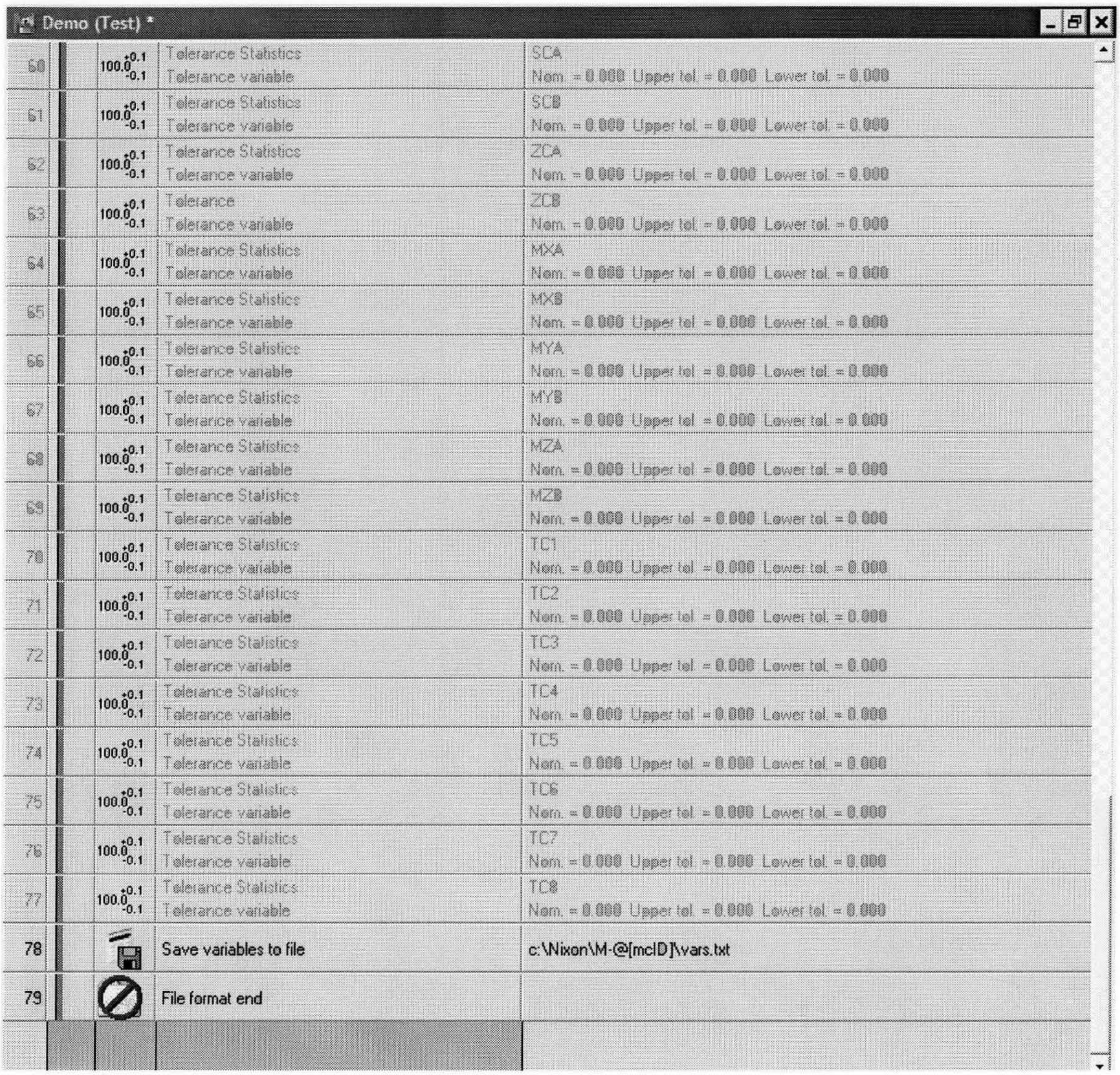

The first and second lines of the program ask the operator to input a cavity ID and nest ID for the part. If the cavity ID was greater than 47, then this indicated that the machine being used is M-127. Lines 9 through 25 were simply used for building the string of the suggested date in the format MMDDYY. Lines 26 and 27 were requesting the operator for date and time string inputs. Line 28 took all of the strings and compiles the filename for the part data file that is located on the network drive. In this example, only the regular C-drive was used. Lines 29 through 41 were a sample CMM program which simply measures circles for example purposes. Lines 42 through 77 were responsible for assigning numerical variables to the data read from the text file and then assigning tolerance statistics to the variable. Placing the variables in the in the *Formula Calculation* commands also allows for the ability to update the variables with some additional calculations, if required. Assigning the tolerance statistic to the variable tells MCOSMOS that this quantity should be reported to the statistical program. When this CMM program is run, MCOSMOS calls MeasurLink to begin the acquisition of the statistical information. The data is then all stored and handled through MeasurLink. For sake of verification, line 78 saved these data to a text file to ensure that they are being correctly processed. The program was then complete.

The program code that is shown here could be easily integrated into any Mitutoyo based CMM inspection site where all of the process monitoring PC's are connected to the same network. It could also be easily altered to accommodate any custom changes to the process monitoring system.